

Technical Report
HARPIA

Team 01 Technical Report to the 2026 EuRoC

Aerospace Team Graz (ASTG)
Graz University of Technology

Graz, October 27, 2026

Contact: Lukas Kolland
l.kolland@astg.at

Abstract

Project HARPIA is the sixth rocket developed by the Aerospace Team Graz (ASTG) and represents the first liquid-propellant launch vehicle of the team. After successfully developing and launching two solid and three hybrid rockets, ASTG aims to advance its propulsion capabilities by transitioning towards liquid propulsion. HARPIA is designed to compete in the liquid 9000 m flight category at the EuRoC 2026. The project's primary objectives are to successfully develop a student-built liquid propulsion system, achieve a nominal flight cycle, reach an apogee of at least 9000 m, and recover the launch vehicle.

The single-stage rocket has a length of 3.94 m, a diameter of 182.4 mm, an estimated dry mass of 34.0 kg, and a launch mass of 58.7 kg. The propulsion system uses nitrous oxide and isopropanol with a regeneratively cooled engine producing 4.9 kN thrust and a total impulse of 39.2 kNs. An actively controlled pressurization system ensures stable propellant feed conditions during the burn.

The aerostructure combines CFRP, GFRP, and aluminum components. A pitot-static probe and a gimbaled camera payload are integrated into the nosecone, while seven cameras record the flight from different perspectives. The recovery system features a dual-deployment architecture with improved lightweight SRAD components, a two-stage shockabsorber, and reinforced parachutes consisting of a 3.2 m main parachute and a para-aramid drogue parachute.

The avionics system uses a distributed architecture with a flight computer, five CANary control nodes, interface PCBs, and a central backplane PCB. A 6S Li-Ion battery supplies onboard power, while LoRa antennas provide communication with the mission control, and filling station and GNSS antennas provide information about the position of the rocket. The avionics software enables autonomous flight control, recovery deployment, and real-time data visualization.

Beyond the participation in EuRoC 2026, project HARPIA aims to establish the foundation for future liquid propulsion projects within ASTG. By developing a liquid rocket, along with the necessary testing procedures and comprehensive technical documentation, this project supports long-term knowledge transfer and advances student rocketry at Graz University of Technology.



Contents

1 Introduction **1**

2 Launch Vehicle System Architecture **3**
2.1 System Overview . . . 3
2.2 Propulsion Subsystem . . . 4
2.2.1 Fluid System . . . 5
2.2.2 Engine Bay . . . 12
2.3 Aerostructure Subsystem . . . 17
2.3.1 Structure . . . 18
2.3.2 Aerodynamics . . . 21
2.4 Recovery Subsystem . . . 23
2.4.1 Overview Recovery Section . . . 23
2.4.2 Redundancy . . . 23
2.4.3 Chargecups . . . 24
2.4.4 First Deployment . . . 24
2.4.5 Second Deployment . . . 25
2.4.6 Parachutes . . . 26
2.4.7 Parachute Lines and Connections . . . 27
2.4.8 Recovery System Tests . . . 29
2.5 Avionics Subsystem . . . 30
2.5.1 Power System . . . 30
2.5.2 Avionics Stack . . . 32
2.5.3 Additional PCBs . . . 35
2.5.4 Recovery Electronics . . . 36
2.5.5 Avionics Telemetry . . . 38
2.5.6 Avionics Software . . . 40
2.5.7 Flight Computer Firmware . . . 41
2.5.8 CANary Firmware . . . 42
2.5.9 Telemetry Firmware . . . 44
2.5.10 TELtalk Communication Protocol . . . 44
2.6 Payload Subsystem . . . 45

3 Mission Concept of Operations (CONOPS) **46**
3.1 Arming . . . 47
3.2 Thrust Curve . . . 48
3.3 Tanking and Pressurizing . . . 48
3.4 Flight Simulation . . . 49

4 Conclusions and Outlook **51**

List of Figures **vii**

List of Tables **x**

Acronyms **xi**

Glossary **xiv**

References xvi

Appendix A: System Data 52

Appendix B: Ground Support Equipment 57
B.1 Filling Station . . . 57
B.1.1 Fluid Architecture . . . 57
B.1.2 N_2 Purging . . . 58
B.1.3 Filling Station Electrical Cabinet . . . 58
B.1.4 Safety Control Box . . . 58
B.2 Launch Rail . . . 59
B.2.1 Fluid Umbilicals . . . 60
B.2.2 Launch Rail Electrical Cabinet . . . 60
B.2.3 Electrical Umbilical . . . 61
B.2.4 Vent Valve Override System . . . 61
B.2.5 Holddown . . . 61
B.3 Mission Control . . . 62
B.3.1 Mission Control Rack . . . 63
B.3.2 Mission Control Box . . . 63
B.3.3 Mission Control Software . . . 64
B.3.4 Antennas . . . 65

Appendix C: Detailed Test Reports 66
C.1 Testing Approval . . . 68
C.2 Recovery System Testing . . . 69
C.3 First Deployment Concept Test . . . 70
C.4 First Deployment Functionality Test . . . 76
C.5 Nosecone Separation Concept Test . . . 79
C.6 Nosecone Separation Test . . . 81
C.7 Second Deployment Concept Test . . . 84
C.8 Second Deployment Functionality Test . . . 90
C.9 KESTREL Calibration . . . 95
C.10 Tension Scale Test . . . 100
C.11 Recovery Vibration Test . . . 109
C.12 First Deployment Vacuum Chamber Test . . . 114
C.13 Vacuum Chamber Test . . . 116
C.14 RTA Windtunnel Test . . . 119
C.15 Drop Test . . . 134
C.16 Main Parachute Pullout Test . . . 139
C.17 Deployment Flight Computer Actuation . . . 141
C.18 Preassembly Test . . . 145
C.19 Shockabsorber Test . . . 150
C.20 Eyebolt Rotation Test . . . 172
C.21 Chargecup Insulation Test . . . 176
C.22 Rope Protection Test . . . 181
C.23 Propulsion System Testing . . . 185
C.24 Cold-Flow 1: Demonstrator . . . 187
C.25 Hot-Fire 1: Demonstrator . . . 197
C.26 Cold-Flow 1: Engine . . . 214
C.27 Hot-Fire 1: Engine . . . 227
C.28 Hot-Fire 2: Engine . . . 244
C.29 Cold-Flow 2: Engine . . . 262

C.30 Hot-Fire 3: Engine . . . 270
C.31 Cold-Flow 3: Engine . . . 284
C.32 Hot-Fire 4: Engine . . . 289
C.33 All Up Vertical Cold-Flow . . . 303
C.34 Hot-Fire 5: Engine . . . 306
C.35 Hot-Fire 6: Engine . . . 323
C.36 Pyrotechnic Ignitor Test . . . 337
C.37 Torch Ignitor Test 1 . . . 346
C.38 Torch Ignitor Test 2 . . . 355
C.39 Torch Ignitor Test 3 . . . 372
C.40 Torch Ignitor Test 4 . . . 380
C.41 Torch Ignitor Test 5 . . . 393
C.42 Torch Ignitor Test 6 . . . 400
C.43 Internal Leak Test . . . 406
C.44 Unloading Test . . . 410
C.45 Fuel Tank Pressure Test . . . 415
C.46 Oxidizer Tank Pressure Test . . . 420
C.47 Combustion Chamber Pressure Test . . . 425
C.48 Electronics Thermal Test . . . 428
C.49 Vacuum Chamber Test . . . 430
C.50 Recovery Igniter Resistance Test . . . 432
C.51 Vibration Test . . . 434
C.52 Long Duration Runtime Test . . . 438
C.53 Range Test Rocket . . . 444
C.54 Range Test Long Range WLAN . . . 447
C.55 Tube Bending Test . . . 449
C.56 Holddown Test . . . 451
C.57 Rail Fit Check . . . 459
C.58 Adhesive Heating Test . . . 461
C.59 Fin Alignment Test . . . 466
C.60 First Launch Dry Run . . . 468
C.61 Second Launch Dry Run . . . 471

Appendix D: Hazard Analysis Report 474
D.1 Hazardous Substances . . . 474

Appendix E: Risk Assessment 480

Appendix F: Compliance Matrix 598

Appendix G: Checklists 614
G.1 ALL: List of all Checklists . . . 614
G.2 ALL: Launch Procedure . . . 615
G.3 ALL: General Abort . . . 620
G.4 ALL: Rocket Recovery . . . 621
G.5 PRO: Cleaning of Fluid Components . . . 623
G.6 PRO: Ground Support Equipment Setup . . . 624
G.7 PRO: Propulsion Stack Assembly . . . 627
G.8 PRO: Combustion Chamber Assembly . . . 628
G.9 AST: Launch Rail Assembly . . . 629
G.10 AST: Holddown Assembly . . . 632
G.11 AST: Launch Preparations . . . 634

G.12 AST: Rocket Integration . . . 636
G.13 AST/AVI: Nosecone Assembly . . . 640
G.14 AST: Rocket Integration Launch Day . . . 642
G.15 AVI: Mission Control Setup . . . 643
G.16 AVI: Rocket Integration . . . 645
G.17 AVI: Ground Support Equipment Setup . . . 647
G.18 AVI: Pre-Launch Checks . . . 650
G.19 AVI: CATS VEGA . . . 653
G.20 REC: Pre-Assembly I . . . 655
G.21 REC: Pre-Assembly II . . . 661
G.22 REC: Final Assembly . . . 663
G.23 REC: First Deployment Assembly . . . 666
G.24 REC: Second Deployment Assembly . . . 668
G.25 REC: Chargecup Preparation . . . 670
G.26 REC: Main Folding . . . 673
G.27 REC: Drogue Folding . . . 677
G.28 REC: Disassembly . . . 679

Appendix H: Further System Details **685**
H.1 Recovery Line Management . . . 685
H.2 KESTREL - Drogue Deployment Simulator . . . 688
H.3 CFD Analysis of Regenerative Cooling Channels . . . 696
H.4 The Sensor Board . . . 698
H.5 Antenna Deepdive - Fundamentals and Patch-Antenna Design . . . 712

Appendix I: Engineering Drawings **725**

Appendix J: PCB Schematics **807**

Appendix K: Detailed Structural and Mechanical Calculations **913**
K.1 Propulsion Calculations . . . 913
K.2 Recovery Calculations . . . 1013
K.3 Aerostructure Calculations . . . 1048
K.3.1 Load Calculations . . . 1082
K.3.2 CFD Analysis Reports . . . 1083

Appendix L: Detailed Flight Simulations **1127**
L.1 Simulation Parameters . . . 1127
L.2 Environment . . . 1129
L.3 Tanks and Engine . . . 1129
L.4 Rocket Body and Aerodynamic Surfaces . . . 1133
L.5 Recovery Devices . . . 1134
L.6 Flight . . . 1140
L.7 Different Wind Conditions . . . 1154

Appendix M: Datasheets **1160**
M.1 Hazardous Materials Datasheets . . . 1160
M.2 Recovery Datasheets . . . 1251

1 Introduction

This document serves as the official technical report for the project HARPIA, presented by ASTG for European Rocketry Challenge (EuRoC). As the team's sixth sounding rocket, HARPIA marks a significant technological milestone: it is the team's first liquid-propellant launch vehicle, engineered to reach an apogee of 9000 m. This introductory chapter outlines the team's organizational framework, history, and the primary objectives driving this year's mission.

Team Characteristics

The ASTG is a student association founded in 2019 at Graz University of Technology (TU Graz). Today, the team consists of 120 members from more than 20 nations. As shown in Figure 1.1, this diverse mix of 21 academic backgrounds is the core asset for managing complex technical projects, and all members share a drive to bring university theory to life.

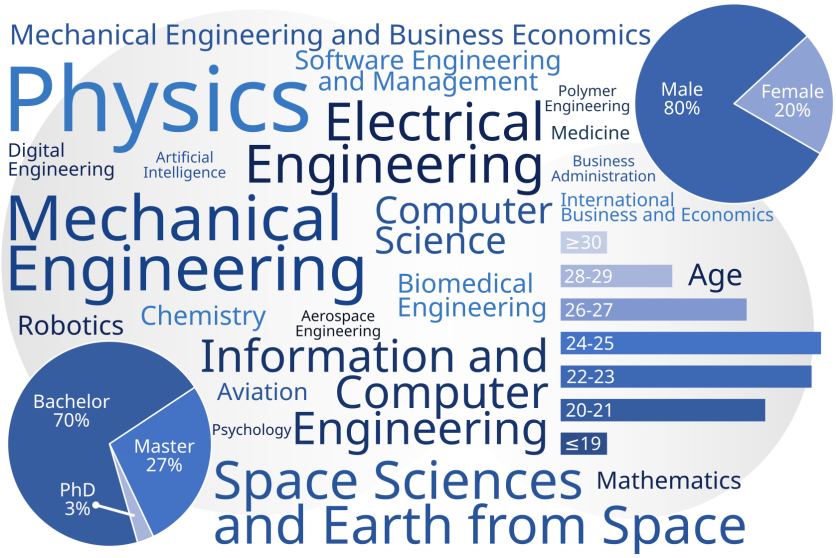


Figure 1.1: Overview of the team demographics showing study levels, gender distribution, fields of study, and age distribution.

Team Structure and Management Strategy

ASTG organizes its workflow into subsystem modules. For HARPIA, Project Lead Management and Project Lead System Engineering supervise the timeline, resources, risks, and interfaces across four main modules: Aerostructure, Avionics, Propulsion, and Recovery.

Development is driven by weekly module meetings, supplemented by on-demand interface meetings for direct cross-module troubleshooting. To maintain oversight, a weekly Lead Meeting brings together project management, the Executive Board, the Safety Officer, and module leaders to align overarching updates, strategic decisions, and safety operations.

Team History

Since its debut at EuRoC 2021, the team's engineering capabilities have evolved rapidly. The progression of the launch vehicles is shown in Figure 1.2. This evolution ranges from the solid-propelled AVES and AVES II to the hybrid-propelled HALCYON, ALCEDO, and ISPIDA, and finally to HARPIA, the team's first liquid-propelled rocket.

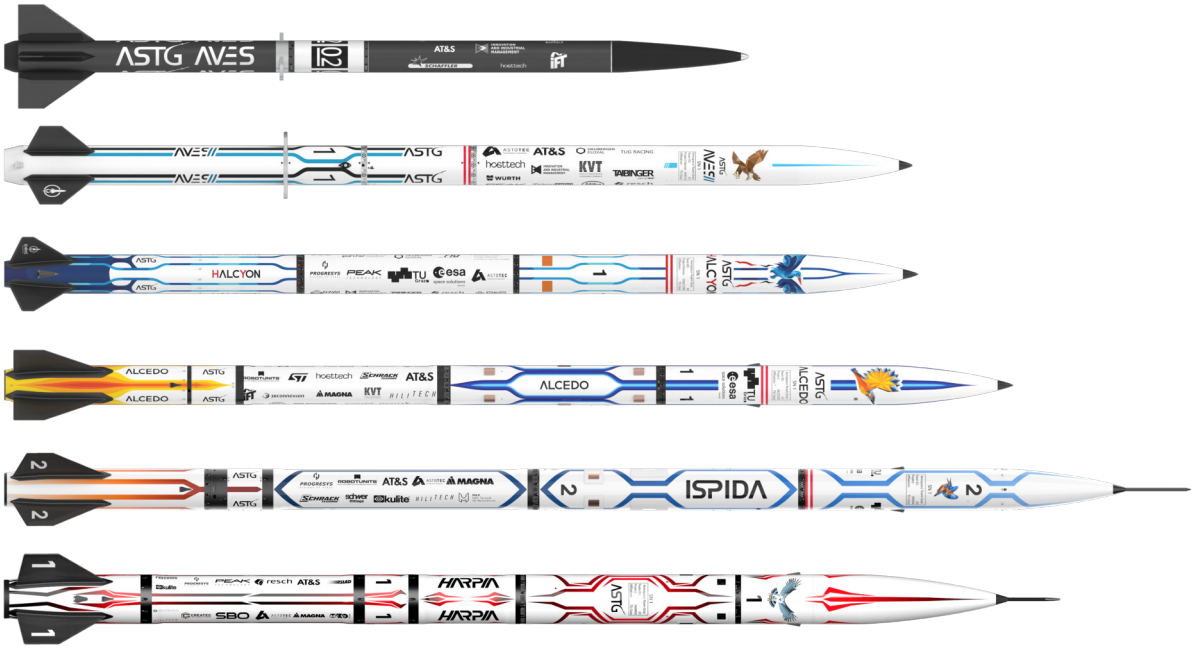


Figure 1.2: Progression of all competition rockets developed by ASTG from 2021 to present.

Stakeholders, Partners and Suppliers

Realizing a project of this scale requires strong collaboration with external partners. ASTG is supported by educational institutions, public funds, and industry partners through monetary donations, materials, manufacturing capabilities, software licenses, and testing facilities. Key sponsors for this year's project include TU Graz, Austrian Research Promotion Agency (FFG), Institute of Production Engineering (IFT), Institute of Innovation and Industrial Management (IIM), Astotec Pyrotechnic Solutions GmbH, Resch GmbH, Peak Technology GmbH, Fuchshofer GmbH, SBO AG, and more than sixty additional contributors.

Project Goals and Technical Challenges

This year, the primary objective is to successfully launch and recover HARPIA, targeting an apogee of 9000 m. Furthermore, ASTG aims to secure at least a top 5 overall placement at EuRoC. Beyond competition, the long-term vision is to establish a reliable foundation for future liquid-propellant rocketry within the team and ensure sustainable knowledge transfer across all modules. Developing the first liquid launch vehicle introduces technical challenges, particularly around complex valve sequencing, an updated rocket diameter, and mitigating parachute deployment shock forces due to greater overall weight. Alongside these engineering hurdles, the project faces severe logistical bottlenecks. Managing extended lead times across supply chains for specialized components is critical to ensuring that the rocket is manufactured and tested on schedule.

2 Launch Vehicle System Architecture

2.1 System Overview

Figure 2.1 shows a cut view of the CAD model of HARPIA and illustrates the overall system architecture and structural partitioning of the launch vehicle. The vehicle is divided into four main parts: the nosecone, recovery section, avionics section, and propulsion system.

From top to bottom, the rocket begins with the nosecone, which houses the pitot-static probe, the CATS Vega, the payload, and the associated electronics. The pitot-static probe enables the acquisition of flight parameters during ascent, while the integrated electronics provide the necessary interfaces for data handling and payload activation.

Connected to the nosecone is the recovery section, consisting of a pressure chamber for the drogue parachute and a main compartment housing the main parachute and the dual deployment system, implemented through the first deployment and second deployment.

Beneath the recovery section is the avionics stack, which contains the flight computer, sensor board, black box, battery pack, and an additional CATS Vega. This section serves as the central interface between the vehicle subsystems, providing data acquisition, system control, power distribution, and telemetry. The external patch antennas mounted on the hull enable communication through LoRa and GNSS links.

The propulsion section forms the lower part of the launch vehicle. It starts with the high-pressure tank and continues with the fuel and oxidizer tanks connected by the Valvebay structure. Three fluid systems - upper, middle, and lower connect the tanks as well as the regeneratively cooled combustion chamber. It is mounted via the Thrust structure and enclosed in the tailcone.

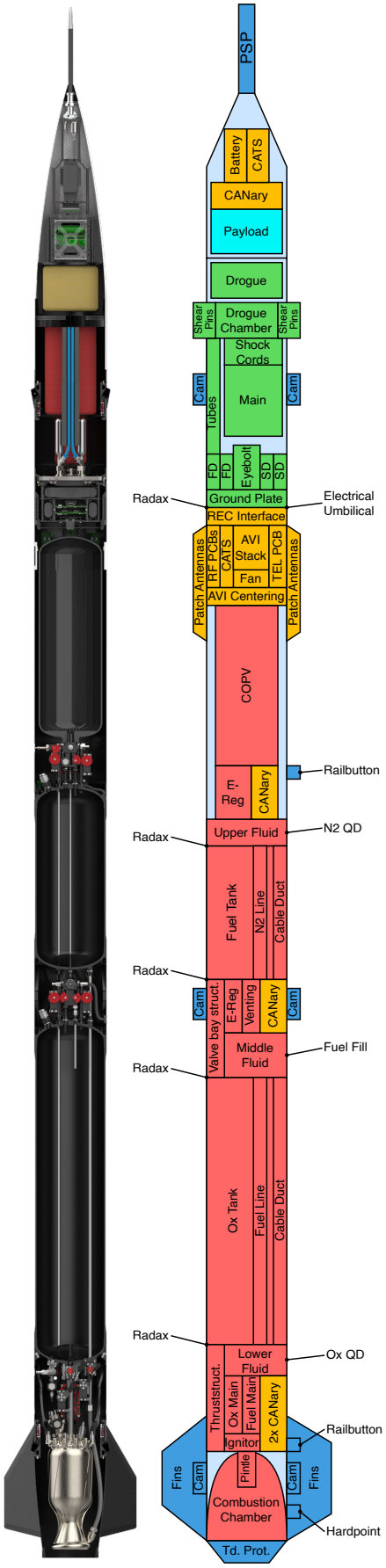


Figure 2.1: Overview of HARPIA.

2.2 Propulsion Subsystem

HARPIA features a bi-liquid propulsion system which aims to propel the launch vehicle to 9 km. It utilizes isopropanol (IPA) as fuel and nitrous oxide (N_2O) as oxidizer. The two propellants are stored in separate structural tanks. Both tanks are pressurized using the same composite overwrapped pressure vessel (COPV), which is located at the top of the propulsion stack.

The structural tanks divide the rocket into three main fluid systems: the upper fluid system between the COPV and the fuel tank, the middle fluid system between the fuel and oxidizer tanks, and the lower fluid system which sits between the oxidizer tank and the engine. The fuel and oxidizer tanks are connected via the Valvebay structure, while the thrust structure connects the engine to the oxidizer tank.

Two pass-through lines run through each tank. One line is a cable duct connecting the printed circuit boards (PCBs) distributed throughout the propulsion stack. In the fuel tank, a N_2 pass-through leads pressurant gas to the oxidizer tank for pressurization. The oxidizer tank houses a fuel pass-through which leads to the engine below.

Table 2.1: Propulsion characteristics.

Characteristic	Value	Unit
Pressurant Tank Pressure	300	bar
Fuel Tank Pressure	42	bar
Oxidizer Tank Pressure	35	bar
Combustion Pressure	26	bar
Fuel Mass	6.3	kg
Oxidizer Mass	15.9	kg
Total Impulse	39.2	kNs
Thrust	4900	N
Burn Time	8.0	s

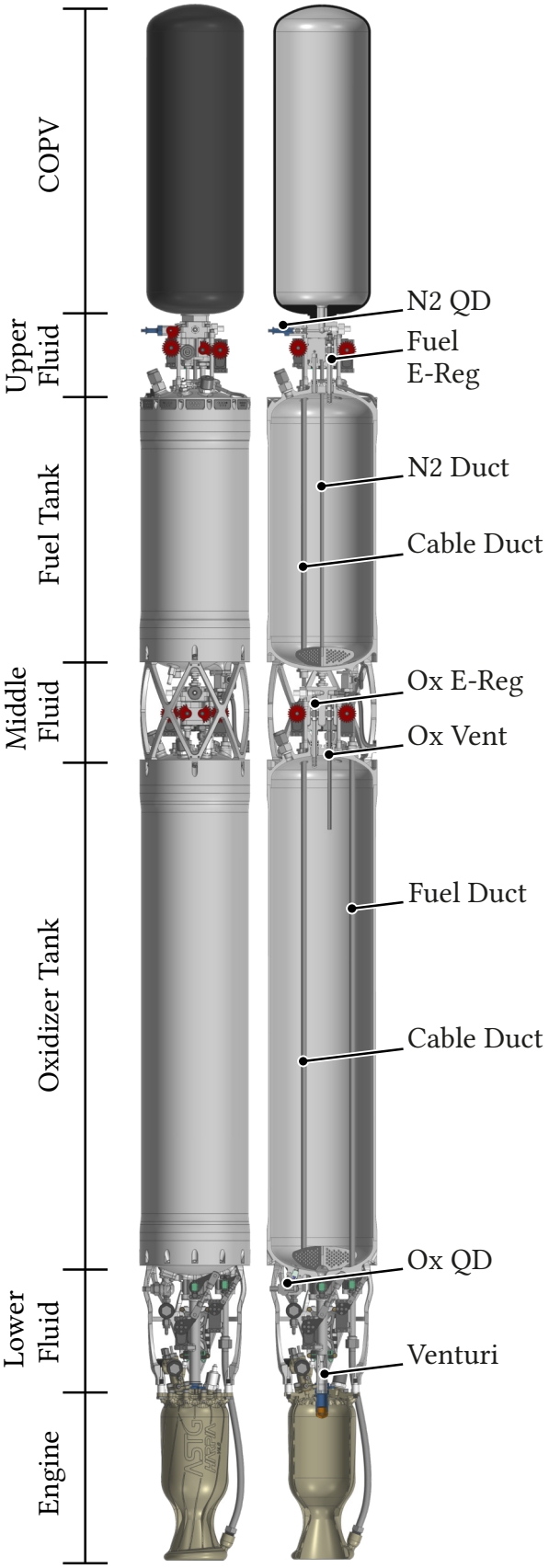


Figure 2.2: CAD of the propulsion stack and a cut view.

2.2.1 Fluid System

Figure 2.3 shows the fluid diagram of the complete propulsion stack. Sensors and valves are described in more detail in later chapters as this section only serves as a first overview.

At the top is the 6.8 L COPV, which is used to pressurize both tanks. The servo-activated N_2 fill valve is used to load the pressurant N_2 into the rocket. The fuel E-Reg pressurizes the fuel tank and uses the four pressure and temperature sensors of the upper fluid system, along with the fuel temperature, for regulation. The fuel depressurization solenoid is used to vent the fuel tank after flight, while the pressure relief device (PRD) and burst disc act as safety devices in case of overpressure.

A manually actuated ball valve positioned at the bottom of the fuel tank serves as the fuel fill valve for the IPA. The N_2 pass-through line feeds pressurant gas to the oxidizer E-Reg, which in turn pressurizes the oxidizer tank. The three pressure sensors of the middle fluid, the temperature sensor of the N_2 in the line below the fuel tank, and the oxidizer temperature are used to regulate the oxidizer E-Reg and supervise the system. The upper oxidizer vent valve is connected to a dip tube which reaches into the oxidizer tank, where liquid venting indicates a full tank. Again, a PRD and burst disc act as safety devices.

Below the oxidizer tank are the two main valves which draw propellants from the aforementioned tank and from the fuel downcomer. While the oxidizer mass flow is further restricted by a cavitating venturi, the fuel is directly led to the inlet at the bottom of the combustion chamber. The oxidizer quick disconnect (QD) contains a check valve and is used to fill the tank with N_2O. One manual and one solenoid valve provide ways to depressurize and detank the oxidizer.

Two solenoids tap off additional fuel and oxidizer to fuel the torch ignitor, which is inserted directly into the engine bulkhead. Additional pressure and temperature sensors monitor the state of the combustion chamber.

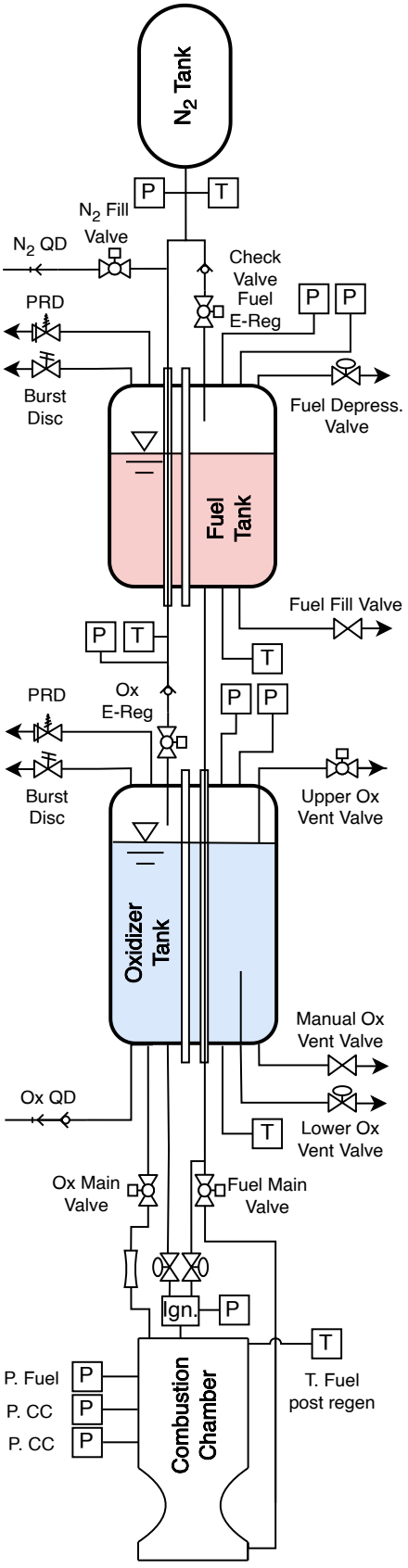


Figure 2.3: Fluid system of the propulsion stack.

Tanks

The fuel and oxidizer tanks each consist of three pieces constructed from EN AW-6082 T6 aluminum. The upper and lower bulkheads are welded to the cylindrical middle section, and the welds are subsequently turned flush. Perforated aluminum plates are welded into the lower bulkheads to suppress vortex formation and prevent gas ingestion by the engine. The lower bulkhead provides connections for the fill line, the main propellant line to the engine, and a temperature sensor. The upper bulkhead features connections for both PRD as well as burst disc, two pressure sensors, and the pressurization line of the corresponding E-Reg.

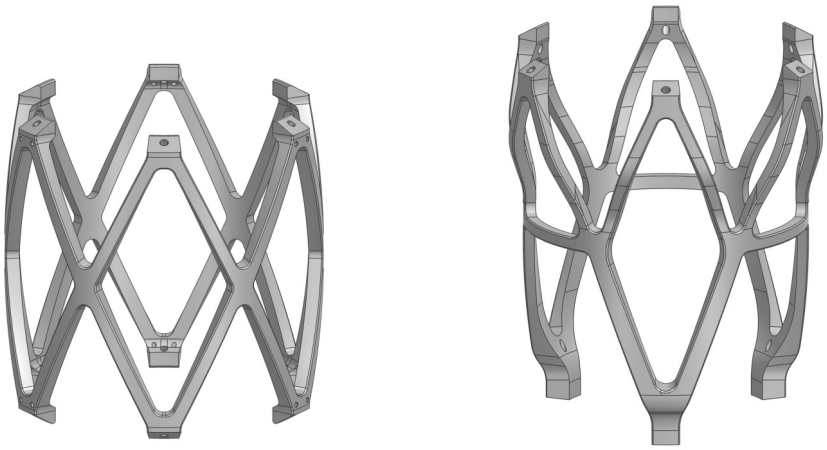
The tanks also act as structural parts of the hull, connecting to the tailcone and Thrust structure at the bottom and to the avionics tube at the top. The tanks are mounted to each other through the Valvebay structure, with all connections being radax interfaces.

The oxidizer tank has a volume of 18.5 L, holding 15.9 kg of N_2O at −20 °C, with 2.6 L ullage. The fuel tank contains 8 L IPA with 1.5 L ullage. Both have been designed to fail by leakage rather than bursting. The cylindrical wall thickness was calculated to withstand more than twice the maximum expected operating pressure (MEOP), and both tanks were fully simulated using finite element analysis (FEA).

Valvebay Structure and Thrust Structure

Each of these structures follows the same philosophy: a lightweight, space-saving yet stiff design that allows full access to the middle and lower fluid systems. Milled from EN AW-6082 T6 aluminum, both designs utilize radax connections for easy integration.

The Valvebay structure is enclosed by three carbon fiber panels. The thrust structure is covered by the tailcone, which uses six of the 12 shared radax connection points on the lower oxidizer bulkhead, leaving six to secure the thrust structure itself. Furthermore, the combustion chamber, equipped with three load cells, is mounted to the lower end of the thrust structure.



(a) Valvebay structure. (b) Thrust structure.

Figure 2.4: Connecting structures of the rocket which envelop the middle and lower fluid system.

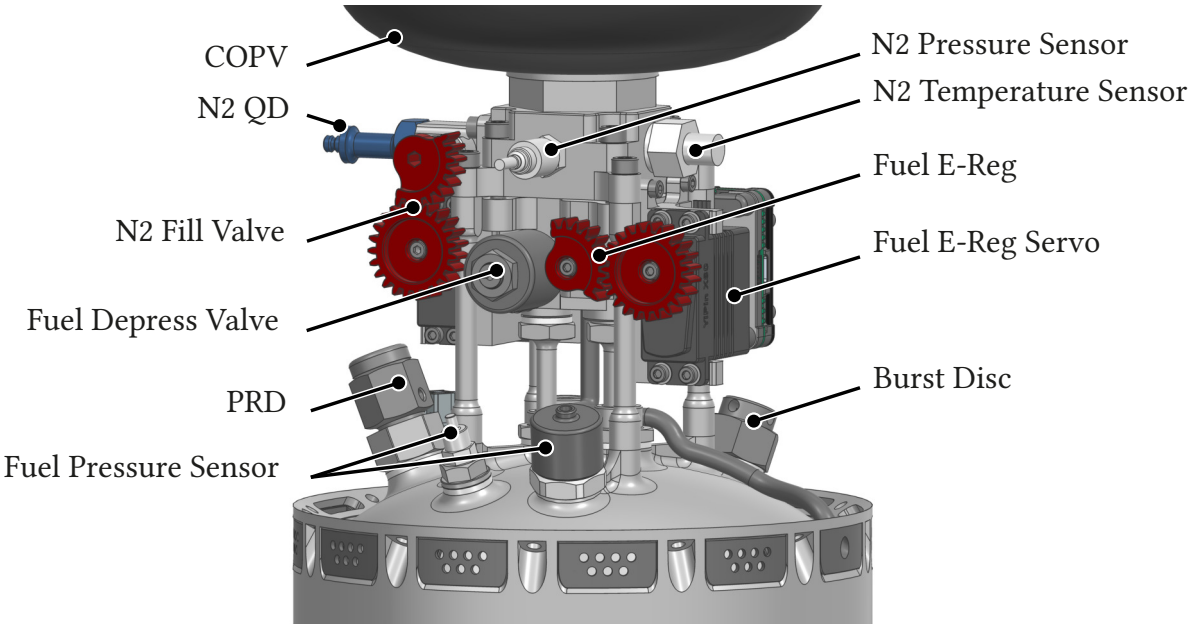


Figure 2.5: View of the upper fluid system.

Upper Fluid

The core components of the upper fluid system are the PT-connector and the attached E-Reg valve body. At its top, the PT-connector interfaces with a 6.8 L commercial-off-the-shelf (COTS) COPV. Its four lateral ports accommodate the N_2 fill valve with its N_2 QD, the N_2 pressure and temperature sensors, and the outlet for the N_2 pass-through line which supplies the oxidizer E-Reg for pressurization.

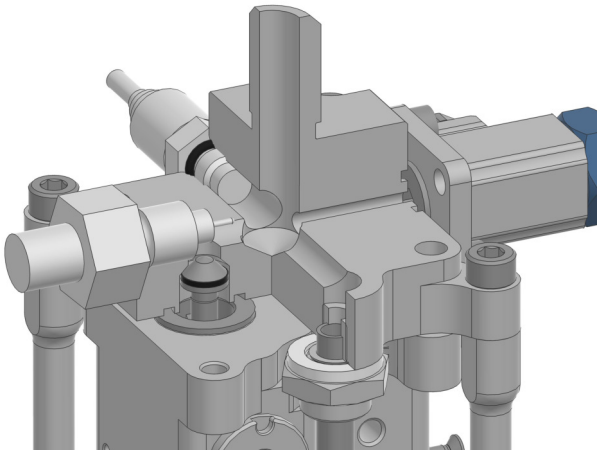


Figure 2.6: Cut of the PT-connector.

The valve body houses the fuel E-Reg alongside a normally closed solenoid valve for fuel tank depressurization. Servos are mounted on both sides of the valve body to actuate the fuel E-Reg and the N_2 fill valve. Their mounts were designed to reduce mechanical play between the servo and the valve, improving valve actuation accuracy.

A CANary is mounted on two of the four rods that secure the entire valve assembly to the fuel tank. The top of the fuel tank provides direct connections for two redundant pressure sensors and two safety devices: a PRD designed to open at 60 bar and a COTS burst disc with a rupture pressure of 67 bar.

All operating procedures are designed to prevent the mixing of oxidizer and fuel in the shared high-pressure system. In case other systems fail, check valves additionally prevent the oxidizer from self-pressurizing into the fuel tank via a depressurized high-pressure system.

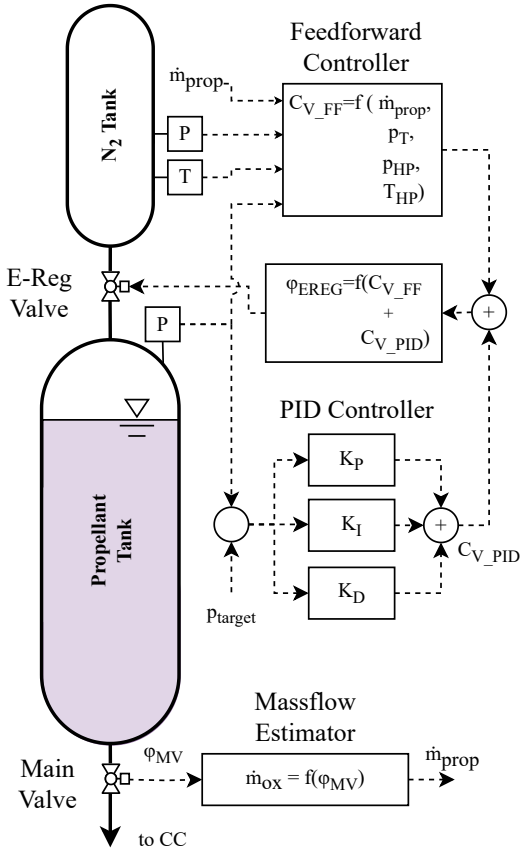


Figure 2.7: Controller overview of the E-Reg.

Pressurizing System

The pressurization of both the oxidizer and the fuel tank is achieved by actively controlled ball valves. A feed forward (FF) as well as a proportional integral derivative (PID) controller are utilized to manage the valves. The control principle, which can be seen in Figure 2.7, is the same for both tanks. Based on the thermodynamic state of the high-pressure side and the main valve mass flows, the FF determines the flow coefficient C_v needed to maintain stable tank pressure. Similarly, the PID controller also calculates a required C_v. Both outputs are then added, and the final valve set-point is passed on.

In normal operation, each E-Reg independently regulates to the set pressure. Should an anomaly emerge before launch, automatic aborts are activated. If communication between the two E-Regs fails during flight or if an abort occurs, conservative fallback curves dictate the valve positions. This ensures the system enters a safe state even in the case of failures.

E-Reg Valve

The E-Reg valve is a self-designed ball valve designed to reduce backlash between the ball and the actuator for more precise positioning. This was achieved by combining the ball and stem into a single component made of AISI 316L stainless steel, featuring a splined shaft for the gearing and a bore diameter of 6 mm.

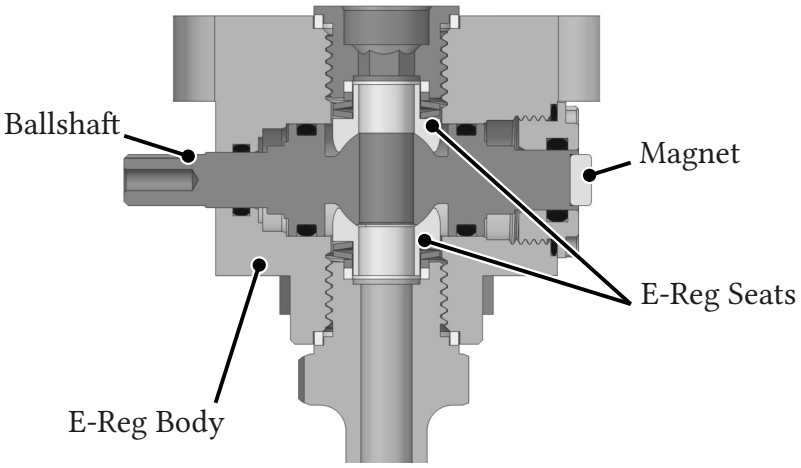


Figure 2.8: Cut of the fuel E-Reg.

The stem is sealed in both the front and the back using two fluoroelastomer (FKM) O-rings. The E-Reg seat for the ball is taken from a COTS valve that uses a combination of polyether ether ketone (PEEK) and polytetrafluoroethylene (PTFE). These seats are held in place with custom end connections. A magnet paired with a matching PCB is mounted to the back of the valve for accurate position feedback. In addition to the two propellant E-Regs, this valve design is also used for the oxidizer vent valve.

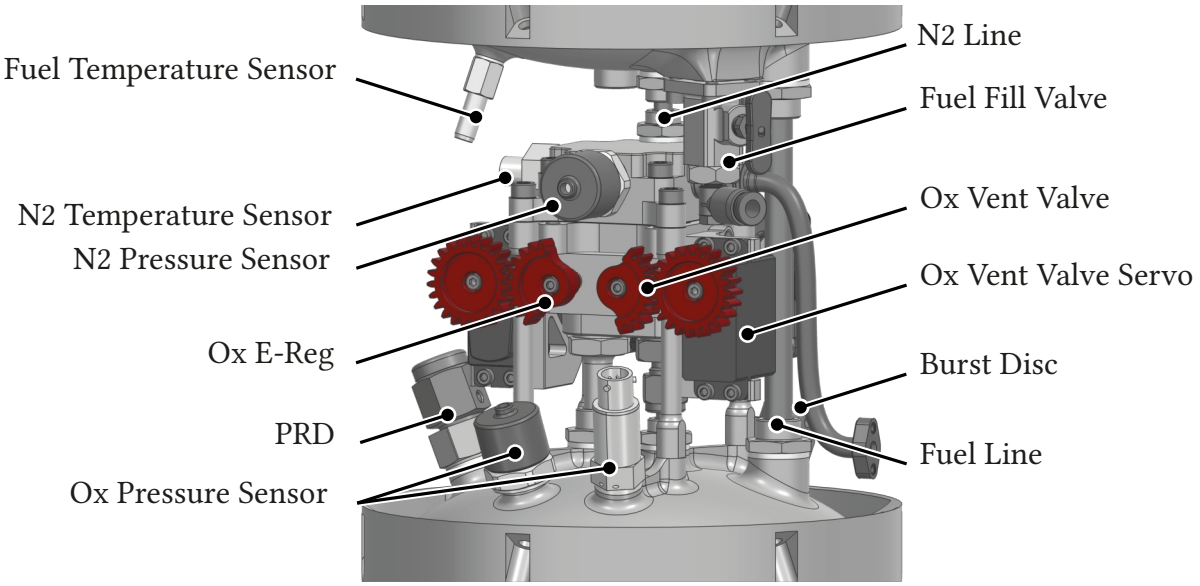


Figure 2.9: View of the middle fluid system.

Middle Fluid

Figure 2.9 shows all components of the middle fluid system. The central oxidizer E-Reg body features two previously mentioned E-Reg ball valves. They are integrated identically to the one used for fuel pressurization. One is used to pressurize the oxidizer tank; the other to depressurize it. On top of the oxidizer E-Reg body, the N_2-manifold connects to the high-pressure N_2 pass-through line, pressure and temperature sensors, and the venting line which guides the gas out to an opening in the hull.

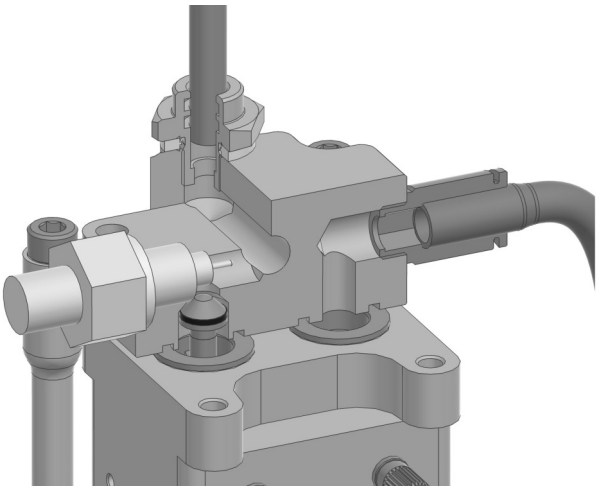


Figure 2.10: Cut of the N_2-manifold.

The manual fuel fill valve is positioned at the bottom of the fuel tank which can be seen in Figure 2.9. A freely rotatable 90° pneumatic connector is used to ensure convenient access for fuel filling. The valve is placed so only one of the three enclosing panels has to be removed for fuel filling.

In the upper oxidizer tank bulkhead, two redundant oxidizer pressure sensors are mounted. These sensors, along with a thermocouple and a pressure sensor for the N_2, are used to control the oxidizer E-Reg. For tank safety, a PRD with an opening pressure of 55 bar as well as a burst disc with a rupture pressure of 61 bar are integrated into the oxidizer tank.

The cable duct, which routes cables inside the tank, is visible in the back. All pass-through interfaces in the tanks are sealed towards the inside with O-rings and to the outside with USIT rings.

Similar to the fuel E-Reg body, a check valve is integrated into the oxidizer E-Reg to prevent mixing of the propellants.

Fill Valve

The fill valve is a COTS 1/8" ball valve featuring a custom-designed body for easier integration and to save space. On one hand it is used as a servo-actuated valve for N_2 filling which requires it to withstand 300 bar and an end connection that includes the QD. It is also used as a manually actuated valve for fuel filling and as an oxidizer relief valve in the event of an abort. The oxidizer relief valve can be actuated from outside the rocket with a hex key.

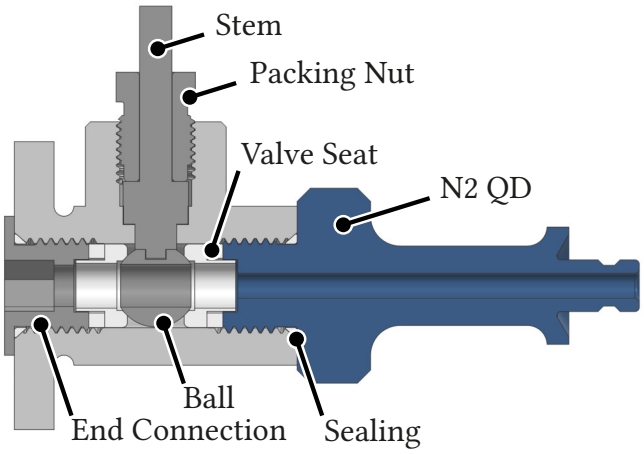


Figure 2.11: Cut of the fill valve at the N_2 QD.

The sealing materials are selected to ensure compatibility with IPA and N_2O, which is achieved through a combination of PEEK and PTFE.

Lower Fluid

Figure 2.12 shows an overview of the main components that are featured in the lower fluid system. This section provides an overview of all components, especially those not explained in greater detail in later sections. Furthermore, it should be noted that while on the launch rail, the whole lower fluid system is purged with N_2 to prevent condensation from forming on any components and to prevent an oxygen-rich atmosphere in case of an oxidizer leak. The purging line is pulled out of the rocket during launch as it merely reaches milli meters into the tailcone.

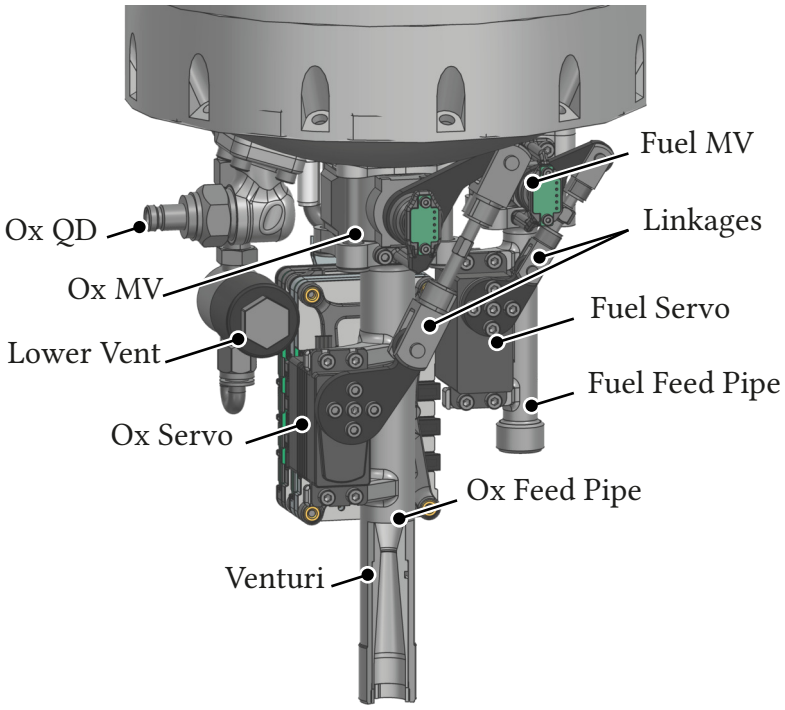


Figure 2.12: View of the lower fluid system.

To the left of the oxidizer main valve sits the oxidizer QD; it is dissimilar to the one used for the pressurant gas. The connector behind the QD is designed to house a screw-in check valve, which prevents oxidizer leaks after the loading lines are disconnected. It is screwed in before the QD-adapter is flanged onto the tank.

Behind the QD sits the lower oxidizer vent valve, which is used if a full offloading of oxidizer is necessary. To prevent freezing during this procedure, the smallest orifice, where the fluid expands, is in the SLS printed pipe leading to an outlet point in the radax. This line can be seen in Figure 2.13 on the right side. Additionally, a heat mat is installed around the solenoid valve to avoid freezing.

Figure 2.13 shows the backside of the lower fluid system. The manual oxidizer vent valve, central in the figure, serves as a fallback for oxidizer detanking if everything else fails. This ensures the oxidizer tank can be emptied in any case, even during rocket recovery when relying on electronics might not be possible. The hex key socket embedded into a linking part can be reached externally through a hole in the tailcone without having to disassemble the rocket.

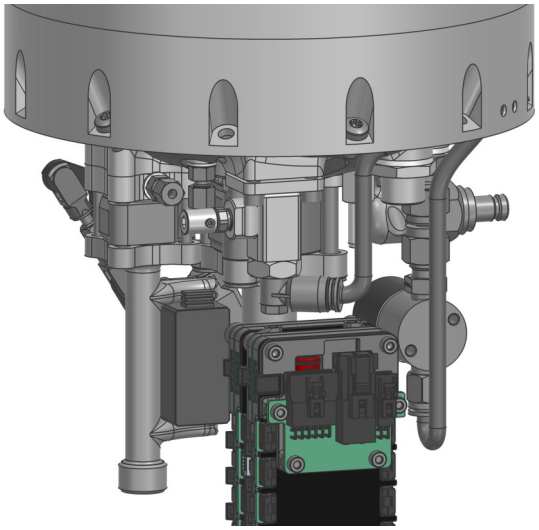


Figure 2.13: View of the back of the lower fluid system.

In Figure 2.13, the two tap-offs for oxidizer and fuel used by the torch ignitor are visible on the left side. Through 1/8” pipes, the propellants are guided to the two propellant solenoids. It can be ignited independently of the main valves by tapping off propellants beforehand.

Main Valves

The two main valves and lines make up the major part of the lower fluid system. Two COTS valves were used as the base components, although the fluid connections on both sides were replaced. This was done to achieve significant weight reductions and a more compact, integrated design. The interfaces on both sides were designed to accommodate the COTS parts. Magnetic angle sensors are used to monitor the position of both of the main valves.

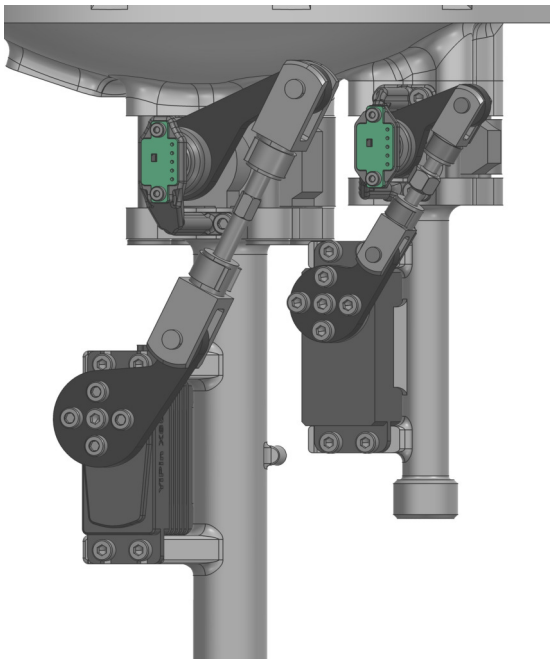


Figure 2.14: Close-up view of the main valves.

In the center, the oxidizer is regulated by a 3/4” ball valve which is directly flanged onto the bottom of the oxidizer tank. The linkages connecting the servo and the valve provide a varying transmission ratio at different opening angles. This helps to overcome the initially high torque required to open the valve. The fuel main valve implements the same principle with a 3/8” valve. For the fuel, an additional flange connects the fuel downcomer to the valve.

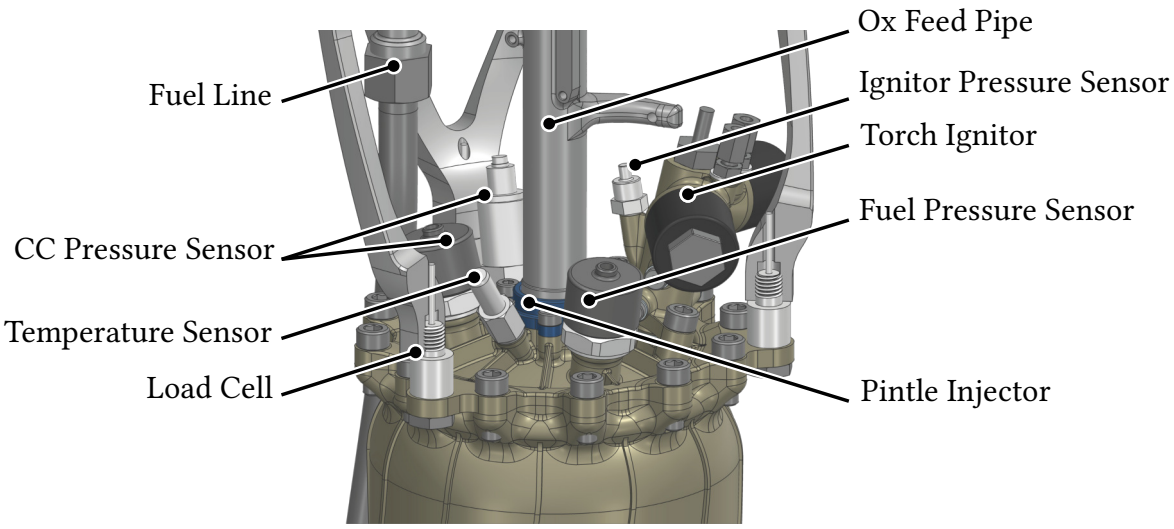


Figure 2.15: View of the engine bay.

2.2.2 Engine Bay

Figure 2.15 gives an overview of the engine bay and its components. The thrust structure connecting the engine to the oxidizer tank is cut to show the integrated load cells for thrust measurement.

The torch ignitor is flanged onto the bulkhead and includes both propellant solenoids, the glow plug, and a chamber pressure sensor. The pintle is slotted into the center of the bulkhead and connects to the oxidizer feed pipe.

Furthermore, to gather data and monitor the system, three pressure and one temperature sensors are integrated into the bulkhead. The fuel temperature is measured after passing through the cooling channels to monitor fuel temperature before injection. Two sensors are used to measure the combustion chamber pressure, with another one to monitor the pressure of the fuel after the cooling channels.

Thrust Measurement

Three tension/compression load cells with a capacity of 5 kN each are installed between the thrust structure and the combustion chamber to measure engine thrust during flight. The three-point arrangement avoids a statically overdetermined system.

Each load cell features an M8 thread on both ends. The axial electrical connection allows for installation without a defined rotational orientation. One side is screwed into the thrust structure, while the other is secured to the combustion chamber using nuts.

Spacers between the load cells and adjacent components ensure proper load introduction and uniform load distribution, reducing local deformations. They also provide a defined shoulder for precise engine alignment.

The load cells use integrated strain gauges in a temperature-compensated Wheatstone bridge configuration. They were selected due to their low mass, compact design, and manufacturer calibration, enabling accurate thrust measurements. Their performance was validated during a horizontal Hot-Fire test by comparison with the test stand's reference measurement system.

Combustion Chamber

The combustion chamber is manufactured from Inconel 718 using laser powder bed fusion (LPBF) and uses IPA as fuel and as the coolant for the chamber wall, which is exposed to the hot gases of combustion. The challenge of designing regenerative cooling for this specific propellant combination is that it requires a high oxidizer-to-fuel ratio (O/F) for optimal performance. This reduces the available fuel mass flow for chamber cooling and requires a careful trade-off between I_{sp} performance and chamber cooling requirements. This is also reflected in the chosen chamber dimensions, which aimed to find a compromise between combustion performance and minimizing the wall area exposed to the hot combustion gases. The throat diameter is 41.6 mm with a contraction ratio (CR) of 6 and expansion ratio of 4.07. The larger CR was chosen to ensure compatibility with the pintle injector, which needs a sufficient diameter for combustion and development of the recirculation zones. L* was set to 1 m, again as a trade-off between efficiency and heat transfer area.

The fuel enters the combustion chamber (CC) at the manifold located at the nozzle exit. The flow area of the manifold decreases linearly in the circumferential direction, which ensures consistent flow velocity and the same inlet conditions for all cooling channels. The channels are incorporated into the walls of the CC, with an inner wall thickness of 0.8 mm to provide good heat transfer between the hot gas and the coolant. The outer wall is 1 mm thick and sized to resist the combustion pressure of 26 bar.

At the interface between the chamber and the bulkhead, the channels are routed in a radial direction, and the interface is sealed with one axial PTFE O-ring on the hot gas side and a radial FKM O-ring on the exterior. This seal configuration was chosen for its compact size, which allows the 12 M6 bolts to be more in line with the load and reduces the maximum diameter, as well as good cooling of the hot gas seal. The bulkhead features 18 threaded holes that optionally receive exchangeable film-cooling orifices, allowing the film-cooling percentage to be varied between tests. After entering the bulkhead, the fuel is routed through converging fuel channels toward the central pintle injector and is homogenized in a tangential channel before entering the injector orifice. The bulkhead cooling channels are arranged in a way that allows for six larger diameter ports to the inside of the CC. These are used for the two CC pressure sensors, the fuel pressure sensor, and the torch ignitor, with an additional port measuring the fuel temperature entering the injector.

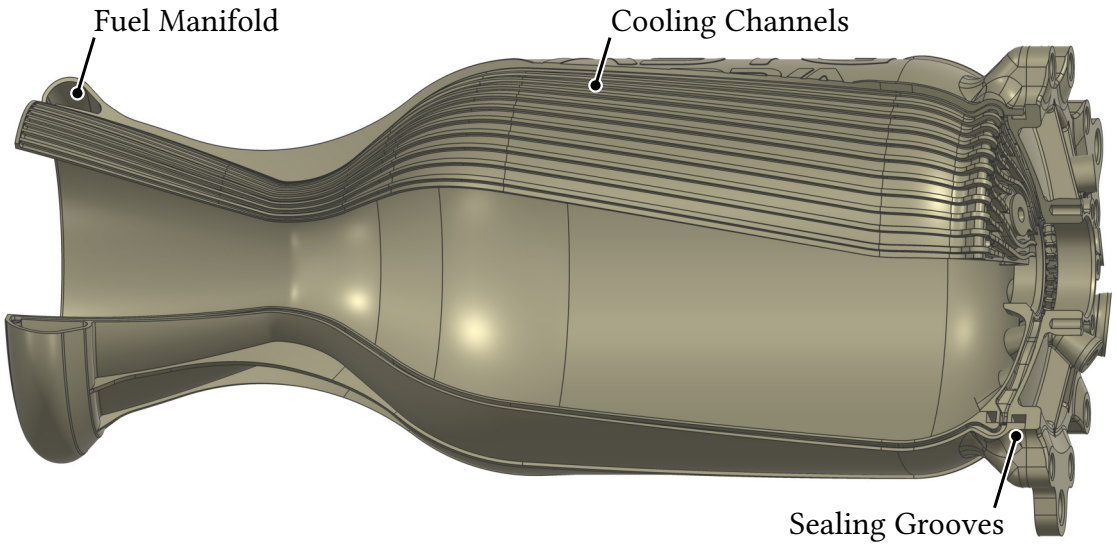


Figure 2.16: Cut of the cooling channels of the combustion chamber.

Regenerative Cooling

The regenerative cooling in the chamber wall consists of 66 cooling channels. The channels are angled 10° to the axis of the chamber, which increases the length of the cooling channel and improves coolant-side heat transfer. In the case of a single (partially) blocked channel, the angle also allows for adjacent channels to partially shield the affected channel from some of the heat load. The combustion gases (and the boundary layer) flow in an axial direction, and an adjacent upstream channel with full flow can therefore provide a relatively cooler boundary layer to the affected channel.

The area of the cooling channel varies along the profile of the chamber to reflect the increased hot gas heat transfer at the throat and to minimize the fuel pressure drop across the cooling channels. The minimum channel size is 1.2 mm x 1.2 mm at the throat and increases smoothly toward the injector and the nozzle exit to 3.6 mm x 1.4 mm and 2.5 mm x 1.4 mm respectively.

The cooling solution was designed using a self-developed 1D heat-transfer model, which was later checked against a computational fluid dynamics (CFD) simulation and test data from the Hot-Fire tests. The starting points are the nominal mass flows and pressure, and NASA CEA is used to determine the stagnation properties of the combustion gas. Then the local gas properties at each axial position in the chamber can be determined.

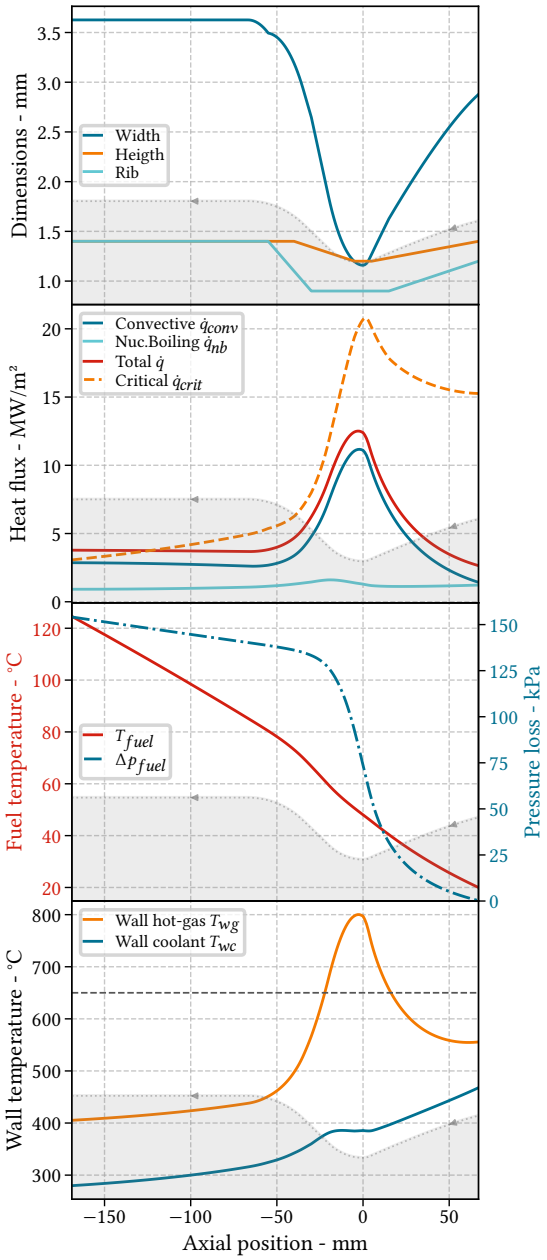


Figure 2.17: Analysis plots of the chamber.

The gas- and coolant-side heat transfer was modeled using the modified Bartz correlation and the Gnielinski correlation, respectively. Together with a factor modeling the fin efficiency of the material between the channels, the heat transfer is solved for each axial position starting at the nozzle exit, determining the wall temperature on both the hot gas and coolant side and the heat flux through the wall. The pressure, temperature, and fluid properties of the fuel are then also updated at each station and used for the next upstream position. Because the coolant-side wall temperature locally exceeds the fuel's boiling point, the Chen correlation is used to estimate the heat transfer enhancement from nucleate boiling, where microscopic vapor bubbles form at the wall, disrupt the boundary layer, and enhance heat transfer. This increase in heat transfer only holds up to a certain critical heat flux (CHF), above which nucleate boiling sharply transitions to film boiling, characterized by the formation of a vapor film on the cooled surface, a reduced heat transfer coefficient, and thus a drastically increased wall temperature. The CHF was thus similarly determined for each axial position using the

modified Tong criterion, originally developed for pressurized water nuclear reactors (PWRs), ensuring sufficient margins in the high heat flux regions. The lowest margins occur at the end of the cooling channel, which coincides with the region where increased heat transfer due to the injector's spray pattern is expected. It was therefore decided to add dedicated film cooling to this region. Due to the many unknowns regarding the injector's effect on heat transfer and the flow field in this region, no analytical estimation of the film-cooling effectiveness was conducted, and instead the film-cooling was optimized during testing using the exchangeable film-cooling orifices.

Pintle Injector

The propellants in the combustion chamber are injected and atomized using a pintle injector, with the fuel being injected axially and the oxidizer radially. A pintle injector was chosen because it offers excellent atomization performance, good integration with the regenerative cooling jacket, inherently stable combustion, and a low part count with few critical dimensions. The injection characteristics can be easily modified by exchanging either the pintle post for the fuel side or the pintle tip for the oxidizer side.

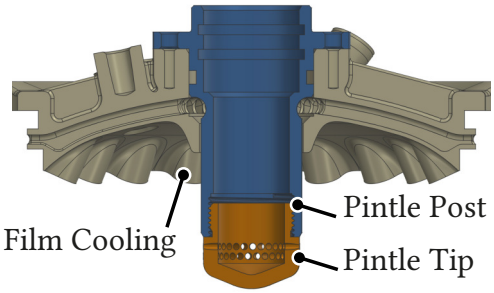


Figure 2.18: Cut of the pintle injector.

An ox-centered configuration was chosen to create a fuel-rich upper recirculation zone, resulting in lower overall temperatures at the bulkhead and seals. The pintle post is constructed out of Ti-6Al-4V, while the pintle tip is made from CuCr[1]Zr, a high-conductivity copper alloy. This combats pintle tip erosion in the high-temperature, oxidizer-rich center recirculation zone. The high O/F ratio of 2.7 makes it difficult to achieve a total momentum ratio (TMR) of 1 between fuel and oxidizer, which is required for optimal atomization. The fuel pressure drop was therefore set higher to 8 bar in comparison to the oxidizer pressure drop of 6 bar. The fuel side consists of an annular axial orifice with an inner diameter of 21.03 mm and a gap width of 0.338 mm. The oxidizer is injected radially at the pintle tip through 38 holes with a diameter of 1.6 mm arranged in two staggered rows. With the resulting TMR of 1.41 this leads to a spray angle of 65.5°.

Cavitating Venturi

The cavitating venturi is installed in the oxidizer feed pipe just below the oxidizer main valve, serving as a passive flow-regulation device. The component has an internal diameter of 6.50 mm and was manufactured in-house out of aluminum. The venturi design promotes controlled cavitation at the throat, ensuring a stable, repeatable mass flow rate once the upstream pressure exceeds the cavitation threshold. As a result, the mass flow rate through the oxidizer feed pipe is independent of moderate upstream pressure variations. A reliable and constant mass flow rate is crucial for operating the engine at the desired O/F.

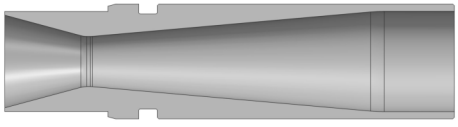


Figure 2.19: Cut view of the venturi.

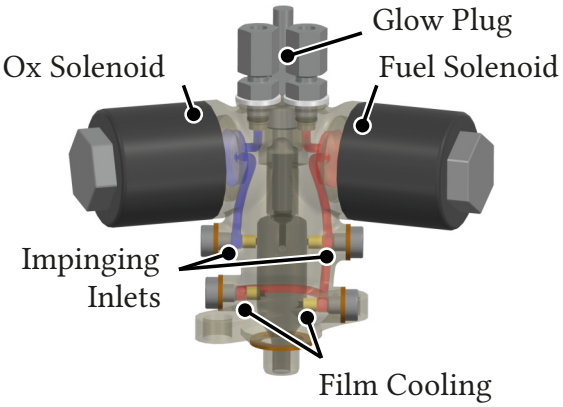


Figure 2.20: Torch ignitor.

Torch Ignitor

A torch ignitor was intended to provide a fast, reusable, and reliable ignition source, reducing the risk of hard starts and ignition delays that can lead to pressure spikes. As an ignition source, a ceramic glow plug was chosen because it can reach temperatures above 1000 °C. Compared to spark-based systems, it eliminates the need for high-voltage electronics and avoids electromagnetic interference (EMI). The glow plug is recessed behind a small orifice, limiting the amount of propellant in direct contact with it and enabling controlled ignition.

Fuel and oxidizer are tapped upstream of the main valves and metered by two integrated solenoid valves. During startup, the propellants are injected as 180° impinging jets with a short fuel lead. The smaller amount of propellant ignited near the glow plug then leads to ignition of the remaining mixture within the ignitor combustion chamber.

To reduce the thermal loading of the throat, fuel is additionally injected tangentially just above the throat, creating a protective film-cooling layer.

The ignitor is mounted to the combustion chamber bulkhead via a flange connection and sealed with a copper gasket, providing a robust mechanical interface and a reliable high-temperature seal.

Pyrotechnic Ignitor

A pyrotechnic ignitor was used for the initial engine tests, providing reliable ignition, as demonstrated in the test engine Gallus. It also provided a fallback solution as the testing of the torch ignitor was insufficient at the time of the report deadline. The pyrotechnic mixture used is similar to the ignitors from the previous hybrid engines and consists of 60 % rocket candy (RC), a mixture of potassium nitrate and sorbitol, 25 % magnesium powder, and 15 % calcium silicide. Additionally, 0.5 % red iron oxide was added as a catalyst to increase the burn rate.

30 g of the mixture is placed around a wooden rod and capped off with circular wooden plates spaced 6 cm apart. The ignitor is inserted into the CC through the nozzle and held in place by a 3D printed base clipped onto the nozzle. The base is additionally held inside by tape going around the manifold to delay the ejection of the ignitor. Four e-matches, secured in place with two layers of painter's tape, are used to ignite the mixture. Once the engine starts, the remaining ignitor structure is ejected by the thrust.

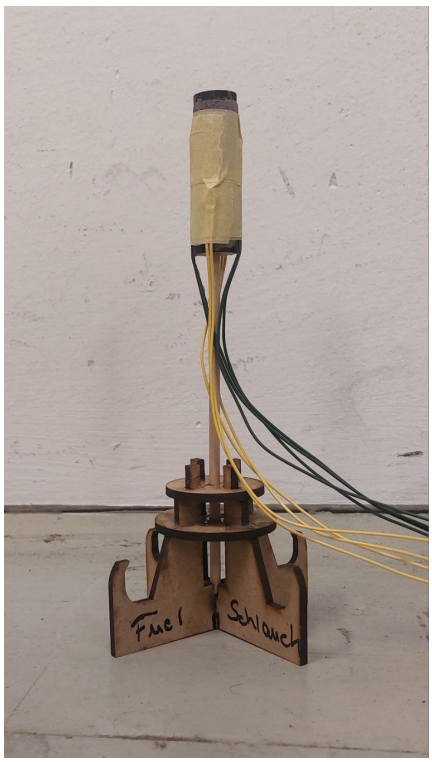


Figure 2.21: Image of the pyrotechnic ignitor.

2.3 Aerostructure Subsystem

The structural airframe is designed to maximize mass efficiency and to sustain multi-axial aerodynamic and mechanical loads. The rocket's structure can be subdivided into seven main sections with different functions:

- Nosecone: houses the CATS Vega, the CubeSat and on the top, the pitot-static probe (PSP) is mounted.
- Recovery section: includes the drogue parachute and main parachute as well as their deployment systems.
- Avionics section: contains the avionics stack, the telemetry system, the COPV, and the upper fluid assembly.
- Fuel tank: part of the propulsion subsystem.
- Valvebay structure: encloses the middle fluid assembly.
- Oxidizer tank: part of the propulsion subsystem.
- Tailcone: includes the lower fluid assembly, the combustion chamber, the hardpoint of the holddown system, and connects the fins.

The different sections of the rocket are connected using either radax joints or coupling interfaces, with the latter being used to attach the nosecone to the recovery section.

The main characteristics of this subsystem are the streamlined integration of the PSP on top of the nosecone to measure barometric speed and altitude, as well as the integrated hardpoint in the tailcone for the holddown system. Additionally, the design of the onboard cameras was optimized to reduce the number of screws in the shells. Furthermore, to accommodate the bi-liquid propulsion system of HARPIA, the airframe has a diameter of 182.4 mm.

All components were designed and validated taking analytical calculations, such as adhesive and screw calculations, along with FEA into account. With CFD simulations, the aerodynamic drag characteristics as well as the pressure distribution and flow behavior of the airframe could be assessed. The resulting load cases have been analytically calculated for nine representative scenarios. All calculations and simulations are documented in the appendix, see Appendix K.3.

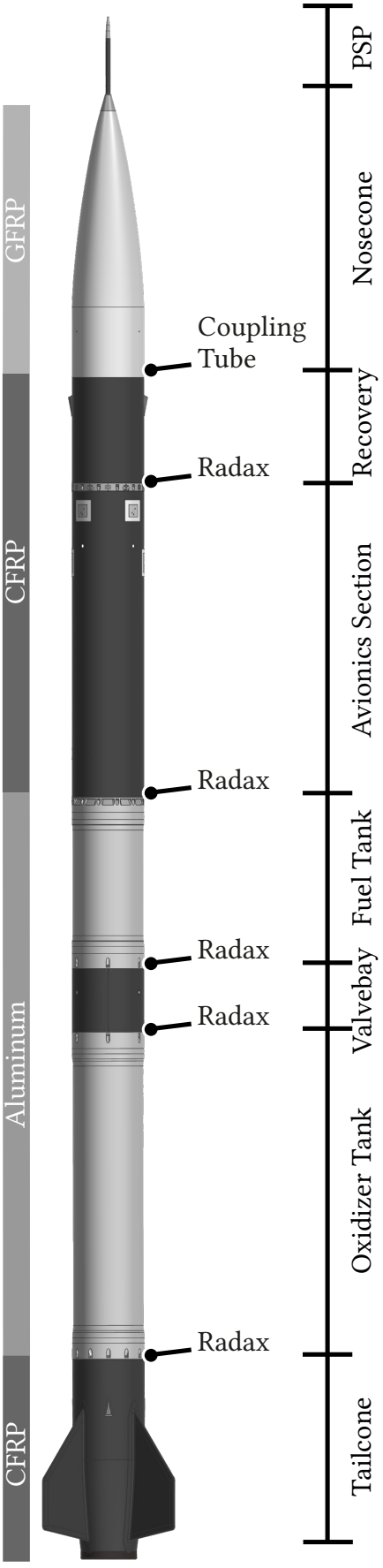


Figure 2.22: Structural overview of the rocket's sections.

2.3.1 Structure

Shell

The majority of the shell is made up of wound carbon-fiber reinforced polymer (CFRP) tubes to ensure low weight and sufficient strength to withstand forces during all flight phases. The rocket's nosecone is made from glass-fiber reinforced polymer (GFRP), which ensures radio frequency (RF) transparency for data transmissions from CATS Vega. In Table 2.2, the lay-up of the recovery shell is listed as an example. All sections feature venting holes to prevent internal pressure buildup. To confirm that the structural integrity under the expected load is maintained, classical laminate theory was used with Altair ESAComp, a tool for composite design and analysis. The structural integrity was then tested under load via a tube bending test, see Appendix C.55.

Table 2.2: Properties of the wound recovery shell.

CFRP	Lay-up [°]	Layer Thickness [mm]
T800	+/- 82	0.4
T800	+/- 45	0.4
T800	+/- 20	0.4
T800	+/- 10	0.4

Radax

All rocket sections are connected using radax-type joints, except for the coupling tube between the nosecone and recovery section. These joints function by pairing two conical surfaces to achieve a self-centering fit when properly assembled.

This design is chosen primarily due to high stiffness under load while only taking up a small amount of internal volume to allow the integration of all components. In addition to their small size, the radax provides precise mounting points, e.g. for the avionics stack.

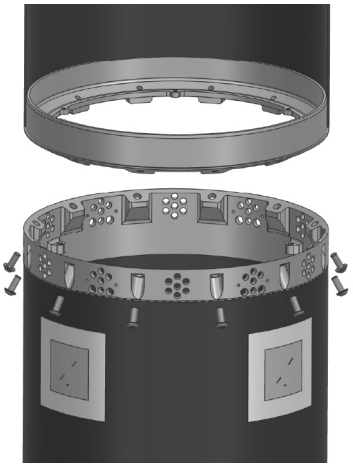


Figure 2.23: Radax connector.

In all joints, the angle of the screw compared to the axis of the rocket is 30°. The two upper joints, connecting recovery to the avionics section and the avionics section to the fuel tank, are designed as 12-point radax joints using M4 screws. The lower ones, Valvebay and tailcone, are 6-point radax joints using M5 screws to compensate for the reduced number of screws. The radax joint on the tailcone is a special case, since it shares the female part of the joint with the thrust structure.

The spaces between the screw pockets are cut out on all joints to reduce unnecessary weight and to allow placement of PCBs. For example, the interface PCBs sit between sections, and the arming PCBs are on the upper radax of the avionics section.

Coupling Tube

To allow the drogue parachute to deploy at apogee, the connection between the nosecone and the recovery section can be released. This connection consists of a coupling tube made of wound CFRP with a wall thickness of 1.5 mm and a length of 180 mm. At one end, the coupling tube is adhered to the recovery shell, while the opposite end fits tightly into the inner diameter of the nosecone shell. In addition, the nosecone is secured to the rocket body by three M2.5 shearpins, which are inserted radially through the nosecone shell and the coupling tube.

Retractable Rail Button

The 12 m-long launch rail guides the rocket during initial acceleration, ensuring a stable flight trajectory. The rocket is connected to the launch rail using two retractable rail buttons. Each rail button houses a spring-loaded mechanism that retracts it into the hull after clearing the launch rail, reducing protrusions from the hull. Additionally, the spring retainer has a design feature that keeps the retainer from rotating, preventing accidental loosening of the screw. The rail buttons are positioned at the rear section and near the rocket's center of gravity.

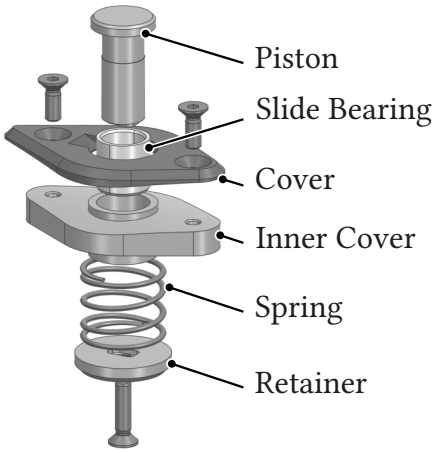


Figure 2.24: Retractable rail button.

Tail Section Heat Management

The tailcone features four NACA inlets at its upper part. The NACA ducts' shallow ramp angle and the curvature profile of the walls create counter-rotating vortices, which deflect the boundary layer away from the inlet and draw in the faster-moving air. These inlets can be dimensioned relatively small for a given airflow compared to other inlets, resulting in only minimal additional drag in the transonic regime. The ducts provide airflow to the tailcone to cool the CC and protect the tailcone's adhesive joints from the heat of the CC.

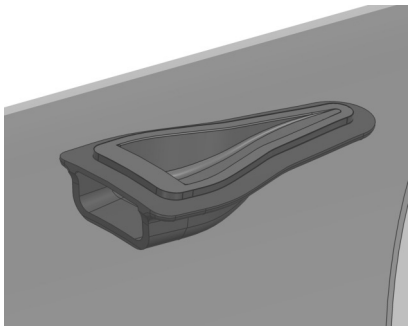


Figure 2.25: NACA duct.

The tailcone's nozzle area, which also features the hardpoint of the holddown system, is protected by a heat shield. The shield is 3D printed from thermoplastic polyurethane (TPU) and features layers of cork and aluminum tape on the inside. These layers prevent the hardpoints' adhesive joints from overheating during burn time. Additionally, the heat shield's 3D printed structure covers the composite end of the tailcone, functioning as touchdown protection during landing. It is designed to wrap around the end of the tailcone to prevent it from sliding away at touchdown.

Nosecone Structure

The nosecone structure provides the mechanical interfaces needed to mount the CubeSat, CATS Vega, and PSP system. It consists of two major components: the groundplate and the stack assembly.
The groundplate is a monolithic piece of machined aluminum fastened with screws to an aluminum ring, which is glued into the nosecone. A polymer bushing pressed into the plate provides mounting for the eyebolt connecting the nosecone to the recovery groundplate via a line. For the CubeSat, an acrylic window is built into the center, allowing the camera to capture nosecone deployment. Four countersunk screws secure the CubeSat to the groundplate while keeping the underside smooth. Finally, a spacer extends along the inner side of the shell from the bottom of the groundplate to the top of the recovery pressure plate.
The stack assembly is a lightweight structure made of CFRP rods and glued 3D printed parts, with heat-set inserts providing the required threads. It is secured to the groundplate using threaded inserts glued into the CFRP rods. Both the PSP assembly and CATS Vega system, including its batteries, are mounted to this structure. The assembly is also supported by the PSP cradle, which is secured into the nosecone shell via the nosecone screw.

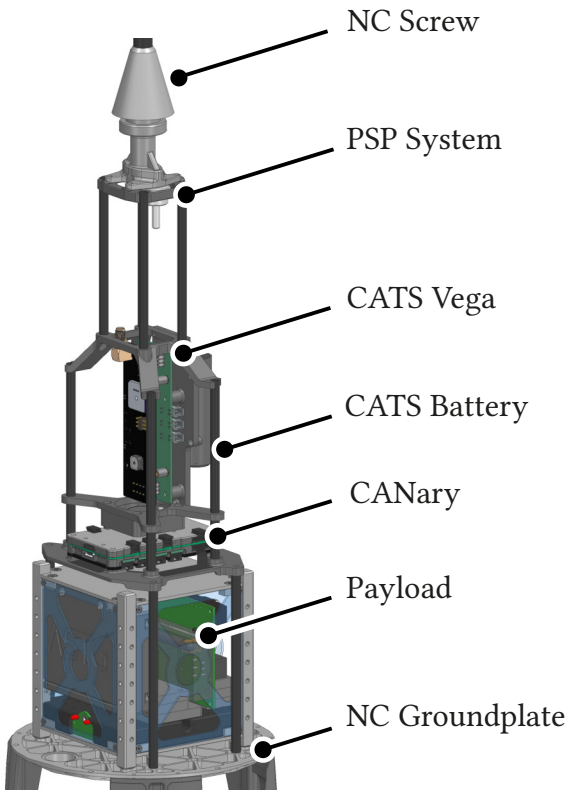


Figure 2.26: Nosecone structure with the CubeSat, the CATS Vega and PSP-system.

Cameras

The recovery section and the tailcone each house two cameras, and three radial cameras are situated in the Valvebay structure. A new clip mechanism was developed to simplify and speed up the mounting procedure; by gluing the camera mount to the inner wall of the rocket, it reduces the number of screws required to attach the camera and the black box. The latter two are removable components; they sit on a hinge and can be extracted by removing the screw at one end of the carrier.

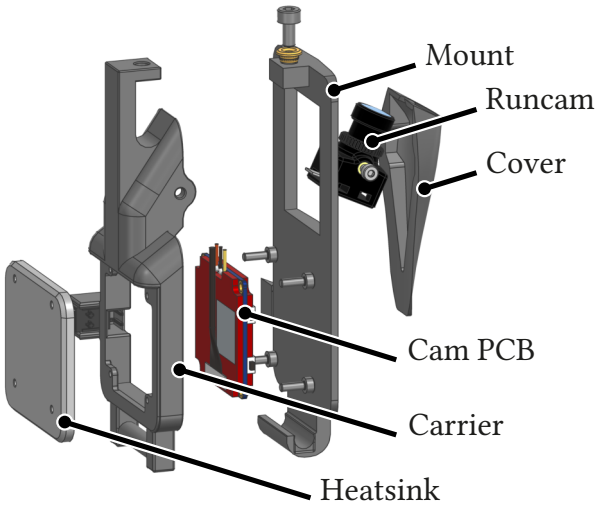


Figure 2.27: Clip mechanism of the onboard cameras.

2.3.2 Aerodynamics

Nosecone and Tailcone

Due to HARPIA's flight profile, the minimization of the drag during subsonic and transonic flight regimes is important. Hence, for designing both the forward and aft sections of the vehicle, a Haack-series profile with a coefficient of $C = 0$ was used, commonly referred to as the von Kármán shape. This geometry provides favorable aerodynamic characteristics and high efficiency within the relevant speed regimes. CFD simulations indicated that using the same profile for the nosecone and the tailcone reduces aerodynamic drag as consistent flow development along the rocket body arises. Furthermore, using the same geometry for both sections streamlines the manufacturing process, as the same mandrel can be used.

The nosecone is made out of GFRP to provide RF transparency to the CATS Vega system, which is located within the nosecone. The tailcone is manufactured from CFRP.

Pitot Static Probe

The PSP system serves to measure the static and dynamic pressure acting on the rocket during flight. The system consists of two components: the cradle, integrated into the nosecone stack, and the removable measuring probe.

The probe has a 3D printed aluminum tip with a double conical geometry. This geometry ensures accurate static pressure measurement, with 8 radial orifices placed at a point that experiences minimal pressure changes compared to static pressure across all flight regimes. Both static and dynamic pressure orifices are connected to pipes routed through the center of the structural CFRP tube. At the rear of the probe, an aluminum piece provides the interface with the cradle and forms a seal using O-rings. Adding this piece significantly reduced the time needed to install the probe.

The cradle provides the mechanical interface for both the PSP and the pressure sensors. The probe is held in place by a tight fit between the structural tube and a set screw. Internal channels distribute pressure to highly precise pressure sensors.

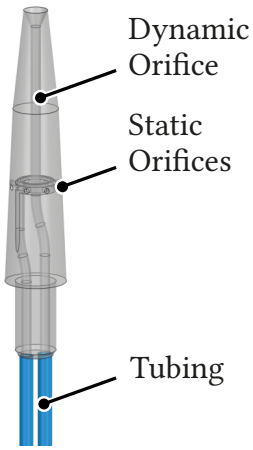


Figure 2.28: PSP - detailed view of tip.

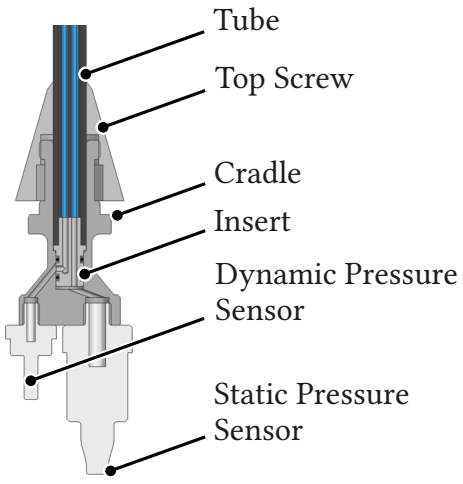


Figure 2.29: PSP - detailed view of cradle.

Fins

The HARPIA fins feature a trapezoidal planform, with the lower base side adapted to the curvature of the tailcone. Their shape is optimized to position the aerodynamic surface as far aft as possible for maximum static stability, while maintaining sufficient ground clearance at the lower tip chord edge. Through this geometry, the fins guarantee rocket stability at ground-level crosswinds of up to 10 m/s. In addition, aeroelastic considerations were directly integrated into the planform geometry to prevent flutter. By intentionally selecting a low aspect ratio and an optimized taper ratio, the bending and torsional modes are decoupled to naturally increase flutter resistance.

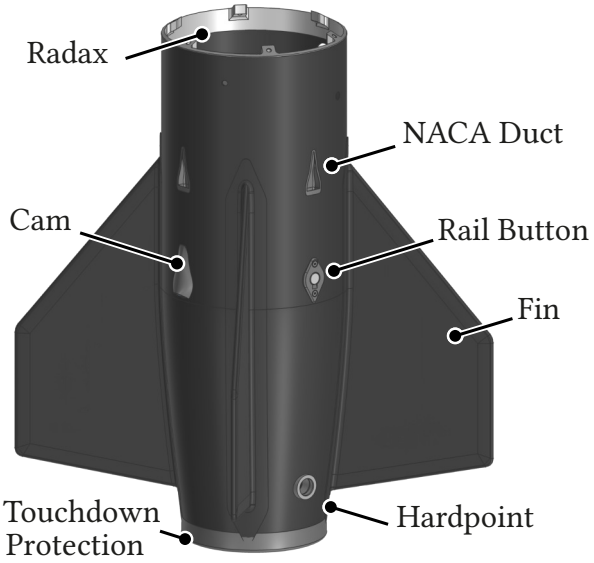


Figure 2.30: View of the tailcone with the fins, the radax and integrated hardpoint.

Six prepreg layups are laminated onto a prefabricated negative CFRP mold using a continuous overlapping technique to manufacture the fins. To facilitate the lamination process and ensure uniform internal compaction during curing, a custom silicone core matching the inner geometry of the fin is used. As it expands slightly under heat, it applies internal pressure against the mold surfaces, effectively eliminating voids. This process allows the entire fin structure to cure as a single piece, avoiding split halves or edge-bonding lines. The resulting hollow core is filled with a liquid-poured microsphere-resin solution in a 60/40 Vol.% ratio to provide high structural stability at a low density of $0.58\,\mathrm{g/cm^3}$.

Finally, an integrated flange, formed seamlessly with the outer prepreg layers, is bonded directly to the airframe tailcone using structural epoxy adhesive, ensuring efficient load transfer into the primary structure.

2.4 Recovery Subsystem

2.4.1 Overview Recovery Section

Figure 2.31 shows the recovery section, which accommodates all structural, electrical, and mechanical components of the dual-deployment recovery system.

At the base of the assembly, the groundplate anchors the recovery system to the rocket body via a radax interface. It serves as a mounting platform for the first deployment (FD) and second deployment (SD) mechanisms, the recovery interface PCB, the SD detection system, and a SRAD rotatable eyebolt for transferring the main parachute load. In addition, the design is weight-optimized through iterative design studies and includes cutouts for clean cable routing.

To initiate nosecone separation at apogee, pneumatic tubes direct pressurized Ar gas released by the FD system into the pressure chamber, which extends into the nosecone. The resulting chamber pressure shears the nylon shearpins that secure the nosecone to the airframe. Within the chamber, a 3D printed structure retains the pressure plate in position and protects the wiring routed into the nosecone. In parallel to the pneumatic lines, flexible electrical wiring runs along the recovery tube, providing uninterrupted power and data transmission to the onboard cameras, sensors, and nosecone electronics.

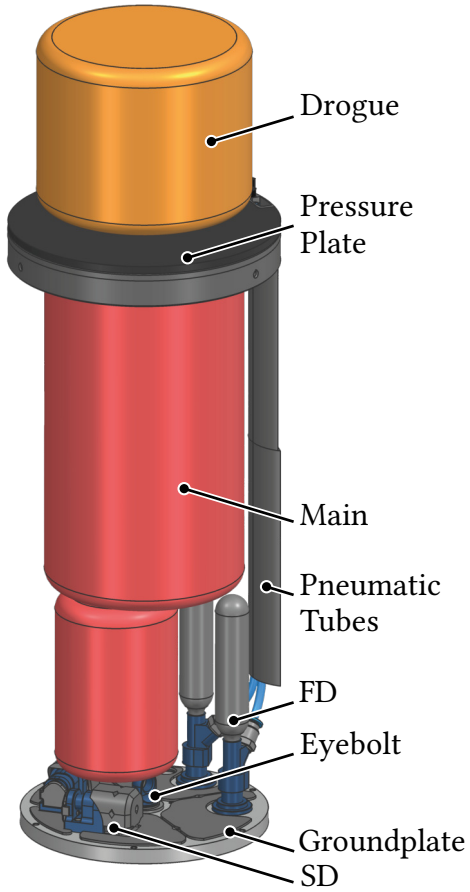


Figure 2.31: Overview of the assembled recovery section.

Between the pressure plate and groundplate, the main parachute is housed in a dedicated deployment bag, with the shockcords stowed neatly around it. The release of the main parachute is controlled by the SD system and occurs at an altitude of 450 m above ground level (AGL).

Pre-Assembly and Integration

To simplify launch-day preparations, the entire recovery section, as shown in Figure 2.31, is assembled the day before launch. On launch day, only the igniters of the FD and SD systems need to be installed from below the groundplate and connected to the recovery interface PCB. This minimizes integration time, while significantly reducing the risk of errors during time-critical launch operations.

2.4.2 Redundancy

The FD and SD mechanisms feature both mechanical and electrical redundancy. Each ejection mechanism is physically installed twice, ensuring successful deployment even if only one unit operates. For electrical redundancy, each unit contains two independent igniters per chargecup, with the igniters connected cross-redundantly to the SRAD flight computer and the COTS CATS Vega, as described in Section 2.5.4. Consequently, activation of a single igniter is sufficient for deployment.

2.4.3 Chargecups

Each deployment mechanism contains two redundant igniters within a titanium chargecup, with one triggered by each flight computer. To provide electrical insulation and seal against hot gases, the igniters are molded in a two-component silicone. This enables quick integration on launch day.

The encapsulation remains intact during igniter activation, protecting the electronics from smoke and residue. Additionally, the electrical connection between the igniters and the flight computer can be verified directly from the mission control during launch operations.

2.4.4 First Deployment

Upon apogee detection, both independent flight computers trigger the igniters located inside the FD chargecup, shown in red in Figure 2.32, which generate pressure that drives the pin upward. The pin pierces the Ar cartridge, allowing the pressurized gas to escape and flow through the pneumatic tubes into the pressure chamber.

There, it pressurizes the pressure chamber, which pushes against the plate of the nosecone. This shears off the shearpins, which secured the nosecone to the rocket body, initiating nosecone separation and deployment of the drogue parachute.

A 3D printed pretensioner prevents the Ar cartridge from loosening under vibration, while a spring ensures that the pin neither pierces prematurely nor remains stuck inside the cartridge. A PTFE plate below the pin protects the casing's thread and the pin from ignition residues (Figure 2.33).

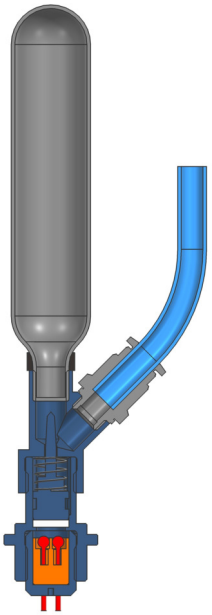


Figure 2.32: Sectional view of the assembled FD.

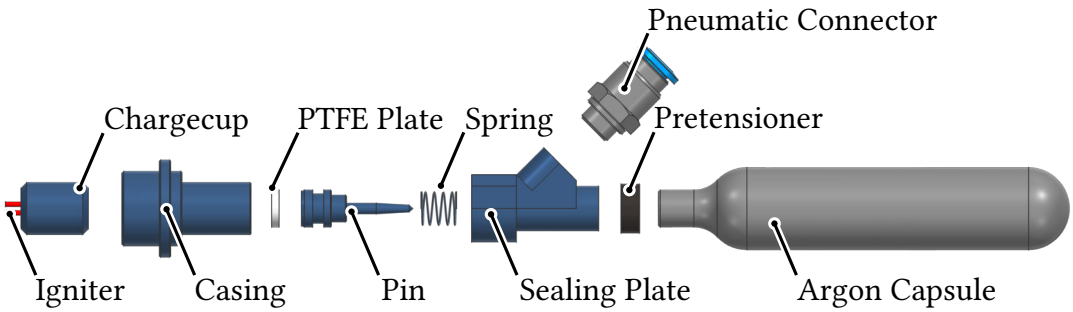


Figure 2.33: Explosion view of the first deployment.

FD Detection

Deployment of the FD is detected through its electrical connection to the nosecone. When the flight computer loses continuity to the nosecone, deployment is detected.

2.4.5 Second Deployment

As the second stage of the dual deployment sequence, the second deployment (SD) mechanism, shown in Figure 2.34, retains the main parachute inside its deployment bag during drogue parachute descent. Main parachute release is withheld until the target altitude of 450 m AGL is reached, at which point the SD releases the main parachute bag, allowing the drogue parachute to extract the main parachute.

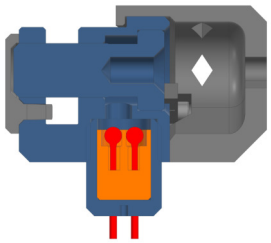


Figure 2.34: Sectional view of the assembled SD.

Structurally, the SD is centered around a Grade 5 titanium housing mounted on the groundplate of the recovery section, see Figure 2.31. A titanium bolt seated inside the housing retains the main parachute bag through a connection line. To prevent premature release, the bolt is fixed by a 3D printed securing element that is screwed into the housing.

Activation of the igniter builds pressure inside the housing, forcing the bolt outward and shearing off the securing. This releases the connection line, resulting in the deployment of the main parachute bag and allowing the main parachute to be extracted. The bolt is subsequently caught and retained by a cover.

An additional lid element clips into the front of the housing, covering the top face of the bolt, which would otherwise remain exposed. This adds a second, physical layer of protection against unintentional release of the connection line during handling or integration.

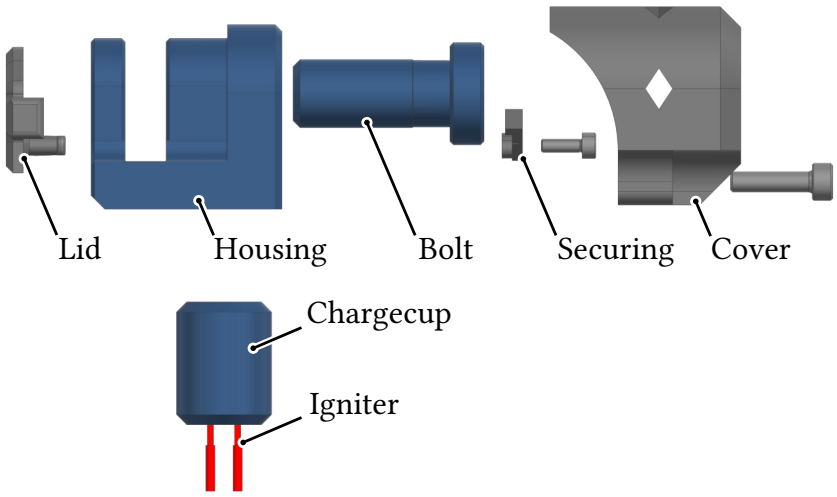


Figure 2.35: Explosion view of the second deployment.

SD Detection

Deployment confirmation is achieved through a cable connecting the main parachute bag to the groundplate, which the flight computer monitors for continuity. As the SD releases the main parachute bag, the connector separates, interrupting the circuit and giving an unambiguous signal that deployment has occurred.

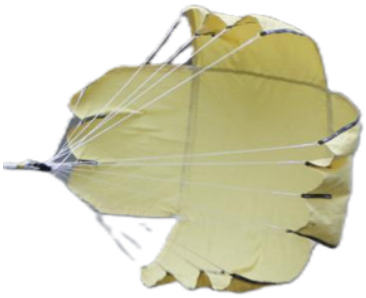
2.4.6 Parachutes

Drogue

The drogue parachute reduces the rocket's descent velocity after nosecone separation and stabilizes it during descent. Manufactured from yellow para-aramid fabric, it is designed to withstand the high shock loads generated during deployment. A cross shape was selected for stability in varying wind conditions. It consists of five square panels arranged around a common center, each with a side length of 50 cm, as shown in Figure 2.36a.



(a) Drogue parachute uninflated.



(b) Inflated drogue parachute.

Figure 2.36: Cross-shape of the drogue parachute in an uninflated and inflated state.

The aerodynamic performance of the drogue parachute was evaluated through flight testing at EuRoC in the previous two years. Based on the test data, the drag-area product was determined to be $c_d A = (0.65 \pm 0.06)\,\mathrm{m}^2$. This value is used to estimate the expected terminal velocity during the drogue parachute descent phase, yielding $v_{\text{drogue}} = (29.7 \pm 1.3)\,\mathrm{m/s}$.

Main

Following the second deployment event, the main parachute reduces the rocket's descent velocity to a safe landing speed. It is deployed at an altitude of 450 m AGL, where the drogue parachute extracts the parachute from its deployment bag.

Orange, purple, and white panels are used to ensure visual distinguishability against every background, see Figure 2.37. This improves tracking during descent and locating the parachute after landing.

Constructed from ripstop nylon fabric, the main parachute has an elliptical shape proven effective in previous systems. The canopy has a diameter of 3.2 m, with a central spill hole with a diameter corresponding to 20 % of the canopy diameter. Ten gores form the canopy, which is connected to twenty shroud lines (see Figure 2.37). Each shroud line has a length of 1.5 times the canopy diameter.



Figure 2.37: Inflated main parachute.

Aerodynamic performance of the main parachute was evaluated through testing with the lower-mass SPATZ test rocket. The resulting drag-area product was determined from the measured test data and is given by $c_d A = 14.6\,\mathrm{m}^2$, see Appendix C.15. Based on the measured aerodynamic performance, the expected terminal velocity of HARPIA under the main parachute was determined as $v_{\mathrm{main}} = 6.2\,\mathrm{m/s}$.

Main Bag

The main parachute bag design is adapted from rescue parachute systems used in skydiving. Constructed from para-aramid fabric, the main parachute bag provides high mechanical durability. To ensure structural integrity and prevent premature main deployment, the bag is securely held closed using a four-leaf configuration, where each leaf has a central lug (see Figure 2.38a). The locking mechanism relies on an elastic loop that is threaded through the lugs and then retained by the main shockcord (see Figure 2.38b). This guarantees that the bag remains closed under vibrations and other loads. The bag opens when the main shockcord is tensioned during the second deployment.

To protect against friction and tearing at the sharp carbon-fiber edges of the pressure chamber ring, at least three layers of para-aramid fabric are integrated around all critical contact areas. Furthermore, a small fabric pocket shields the main shockcord during drogue parachute descent.



(a) Main bag opened. The shroud lines of the folded main parachute are visible.

(b) Main bag closed. The main shockcord seals the bag in place.

Figure 2.38: Main parachute bag with a folded main parachute inside, shown open and closed.

2.4.7 Parachute Lines and Connections

Eyebolt

During main parachute descent, the parachute may begin to rotate relative to the rocket body. To prevent excessive twisting and potential damage to the main shockcord, a rotatable connection between the shockcord and groundplate is required.

For this purpose, a SRAD eyebolt is utilized. It features a closed eye and is supported by a plastic plain bearing, as shown in Figure 2.39. A circlip combined with a washer is used for axial fixation.

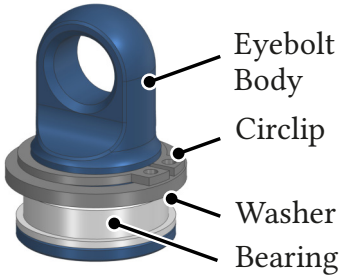


Figure 2.39: Overview of the eyebolt and its components.

The eyebolt and its associated components weigh approximately 80% less compared to the COTS solution previously used. It is machined out of Grade 5 titanium. An FEA for the maximum expected force verifies sufficient material strength, yielding a safety factor (SF) greater than 2.7 against breaking Appendix K.2. In addition to connecting the main shockcord and the groundplate, the same eyebolt is used a second time as the connection between the nosecone and the nosecone connection line.

Pressure Plate Connection Bolt

The pressure plate connection bolt does not need to rotate and is glued into the pressure plate. It features a closed eye on both sides and connects the pressure plate to the shockcords. As with the eyebolt, it is manufactured from Grade 5 titanium. An FEA verifies sufficient material strength for the maximum expected force during drogue deployment, yielding a SF greater than 2.6 against breaking Appendix K.2.

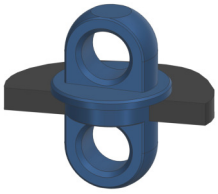


Figure 2.40: Pressure plate connection bolt.

Swivel Links

In addition to the eyebolt, two rotatable steel swivel links are used to decouple the rocket body from any potential rotation of the parachutes. These swivels, as in Figure 2.41, serve as direct connections between the shockcords and the shroud lines of their respective parachutes.



Figure 2.41: Rotatable swivel.

Shockcords

The shockcords connect the main rocket body to the parachutes as well as the nosecone. Their lengths were determined using a CFD analysis, see Appendix H.1.

In tests with different kinds of shockcords (Appendix C.19), a twisted polyamide shockcord, as used in previous years, showed the best performance, as the line is best able to absorb shock loads through stretching.

To protect the lines from abrasion against the rocket body, para-aramid fabric sleeves are added at critical points, and metal thimbles are installed to reinforce the spliced loop ends, see Figure 2.42. All lines are color-coded to ensure correct assembly.

The transition of the rocket from deployment into the steady-state descent phase after nosecone separation represents a critical dynamic regime. To further determine these complex line and parachute dynamics in future iterations, the internal numerical simulation tool KESTREL (see Appendix H.2) is currently under development.



Figure 2.42: Shockcord with thimble and rope protection.

Softshackles

The SRAD Dyneema softshackles, Figure 2.43, are used to connect the shockcords and bolts, replacing conventional metal quicklinks to reduce overall system mass. In addition to their significant weight advantage, they offer a SF greater than 5 (as has been tested in Appendix C.10). The latest iteration features a fixed-size eye, which further reduces the already low probability of accidental opening, improving reliability during operation.



Figure 2.43: Closed softshackle.

Shockabsorber

To dampen the shock loads during drogue parachute deployment, a student researched and developed (SRAD) shockabsorber is added to the line arrangement below the pressure plate. It is made out of a folded Dyneema strap, sewn together with multiple polyester threads. It consists of two stages of differing strength, with the longer main stage tearing at 900 N. As the shockabsorber opens, the seams tear and thus decrease the peak shock force during drogue parachute deployment, see Appendix C.19. In case of failure, a Dyneema bypass-line is added.

The shockabsorber is not critical, as all elements of the recovery system are able to handle the expected shock force even if the flight is not nominal; however, it further increases the safety margin.

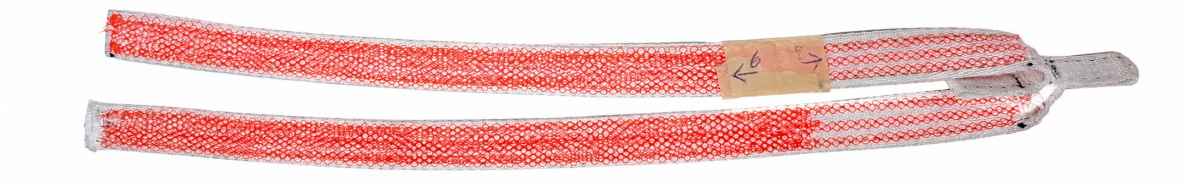


Figure 2.44: The shockabsorber as manufactured for flight.

Line Management

A detailed schematic of the line management, including all connection points, the placement of the parachutes and their lines, and the lengths of the lines, can be found in Appendix H.1.

2.4.8 Recovery System Tests

The overall recovery system test strategy, including a detailed description of the approach, an overview of all performed ground and flight tests, as well as all corresponding test reports, is provided in Appendix C.

2.5 Avionics Subsystem

The avionics subsystem of HARPIA spans a wide range of critical functionalities. It ensures successful and safe operations by enabling continuous control, monitoring, and communication for the rocket and ground support equipment (GSE) systems.

2.5.1 Power System

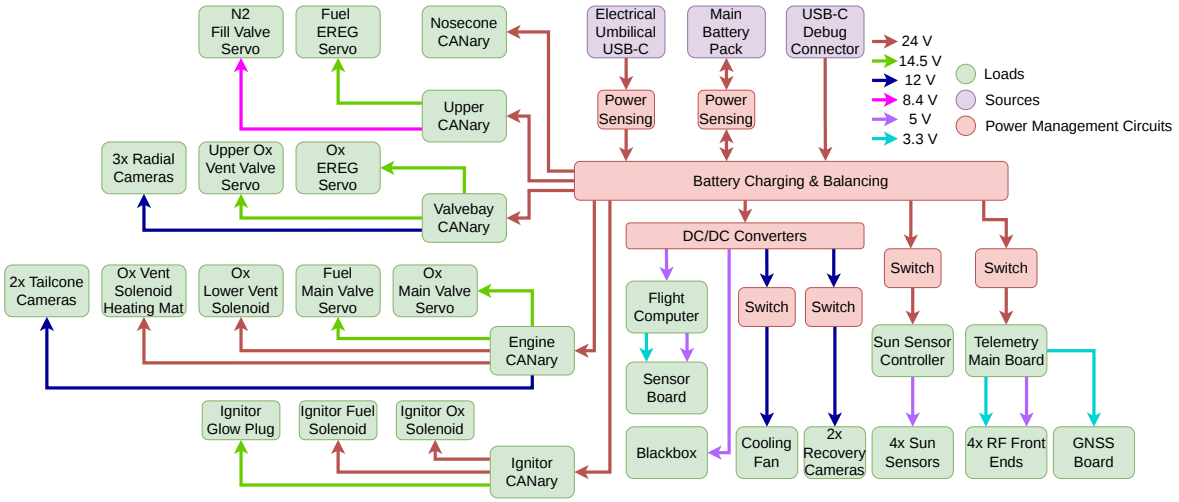


Figure 2.45: Overview of the main power bus of the rocket.

The power system of HARPIA, illustrated in Figure 2.45, shows the main power distribution of the system, excluding the recovery system. It includes the internal electrical umbilical PCB, the main battery pack, the USB-C debug connector, and various subsystems connected to the main power bus.

Main Battery Pack

The rocket's main power system is a custom-built 6S (six cells in series) lithium-ion (Li-Ion) cell battery pack. The battery pack shown in Figure 2.46 was redesigned to accommodate the larger current draws anticipated in HARPIA's system.
The pack is designed to support the rocket's system for up to 3 hours without being charged. To support the growing power demands, the battery pack uses six 21700 5000 mAh cells.
Integrated in the battery pack is an interface PCB that routes the balancing cables to the main connector.

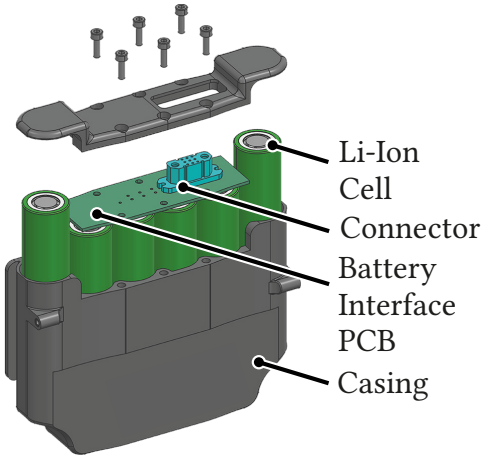


Figure 2.46: The main battery pack.

Main Battery Pack Cell Balancing and Charging

As the main battery pack contains six 21700 cells in series, it requires additional attention regarding protection and management.

A standalone 3- to 8-cell lithium-ion (Li-Ion) battery pack monitor, the ISL94202, provides this protection and is located on the backplane PCB. This protects the battery against overcharging, undervoltage, and short circuits. Furthermore, the integrated circuit (IC) can balance each cell individually through an external circuit. The chip communicates with the flight computer via the Inter-Integrated Circuit (I2C) interface, which allows reading data such as battery current, cell voltages, and temperatures.

Supplying power to the avionics stack can happen through three separate paths: the main battery pack, the electrical umbilical connection, and the external debug power USB-C connector on the backplane. When any charger is connected, the ISL94202 automatically wakes up and checks for acceptable charging parameters. Provided this check is successful and the connected power supply can deliver the necessary charging current, the battery pack begins charging.

Charging current is dynamically reduced, depending on whether ground power over the umbilical or debug power is connected. Through the umbilical connection, a maximum charging power of 120 W (5 A at 24 V) can be achieved.

Subsequently, power is routed through a combined buck-boost battery charger, the LTC4020, which ensures a floating output voltage of 25.2 V. This corresponds to 4.2 V per fully charged cell. When no battery pack is present, the entire avionics stack can still be powered solely through the LTC4020, bounded by the power supply capabilities outlined above. The current on the primary side of the buck-boost circuit can reach up to 5 A. The charging circuits are located on the backplane PCB described in Section 2.5.2

Additional Battery Packs

In addition to the main battery pack, there are three battery packs with a 2S Li-Ion 18650 3500 mAh cell configuration.
Two are located in the avionics stack and are responsible for the independent CATS Vega flight computer and the SRAD recovery igniter system, respectively.

The third one is located in the nosecone and supplies the CATS Vega tracking flight computer.

The battery packs in this configuration have been used in the past and have proven that they can supply the system for up to 8 hours without charging.

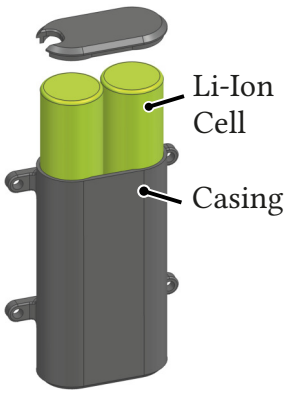


Figure 2.47: The small battery pack.

Cable Management

To ensure safe operation under all conditions, internal rocket cables utilize the UL1332 specification with fluorinated ethylene propylene (FEP) insulation, rated for the complete temperature range expected during operation. Additionally, all connectors use either integral locking mechanisms or are mechanically secured with screws during assembly to prevent inadvertent disconnection.

To simplify assembly, all cables requiring connection during assembly use blind-mating connectors within the radax connections, and all cables are secured with cable ties.

2.5.2 Avionics Stack

The avionics stack serves as the main structural housing for the internal flight electronics and power supply. It is designed to withstand the physical forces experienced during flight and landing while keeping all internal parts safely supported and cooled.

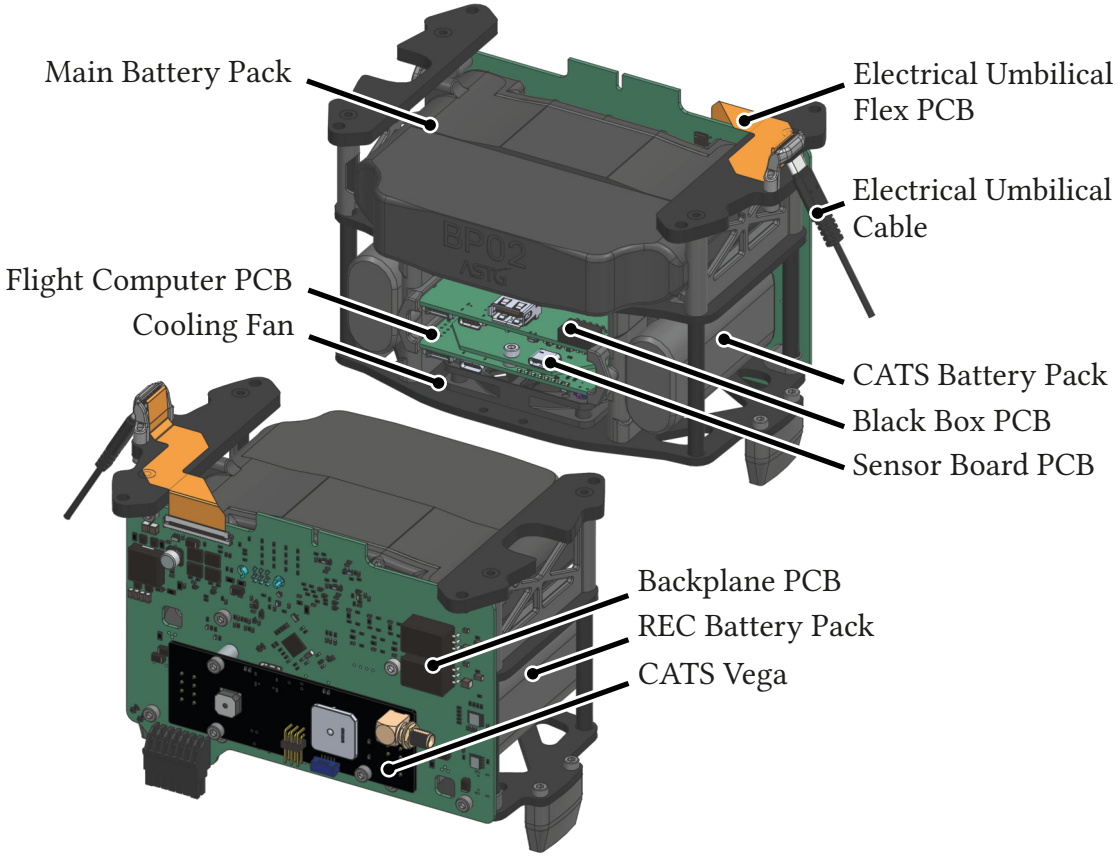


Figure 2.48: Overview of the avionics stack.

The main frame consists of two CFRP plates held together by four long CFRP rods, glued into place with structural epoxy adhesive. Four shorter CFRP rods provide extra support between the lower and middle plate. The space between these two bottom plates is filled with a custom 3D printed nylon core. This printed piece has several functions: it provides rails for the flight computer and black box to slide into, includes mounting points for the recovery and CATS Vega battery packs and the backplane PCB, and has built-in slots to lock the PCBs in position. To generate airflow in the avionics stack, a cooling fan is built in.

The black box PCB and the main flight computer PCB are held in place by their main PCIe connectors, but a small selective laser sintering (SLS) print is also screwed into the SLS core to act as an extra safety lock. The main battery pack sits on top of the middle CFRP plate, guided and held in place by SLS prints and two mounting screws. At the top, two CFRP handles are attached to radax with two screws each. One of these handles holds the umbilical adapter, which supports the USB port of the electrical umbilical flexible printed circuit (FPC). The electrical umbilical FPC connects the electrical umbilical USB-C cable to the backplane.

The backplane itself mounts to the back of the stack using eight screws, and the CATS Vega board attaches directly to it via pin-headers. To make integration easier, the avionics stack uses two alignment pieces on the bottom CFRP plate that slide into a centering ring inside the avionics tube, guiding it straight into place.

Main Flight Computer

HARPIA's main flight computer is responsible for critical in-flight operations such as data processing and the actuation of the recovery system. Powered by an STM32H745ZIT3 microcontroller unit (MCU), it integrates a 3.3 V regulated voltage supply and three connectors for the sensor board.

The flight computer interfaces with the backplane via a PCIe connector, which simplifies system integration. The flight computer includes a buzzer that indicates whether the SRAD arming circuits are armed.

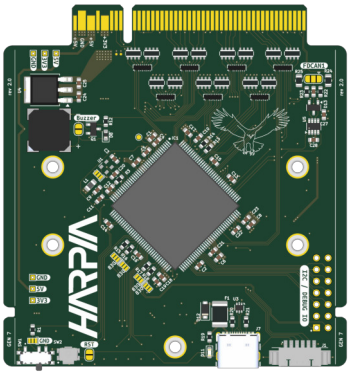


Figure 2.49: The flight computer PCB.

Sensor Board

The sensor board of HARPIA features a field programmable gate array (FPGA) for sensor data acquisition and processing. The board itself hosts two inertial measurement units (IMUs), accelerometers, gyroscopes, and barometers.

The sensors are connected to the FPGA via the Serial Peripheral Interface (SPI) bus. To accommodate the FPGA, the PCB features several voltage regulators, additional DRAM, and an FTDI Universal Serial Bus (USB)-C to UART IC. The PCB is mounted on the flight computer with five M3 screws and connects with three board-to-board connectors.

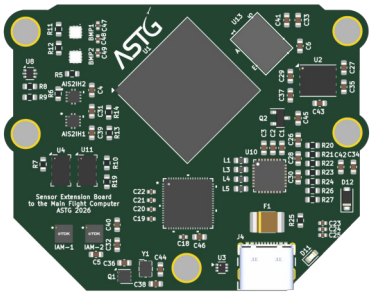


Figure 2.50: The sensor board PCB.

Black Box

For HARPIA, a flight-proven black box PCB design is used. It features a real-time clock for precise timestamps on all data packets stored on the SD card, which is encased in CFRP. The real-time clock is powered by a Li-Ion button cell battery.

The black box integrates its own STM32 MCU and controller area network (CAN) bus transceivers to monitor both CAN buses in the rocket. It can store data packets on the SD card with write speeds up to 300 KiB/s.

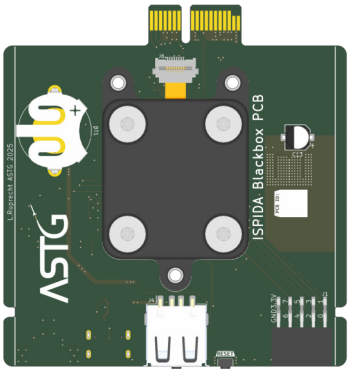


Figure 2.51: The black box PCB.

Backplane

The rocket's backplane PCB extends along the entire backside of the avionics stack and acts as the main power and signal distribution hub for all subsystems. It hosts interfaces such as PCIe style sockets and battery connectors, which facilitate efficient and organized wiring within the rocket. Specifically, it has three battery connections for the main battery, the recovery battery, and the CATS Vega secondary flight computer. Power from both the SRAD and CATS Vega batteries is routed through separate, identical arming PCBs, which are surface-mounted on the backplane and further described in Section 2.5.4.

To optimize space, the COTS CATS Vega secondary flight computer is mounted on the backplane via pin headers. The power supply as well as the recovery igniter traces of the CATS Vega are independent of any SRAD traces. The black box and the main flight computer are mounted via the PCIe connectors mentioned above.
Additionally, the backplane provides subsystems for current measurement in various paths, an analog multiplexer to measure selected voltages, detection and resistance measurement of SRAD FD and SD igniters, and digital power output switches.



Figure 2.52: Backplane PCB.

Recovery Interface PCB

The primary function of the recovery interface PCB is to provide an electronic connection between the backplane, the flight computer, and the pyrotechnic igniters that trigger the recovery systems FD and SD.

Furthermore, a smaller PCB which includes screw-switches that can be actuated from the outside is mounted on the interface PCB. The screw-switches are used to pre-arm the rocket.

The connection to the backplane is provided by an edge connector, while the pyrotechnic igniters, which trigger the recovery systems, connect via four terminal connectors.

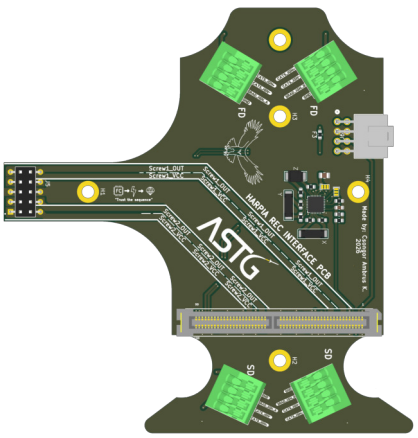


Figure 2.53: Recovery Interface PCB.

Electrical Umbilical FPC

The electrical umbilical uses a USB-C connector with custom pin-out to provide all necessary electrical connections while the rocket is still on the launch rail: 24 V power, engine and holddown ignition signal, reset input/output, four arming channels (two each for the SRAD and COTS recovery systems), and four corresponding disarming channels. The USB-C plug is soldered to an FPC, which connects to the rocket's backplane.

2.5.3 Additional PCBs

CANary PCB

The CANaries are SRAD PCBs that both sample sensors and control actuators while communicating with the flight computer via a CAN bus. The board offers eight sensor channels that can be configured individually for either thermocouples, various pressure sensors, or strain sensors. This approach provides maximum flexibility for later design decisions and supports a wide range of applications with the same hardware.

Each CANary board includes two types of actuator controls: two pulse-width modulation (PWM) channels with adjustable voltage supply for servo outputs, and three high-power digital outputs for other actuators such as solenoid valves, heat mats, or cameras.

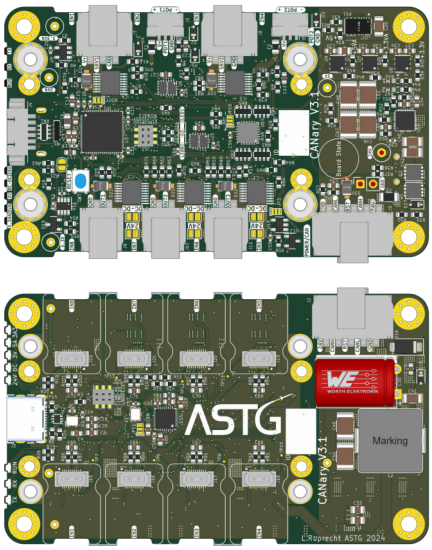


Figure 2.54: The CANary PCB.

Sun Sensor PCBs

The sun sensor subsystem consists of four sensor PCBs and one controller/main-board PCB. Its main function is to estimate the solar vector relative to the rocket during flight and assist with active attitude determination.

The sun sensor PCBs contain the circuitry required to amplify and convert the electrical current signal of the two-dimensional photo-sensitive diode (PSD) into a digital value. The sun sensor controller PCB can access and drive each of the four sun sensors' ADCs using the SPI bus. It samples the raw PSD values from each sun sensor, then filters, processes, and converts them into a single normalized solar vector in the rocket's reference frame.

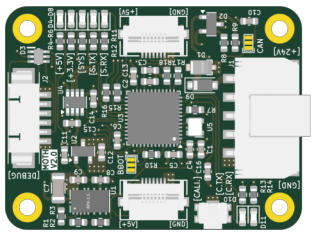


Figure 2.55: Controller PCB.

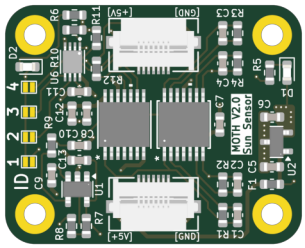


Figure 2.56: Sun sensor PCB.

Interface and Distribution PCBs

Several smaller PCBs are distributed across the rocket to help simplify overall system integration.

- **Radax Power Interface**: mounted in the avionics tube lower radax, it connects power cables to the fuel tank power interface PCB during integration.
- **Radax Data Interface**: mounted in the avionics tube lower radax, it connects avionics section CAN bus and reset lines to the fuel tank data interface PCB during integration.
- **Fuel Tank Power Interface**: mounted on the fuel tank, it links the corresponding radax power interface and distributes power lines to the upper CANary and to the rest of the propulsion stack.
- **Fuel Tank Data Interface**: mounted on the fuel tank, it links the corresponding radax data interface lines to the upper CANary and the rest of the propulsion stack.
- **Arming Screw PCB**: two M3 screws to mechanically disconnect battery power from recovery electronics.
- **Arming Indication**: two light-emitting diodes (LEDs) indicating the arming status of the rocket or nosecone.
- **Angle Sensor**: measures the absolute angle of servomotors using an AS5600 sensor.
- **Solenoid vent valve override (VVO)**: enables solenoid valve actuation with an external voltage.
- **Servo VVO**: enables and generates a PWM signal to override servos with an external voltage.

2.5.4 Recovery Electronics

Arming System

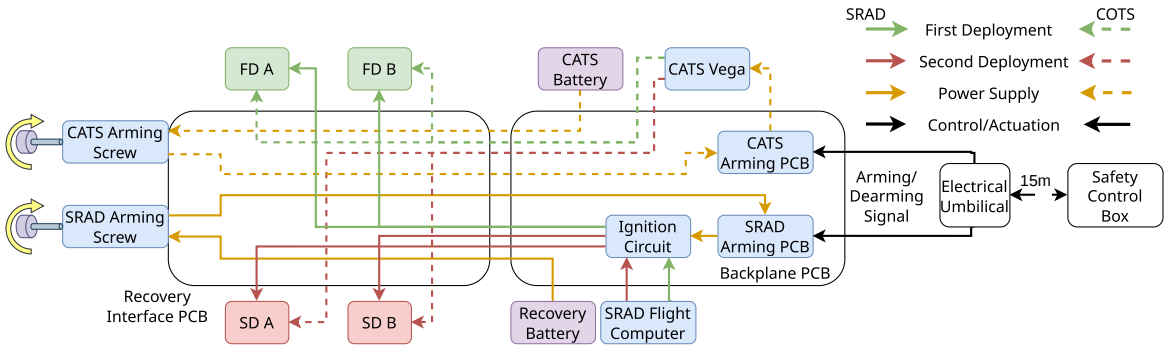


Figure 2.57: Overview of the recovery arming system.

Because the propulsion system's length prevents ground access to the avionics stack, a cable-based, fully redundant arming system was developed using the umbilical USB-C cable to provide arming and disarming signals.

The system features two mechanical screw switches secured with hex keys through designated access holes. When connected, these switches supply power to the arming PCBs on the

backplane. From the arming PCBs, power is supplied to the SRAD and COTS recovery electronics.

The recovery interface PCB acts as a passive connector, routing pyro-channels to terminal blocks for igniter connections. All connections between the recovery interface, arming screws, and backplane are redundant, using at least two connector pins placed on both sides of the PCB connection.

The main flight computer continuously measures igniter resistance through dedicated sensing circuits to verify proper igniter connections and detect wire breaks or short circuits before and during flight operations. Two independent MCU input/output (I/O) pins control the SRAD igniter circuits, with separate metal–oxide–semiconductor field-effect transistors (MOSFETs) for each igniter, providing four independent ignition channels in total.

Arming PCB

The arming PCB features four identical redundant circuits, each containing two input comparators, one flip-flop, and one p-channel MOSFET.

The comparators compare the arm and disarm signal levels to a fixed reference voltage. When exceeded, the flip-flop switches accordingly and directly controls the MOSFET. The four MOSFETs are arranged in a 2x2 configuration with two in series per branch and two branches in parallel, ensuring full functionality even if one circuit fails. All sub-circuits are individually fused.

The four arming and disarming inputs connect to two redundant cable pairs to allow disarming even if one cable breaks, while preventing arming.

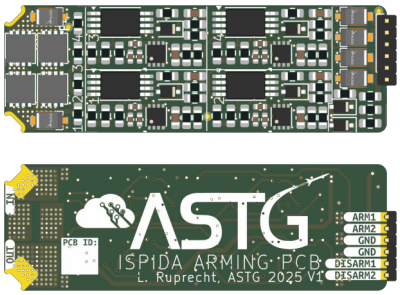


Figure 2.58: Arming PCB.

Arming Feedback

To provide feedback about the arming status of the rocket, multiple separate methods are used:

- A small voltage, well below the arming threshold, is applied to the arming input connection and activates an indicator light inside the safety control box.
- Multiple bright red LEDs that light up if any system is armed are placed around the circumference of the upper avionics radax.
- The SRAD and COTS flight computers have buzzers that produce an audible, distinguishable alarm to indicate that they are armed.
- All arming voltages are measured and the values are sent over telemetry to the mission control.

2.5.5 Avionics Telemetry

Main Board

The telemetry main board brings together all parts of the wireless system, controlled by an MCU, which then communicates with the rest of the rocket via a CAN bus. Using flexible flat cables (FFCs), the global navigation satellite system (GNSS) board, the RF frontends, and the Ethernet PCB are also connected to this PCB and form the rest of the telemetry system.
This board also contains the SX1280 LoRa transceiver with a matching network and bandpass filter, which generates the RF signals and distributes them to the frontends through either a 4-way splitter or a single output.
The main board also integrates a micro SD card slot for local data storage.

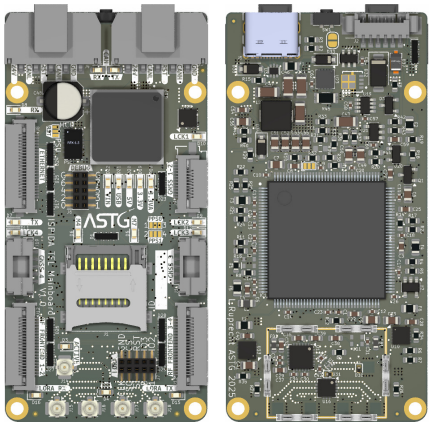


Figure 2.59: Telemetry main board front and back.

RF-Frontend PCB

Antennas on the rocket and on the ground stations are used for reception and transmission of the 2.4 GHz link. To improve the link budget and increase the range of the half-duplex telemetry system, a dedicated RF front-end PCB is used. The front-end incorporates two distinct modes for both transmission and reception, each featuring a dedicated amplifier. Two absorptive RF switches (SKY13348-374LF) are used to insert either the power amplifier (PA) or LNA in the signal path. Special care was taken to implement the desired frequency response, limiting the switch to RF signals.
To increase the received signal strength, a SKY65971-11 LNA amplifies the antenna signal by 14.5 dB. This LNA has the option to be electronically switched to a 7 dB attenuator.
This prevents signal overdrive while the rocket is still on the ground and the transmitter and receiver are close.
In transmission mode, a SE2623L PA is used to boost the signal power up to 27 dBm (500 mW).

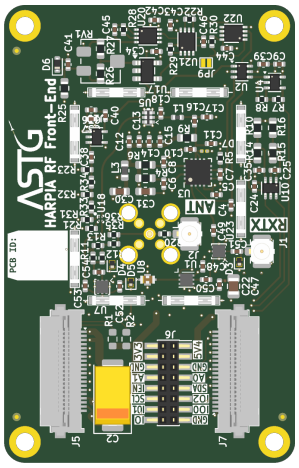


Figure 2.60: The RF-Frontend PCB.

Because this amplifier outputs higher power, it needs protection against incident reflected power in case of a mismatched antenna. To implement this protection, two features are added to the amplifier circuit. First, a transient-voltage-suppression (TVS) diode at the amplifier output limits the voltage on this port, protecting the circuit from overvoltage. A cross-coupler and an active detector (MAX2204) measure the power reflected from the antenna port. If the reflected power exceeds a preset value, a latching circuit activates and disables the PA until the mode is set to reception and then back to transmission.

GNSS PCB

In order to accurately and reliably provide GNSS-derived position information on the rocket, a GNSS PCB is added to the telemetry system. On the PCB are two interchangeable GNSS system-on-modules (SoMs) used to decode the signals of various GNSS systems. The signals received from both antennas are amplified by 19.6 dB using a BGA524N6 LNA for each of the two antennas. The amplified signals are then combined and split by a resistive combiner/splitter. This is implemented so that each GNSS's LNA receives a signal from both antennas.

To further improve the reliability and availability of GNSS information, a back-up battery on the PCB supplies the SoMs throughout periods where there is no power supplied by the main board (e.g., reboot of the avionics). This enables the SoMs to receive GNSS signals continuously and hold their lock, which otherwise would take up to 1.5 min to establish.

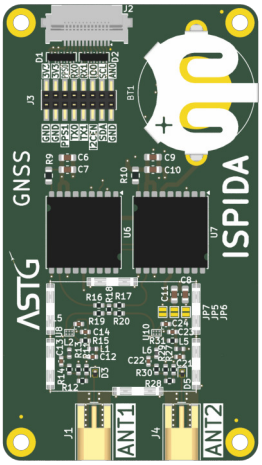


Figure 2.61: The GNSS PCB.

Patch Antenna System

The antenna system acts as the interface between transmission-line-bound signals and freely propagating electromagnetic waves, enabling communication between the rocket and the ground station.

As in previous years, a ring of patch antennas is uniformly mounted on the rocket's outer shell. This approach reduces mass and installation space while maintaining the required performance.

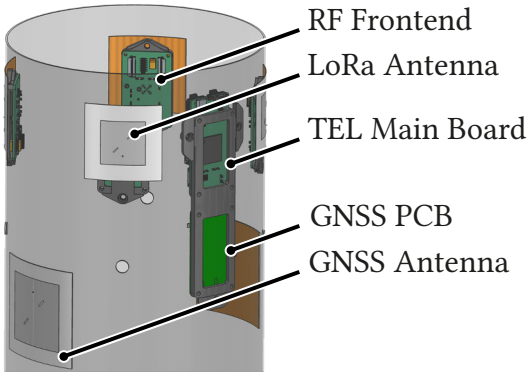


Figure 2.62: Antenna section.

Due to their proximity, the individual antenna elements are strongly coupled in the near field, while their radiated fields combine to form the overall far-field radiation pattern. The system is designed to maintain a stable communication link independent of the rocket's rotation. This year's system adds a thin electroplated silver layer on the exposed copper surfaces to protect against oxidation and physical wear.

2.4 GHz Antennas

The LoRa transceiver operates from 2.4 GHz to 2.5 GHz, overlapping with the 2.4 GHz ISM band from 2.400 GHz to 2.4835 GHz. The antennas are designed for a resonance at 2.47 GHz, as post-processing steps such as electroplating and coatings are expected to lower the resonant frequency.

One challenge of last year's design was the coupled optimization of S_{11} and axial ratio (AR). The asymmetric corner-cut geometry was suspected to be sensitive to cylindrical bending and was therefore replaced by a diagonal-slot approach. This allows the two orthogonal patch modes to be perturbed closer to the patch center and enables more independent optimization of impedance matching and axial ratio.

Different substrate thicknesses and dielectric constants were investigated. Higher dielectric constants reduce antenna size at the cost of bandwidth and increased tolerance sensitivity, while thicker substrates generally improve bandwidth and efficiency but increase mechanical strain during bending. Due to delamination observed with the 37 mil (0.93 mm) substrate, a 20 mil (0.51 mm) substrate was selected. Together with the increased dielectric constant, this reduced the antenna size by approximately 55 % compared to previous designs.

GNSS Antennas

Two patch antennas mounted adjacent to the LoRa antenna ring are used to receive GNSS signals. They operate in the GNSS L1 band at 1.575 42 GHz and follow the same general design concept as the LoRa antennas, although their operating frequency is fixed by the GNSS signal. The initially selected 37 mil (0.93 mm) substrate was replaced due to the observed delamination. A 30 mil (0.79 mm) substrate was chosen to retain higher efficiency, while an increased dielectric constant compared to last year's design reduced the antenna size by approximately 55 %.

2.5.6 Avionics Software

The Avionics software operates as a distributed system, with the mission control server as its controller node during pre-launch and the rocket's flight computer during flight operations, as shown in Section 2.5.7. An overarching state machine controls the whole system and when actions can be taken. It is described in detail in Section 2.5.6. Configuration files on all nodes support quick changes to the software during the testing phase and, at the same time, provide documentation

The software supports communication over a single packet protocol, which is described in Section 2.5.10. Real-time operating systems are used to make maintenance easier and programming more modular.

State Machine

The state machine system is present in both the flight computer and the filling station. It tracks the system states and is synchronized with the pre-launch checklists.
The state machines on the flight computer and the filling station run in parallel. The states are categorized as 'green' or 'red'. The green states are not synchronized between the flight computer and the filling station, while the red states are synchronized. After ignition, the flight computer state machine tracks the flight autonomously. See Section 2.5.7 for more details. The filling station state machine transitions into a Post Flight State.
The state machines prevent actuation of pyrotechnical channels and the torch ignitor. Other signals can also be gated behind the state machines if needed.

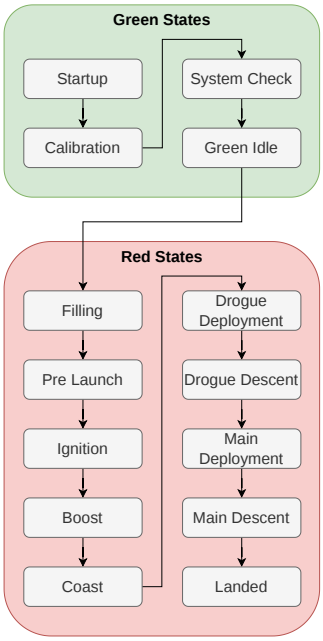


Figure 2.63: The rocket's state machine.

2.5.7 Flight Computer Firmware

The flight computer handles in-flight operations. It runs the final 20 s countdown, coordinates timing of autonomous system activations in the countdown, and decides when the FD and SD are actuated based on the automatic state detection Section 2.5.7. The flight computer runs the SRAD real-time operating system RavenOS. Flight operations are handled by the CM7 core while reading flight critical sensor data and the calculation of the altitude Kalman filter described in Section 2.5.7 is allocated to the CM4 core. Both cores communicate over a shared memory section which is synchronized by a hardware semaphore.

Automatic State Detection

To determine what phase of flight the rocket is in, the flight computer uses a linear finite state machine. The state machine waits for conditions to be true and only then advances. The stages are described as follows:

1. The flight computer is in the 'Ignition State' until the rocket is 75 m above ground.
2. Then it transitions into the 'Boost State', which ends when the vertical acceleration falls below zero.
3. The rocket remains in the 'Coast State' until the vertical velocity becomes negative, just after apogee.
4. Then, in the 'First Deployment State', the flight computer triggers the drogue parachute deployment. This trigger is active for at least one second.
5. This transitions the state machine into the 'Drogue Descent State', which lasts until the rocket is detected to be 450 m above ground.
6. At which point the flight computer in the 'Second Deployment State' triggers for at least one second to deploy the main parachute.
7. Thus entering the 'Main Descent State' and remaining in it until the vertical velocity is above −100 mm/s. The slightly negative threshold is chosen to reliably detect the landing event.

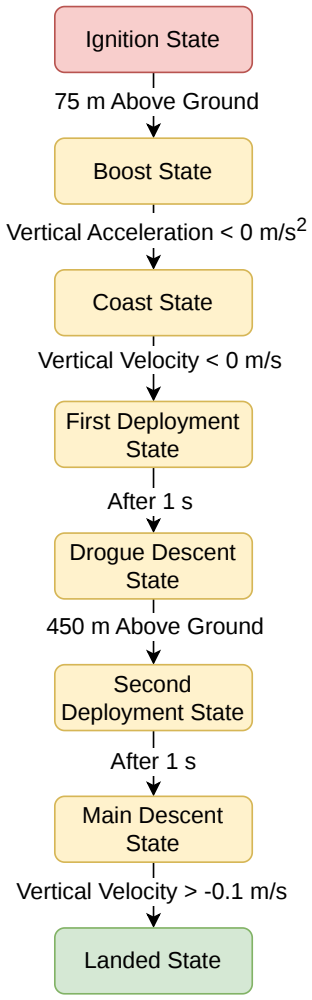


Figure 2.64: Graphical representation of the automatic state detection.

Filter for Altitude and Attitude Calculation

Two different extended Kalman filters are used on the flight computer. One is used to calculate altitude and velocity, and the other for attitude determination.

The altitude filter uses the 4 barometers, 2 IMUs, 2 accelerometers, and 2 gyroscopes. Because velocities above Mach 1 can cause anomalies in barometric data, the altitude filter also estimates an anomaly variable to capture the offset between barometric data and what it should be.

The attitude Kalman filter is purely experimental, as the data is stored only during flight and can be used afterward for flight analysis. In addition to the 2 IMUs and 2 gyroscopes on the sensor board, this filter also uses the magnetometer and the sun sensors. For calculations, a quaternion is used to prevent gimbal lock.

2.5.8 CANary Firmware

CANaries run FreeRTOS as its real-time operating system to ease development. Because there are 5 CANaries in HARPIA the firmware has to be highly customizable for the different use case of each specific CANary. This is done with a configuration file that defines the behaviors of the PCB's inputs and outputs. As CANaries can be used in multiple projects, each requiring different behaviors, this configuration is split into a base and service configuration. The base configuration handles features needed in every project. This includes sensor inputs, digital and servo outputs, and the DC-DC controller. Services handle project-specific behavior. For example, the E-Regs, abort system which is run on every CANary, or main valve service. The abort system as seen in Section 2.5.8 is configured on each CANary. To prevent delays caused by communication over CAN bus or routing, services are run on those nodes where the needed sensor data is read, or valves need to be actuated.

Nosecone CANary

The Nosecone CANary handles reading the PSP. It is configured to read out the two pressure sensors and sends them over the CAN bus to the flight computer and black box. The flight computer then routes it to the telemetry main board. Digital outputs are configured to power on payload and the tracking CATS Vega.

Upper CANary

The Upper CANary is used to keep the pressure of the fuel tank at a specific value. This is done with the E-Reg service which is explained in more detail in Section 2.5.8. For this it is configured to read the fuel tanks and COPV pressure and temperature sensors. Furthermore, a digital output is configured to actuate the depressurization valve and a servo output to actuate the E-Reg.

Valvebay CANary

Similar to the Upper CANary, the Valvebay CANary is used to keep the pressure of the oxidizer tank at a specific value with the in Section 2.5.8 E-Reg service. Furthermore, the vent valve service uses a servo output and a oxidizer pressure sensor to vent excessive pressure from the tank during oxidizer filling. The service uses a similar PID-regulator as the E-Reg service. The Valvebay CANary is configured to read the pressure and temperature of the oxidizer tank and COPV. Furthermore, both E-Reg and vent valve servo motors are actuated by this CANary.

Engine CANary

The Engine CANary is used to actuate the main valves in a way that both propellants enter the combustion chamber at the same time. For this one has to configure the main valve service where states can be defined which are played through upon main valve service open actuation. The CANary has for this both main valves with potentiometers configured. Furthermore, the pressure of the combustion chamber is monitored here.

Ignitor CANary

The Ignitor CANary is used to actuate the torch ignitor. For this multiple services are used. The current control controls the heat up of the glow plug via a servo output. Furthermore, the torch ignitors valves need to be opened in a specific way to produce a combustion. For this the torch ignitor was developed in a similar way as the main valve service. States can be defined to actuate configured digital outputs in a specific way. Furthermore, this CANary monitors the ignitor's pressure and temperature.

E-Reg Service

The E-Reg Service is used to actuate fuel and oxidizer E-Regs of the propulsion system. It supports pressurization, holding the pressure and actuating the valve directly by the operator.

To hold the pressure in its tank, it uses a PID-regulator. It uses the two pressure sensors of the tank, COPV pressure, and the angle sensor of its tank's main valve to hold the pressure.

The direct actuation of the E-Reg has a built-in safety software. If pressure is present in the tank, it cannot be normally actuated to prevent user error. If movement of the valve is desired, the E-Reg service needs to be set into the override mode.

Abort System

The abort system was designed to prevent engine damage during testing operations. Based on predefined conditions, a CANary node can initiate an abort. It first executes its local abort functions and subsequently broadcasts the abort signal to the network. Upon receiving this signal, each connected node executes its own system-specific abort handling routines. The architecture distinguishes between two response levels:

- A Hard Abort is triggered during critical failures and results in an immediate launch abort or engine shutoff to ensure system safety.
- A Soft Abort operates under soft real-time constraints to handle non-critical anomalies. Instead of a full shutdown, it implements fallback strategies, such as polling redundant sensors to avoid reliance on a single faulty data point.

2.5.9 Telemetry Firmware

FreeRTOS is used as the operating system for the telemetry firmware. The software architecture is modular, so common components can be reused across the different telemetry nodes, including the onboard system, the mission control receiver, and the filling station.

The STM32H745 contains two processor cores, each running a separate FreeRTOS instance. Radio communication via LoRa is assigned to the CM4 core, whereas the CM7 core is responsible for the remaining functionality. This includes exchanging data with other rocket subsystems over CAN, receiving GNSS information via UART, and acquiring voltage, current, and temperature measurements using an ADC. The cores transfer information using a queue in shared memory. Access to the shared data is synchronized using hardware semaphores. The radio transceiver is connected through SPI. UART, ADC, and SPI transfers make use of direct memory access (DMA) to limit the processing overhead on the MCU.

Different communication interfaces are used depending on the system part. LoRa provides the wireless link between the rocket and mission control, CAN is used for communication within the rocket and the GSE, and the ground systems communicate with each other over UDP. Regardless of the underlying transport, all communication uses the custom TELtalk protocol, which provides a common format for packet handling, routing, and integrity verification.

2.5.10 TELtalk Communication Protocol

TELtalk regulates how the various MCUs communicate. It encodes the data into an efficient bit-level-packed representation and implements pings, log messages, commands, a special format for high-frequency sampled data points, network statistics, packet fragmentation, and integrity checksums.

TELtalk is agnostic about its lower transport layers. Ethernet, IPv4, UDP, LoRa, and the CAN bus are used across the network.

Both C and Python libraries are generated from a spreadsheet, enabling rapid development when a new command or sensor is added. To avoid version conflicts, the command and data packets include identifiers based on a hash of their definition, virtually eliminating the possibility of parsing an incompatible packet.

2.6 Payload Subsystem

HARPIA is designed to carry one 1U CubeSat with a total mass of 1 kg in the nosecone. This year's payload is based on COLIBRI, a member's bachelor's thesis, and was further developed by a high school student.

The payload's task is to capture clear, steady video footage during and after drogue parachute deployment, through touchdown. Since the nosecone can spin freely around the lines of the parachute, the challenge was to stabilize the camera along the vertical axis like a gimbal. To achieve this, a servo motor can move the camera and its PCB to any desired position. The camera electronics are electrically connected to the payload through a spring-loaded contact via a sliding contact interface.

The control system is based on an ESP32 MCU and uses an Adafruit BNO085 IMU to measure acceleration and angular velocity. An AS5600 magnetic encoder provides the motor position and rotational speed feedback. A field-oriented controller drives the motor using the DRV8313 motor driver. A BMP390 barometric sensor, reused from the original COLIBRI payload, provides pressure and altitude measurements.

The payload is integrated into the nosecone before flight. During the procedure, an arming PCB gets a signal from the nosecone CANary to switch on the power of the CubeSat. It is powered by its own 4S 18650 Li-Ion battery pack, and it stores data locally on a physical storage device.

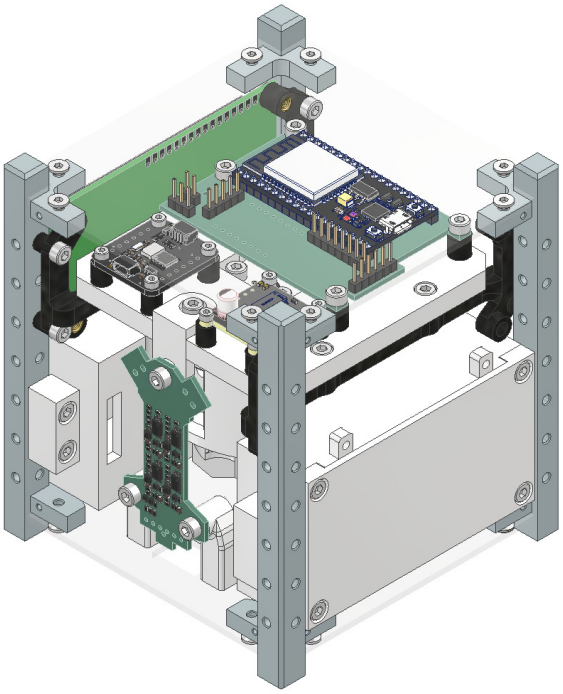


Figure 2.65: Internal view of the CubeSat showing the structure and electronics.

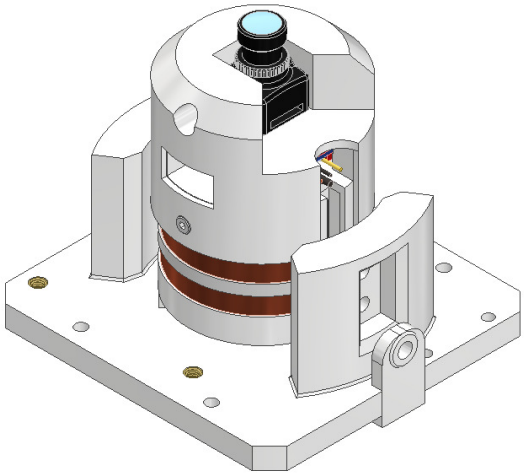


Figure 2.66: Camera stabilization mechanism of the CubeSat.

3 Mission Concept of Operations (CONOPS)

Mission/ Operational Phase		Appr. Time (Start)	Phase Start	Phase End	Integration Tent Team	Mission Control Team	Launch Rail Team
Storage & Transport		T-7d		Arrival at the launch site	Parts are stored in boxes, The propulsion stack is preassembled, The recovery subsystem is preassembled	The mission control monitors and parts are stored in boxes	The launch rail is disassembled
Pre-flight	Assembly	T-3h		The rocket is fully assembled and ready to be brought to the launch rail	Final assembly of the rocket, Visual inspection of the preassembled propulsion stack, Final test actuation of the flight hardware	Setup of the mission control, Establish connection with the filling station and its cameras, Establish communication, Report first sensor data of the filling station	Setup the launch rail, Setup the filling station and its antennas, Install the N2O and N2 bottles, Purge the filling system
Pre-flight	Pre-flight handling	T-1h	Assembly is completed	Pre-flight checks are completed, Rocket is armed, Launch rail team leaves the launch pad		Final checks of the filling station	Mount rocket to the launch rail, Connect all umbilicals, Fill fuel, Arm rocket, Open manual N2O valve
Pre-flight	Tanking	T-30 min	EuRoC gives GO for tanking	Propellant loading and pressurization are completed, loading lines are disconnected		Controlling the tanking procedure, Final go/no go round for launch, Remote disconnection of the fluid umbilicals	Stay alert in case of an abort, Possibility of manual umbilical disconnection or manual depressurization

Mission/ Operational Phase		Appr. Time (Start)		Phase End	Aerostructure	Avionics	Propulsion	Recovery	Payload
Ignition		T-2s	Ignitor starts	Ignitor is burning		Ignitor is triggered	Ignitor is ignited		Payload is recording
Flight general	Lift-Off	T=0s		The holddown mechanism is deployed and the rocket starts moving under its own thrust	Rail buttons provide stabilization on the launch rail	Open the main valves	Engine ignites after the main valves are opened		
Flight general	Boost Phase	T+0s		The main valves are closed		Detects liftoff	E-Regs regulate pressure in propellant tanks		
Flight general	Coast Phase	T+8s		Apogee is detected by the flight computers		Detects apogee and triggers first deployment	Tanks are depressurized		
Flight general	Drogue Descent	T+42s		Reaching an altitude of 450 m		Detects 450 m and triggers second deployment	Vent valves open to fully vent the tanks	The drogue parachute slows the rocket to 29 m/s	Payload camera is gimbaled to record drogue
Flight general	Main Descent	T+284s		The rocket lands				The main parachute slows the rocket to 6 m/s	
Flight general	Landing	T+347s		The area is free for recovery operations					

Mission/ Operational Phase		Appr. Time (Start)		Phase End	Integration Tent Team	Mission Control Team	Launch Rail Team
Post flight	Landed	T+30 min		The rocket is brought into the assembly tent	Prepare to receive the rocket for final disassembly	Provide the recovery team with GNSS data, Check filling station data	Close the gas bottles, Depressurize the filling station

Figure 3.1: HARPIA CONOPS.

The mission concept covers HARPIA's complete operational sequence, from ground preparation through launch, flight, recovery, and landing. Before lift-off, the vehicle is integrated, filled, and armed while the different parts of the ground support equipment, like the mission control, the filling station, and the launch rail, are set up. Figure 3.1 summarizes the vehicle's nominal operation and subsystem responsibilities throughout these phases, including the respective phase-transition criteria.

The flight itself is divided into the ignition, boost, coast, drogue descent, main descent, landing, and post-flight phases, with transitions defined by key mission events such as ignition detection, lift-off, engine shutdown, apogee detection, parachute deployment, landing, and clearance for recovery operations, as illustrated in Figure 3.2.

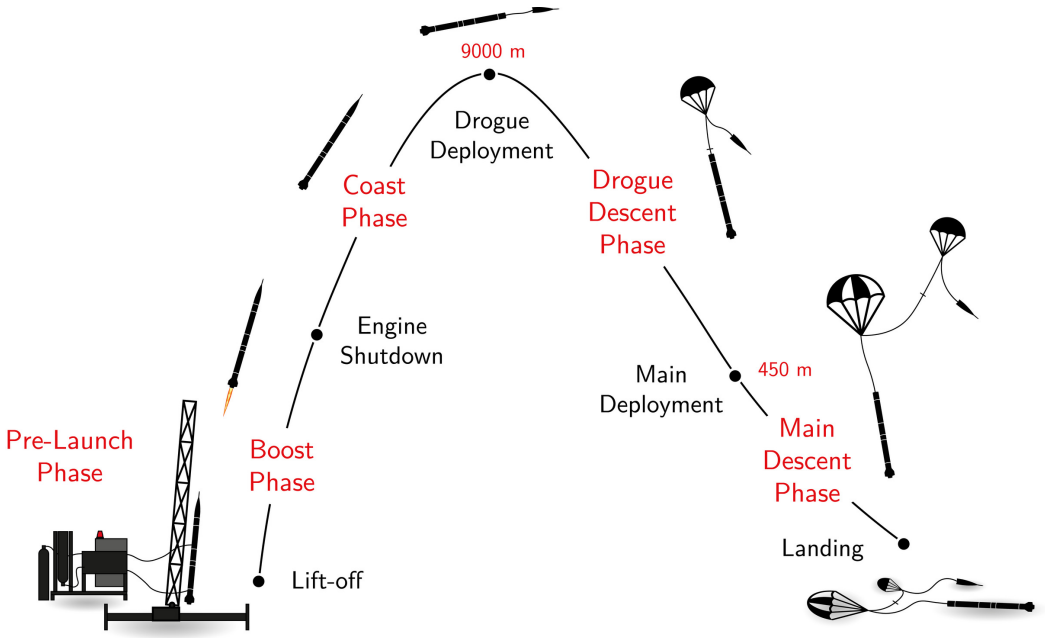


Figure 3.2: HARPIA flight phases.

3.1 Arming

Integration and Transport: The arming screws are open, mechanically disconnecting all energetic devices from power sources.

At the launch rail: After the rocket is mounted on the launch rail in a horizontal position and all umbilicals are connected, the arming screws will be tightened. The igniter circuits are still disconnected from the rocket's flight computers by the arming PCBs.

Before launch: When the launch rail team leaves the launch site, the rocket is armed using a key switch in the safety control box. This sends signals over two redundant electrical connections, each with a separate mechanical switch. This enables the redundant MOSFETs on the arming PCBs, supplying power to the igniter circuits. A separate key switch also arms the holddown circuit.

3.2 Thrust Curve

Figure 3.3 shows all thrust curves recorded during the successful static Hot-Fires. For the flight simulation, the thrust curve of Hot-Fire 6.2 was used.

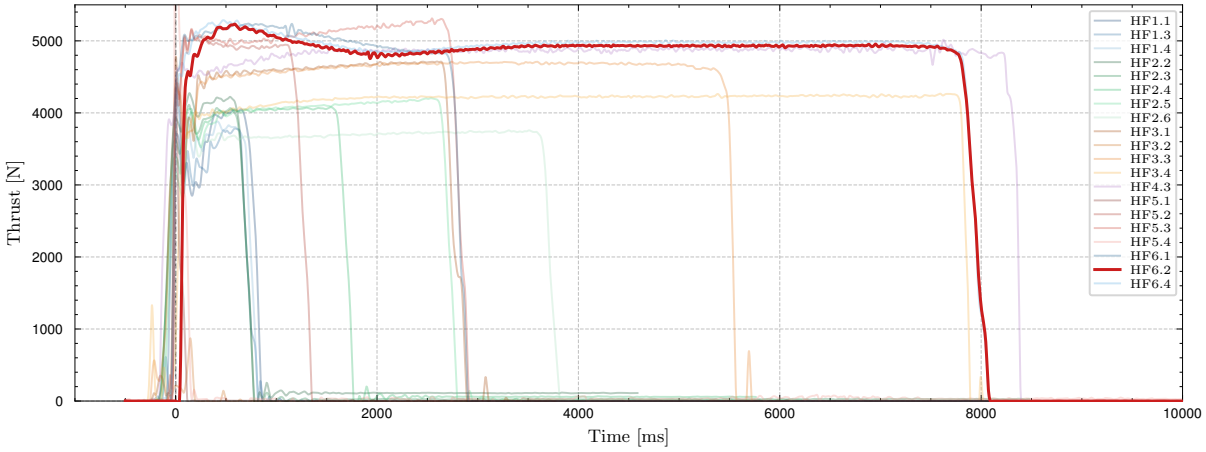


Figure 3.3: All thrust curves recorded during the static Hot-Fires. The thrust curves were filtered with a Butterworth filter (order=2, f_crit=20 Hz, python scipy, filtfilt function) for better visibility. The unfiltered thrust curves can be looked up in the corresponding test reports.

3.3 Tanking and Pressurizing

Fuel is filled as one of the last steps before the launch rail team leaves the launch pad. The oxidizer and pressurizer are tanked as soon as everyone is away from the rocket. The oxidizer and pressurizer tanking procedure involves the following steps:

- Set the vent control to 15 bar and open the oxidizer fill valve completely.
- Once liquid venting is observed at the upper vent valve, close the oxidizer fill valve.
- The system enters standby mode, awaiting pressurization and the launch GO from EuRoC.
- Perform a top-off: reopen the oxidizer fill valve until liquid venting resumes, then close it again.
- Vent the oxidizer fill line and disconnect the oxidizer QD.
- Open the first pressurizing fill valve to pressurize the pressurant tank to approximately 280 bar.
- The fuel tank is pressurized to 42 bar and the oxidizer tank to 35 bar via the internal COPV and the pressurization systems.
- Reopen the first N_2 fill valve to bring the pressurant tank to approximately 260 bar.
- Open the second N_2 fill valve until the COPV reaches approximately 300 bar.
- Close both N_2 fill valves, vent the N_2 fill line and disconnect the N_2 QD.

3.4 Flight Simulation

Figure 3.4 depicts the trajectory of a HARPIA flight simulated using RocketPy. With average EuRoC weather conditions, the rocket reaches an apogee of 9440 m. The thrust curve used is the one from Hot-Fire test 6.2 Appendix C.32, as seen in Figure 3.3. The off-the-rail velocity exceeds 30 m/s in every simulated environment, and the stability margin never drops below the stated requirement of 1.5 calibers.

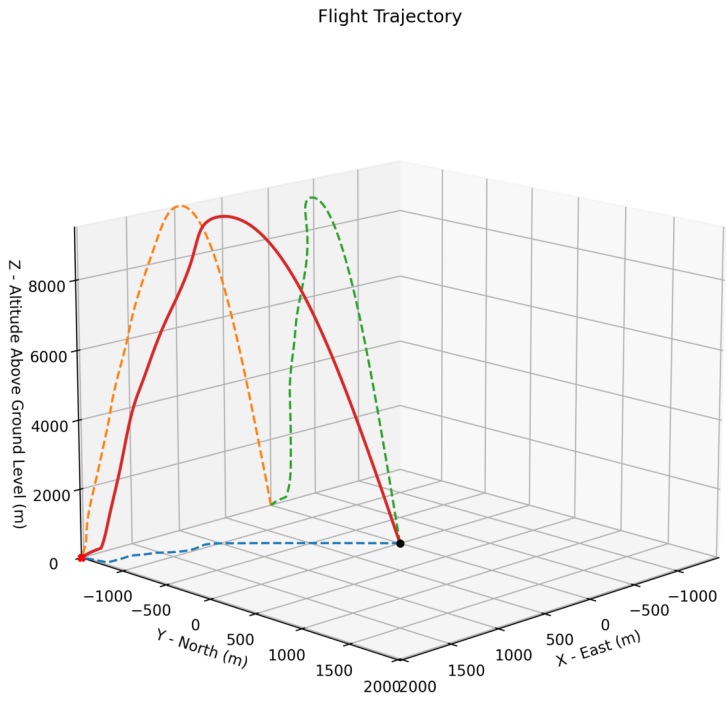


Figure 3.4: Flight trajectory of a HARPIA flight using the average weather conditions at the EuRoC launch site.

Multiple trajectories for different wind speeds were simulated. The most important parameters are listed in Table 3.1.

Table 3.1: Apogee, stabilities, and drift distances for different surface wind speeds simulated with RocketPy.

Wind speed [m/s]	Apogee [m]	Drift [m]	Off-rail stability [cal]	Max stability [cal]
0.0	9324.4	1825.1	3.53	5.28
2.0	9368.0	1837.8	3.53	5.28
4.0	9379.7	1835.8	3.53	5.28
6.0	9358.7	1826.4	3.53	5.28
8.0	9307.0	1816.3	3.53	5.28

More detailed information on aerodynamic stability over velocity/mission time and simulated acceleration, descent rates, and center-of-gravity/pressure positions is available in the detailed flight simulation in Appendix L.

4 Conclusions and Outlook

Project HARPIA marked an important milestone for ASTG, as it was the team's first liquid-propellant launch vehicle and was developed within a single project year. Building on experience with previous hybrid propulsion systems, the project expanded the team's capabilities toward liquid propulsion and required the development of new fluid, structural, recovery, and ground support systems. In particular, the regeneratively cooled CC and its associated fluid system introduced a considerably higher level of system complexity than previous projects.

In various areas, this project significantly advanced the team's capabilities: Within Aerostructure (AST), manufacturing was improved through dedicated tooling and new manufacturing approaches, including streamlined methods for tube cutting and fin production. The Recovery (REC) module gained further experience with shockabsorber behavior and developed a simulation tool, KESTREL, for parachute-opening dynamics. These developments will support the design and analysis of future vehicles.

One of the main lessons learned during the project was the importance of considering backward compatibility during development. Keeping compatibility with previously developed and tested components, interfaces, and procedures allows subsystems to fall back on proven solutions if newly developed hardware or external manufacturing causes problems. This makes the overall system less dependent on individual components and reduces the effects of failures or delays. For a student engineering project with limited development time and manufacturing capacity, these fallback options are particularly useful.

The project also showed where the development process can be optimized. The transition from design to manufacturing should be coordinated more closely to avoid misunderstandings and late design changes. Manufacturing capabilities and limitations should be considered earlier in the design process. Where possible, critical components should not depend on a single manufacturer. Alternative manufacturing options reduce scheduling risks and make it easier to respond to delays or manufacturing problems.

Several aspects have the potential for future improvements. The REC simulation tool KESTREL can be further refined and validated using flight test data, which would provide more accurate predictions of parachute deployment behavior. Within Propulsion (PRO), better accessibility of components and interfaces would simplify assembly, inspection, and maintenance. For Avionics (AVI), better adherence to the overall project schedule and a more even distribution of tasks would help reduce the workload towards the final phase of the project.

Overall, developing HARPIA was an important step for ASTG. The transition from hybrid to liquid propulsion required new technical solutions and the implementation of more complex systems. The experience gained during the vehicle's design, manufacturing, testing, and integration can be used directly in future projects.

List of Figures

1.1 Overview of the team demographics . . . 1
1.2 All ASTG rockets . . . 2

2.1 Overview of HARPIA . . . 3
2.2 Propulsion Stack . . . 4
2.3 Fluid system . . . 5
2.4 Valvebay and Thrust structure . . . 6
2.5 Upper fluid . . . 7
2.6 PT-Connector . . . 7
2.7 E-Reg controller . . . 8
2.8 E-Reg cut view . . . 8
2.9 Middle fluid . . . 9
2.10 N_2-manifold cut view . . . 9
2.11 Fill valve cut view . . . 10
2.12 Lower fluid . . . 10
2.13 Back view of lower fluid . . . 11
2.14 Main valves . . . 11
2.15 Engine bay . . . 12
2.16 Combustion chamber cut view . . . 13
2.17 Analysis plot of the chamber . . . 14
2.18 Pintle injector . . . 15
2.19 Venturi . . . 15
2.20 Torch ignitor . . . 16
2.21 Pyrotechnic ignitor . . . 16
2.22 Structural overview of the rocket's sections . . . 17
2.23 Radax . . . 18
2.24 Retractable rail button . . . 19
2.25 NACA duct . . . 19
2.26 Nosecone structure . . . 20
2.27 Clip mechanism of the cameras . . . 20
2.28 PSP tip . . . 21
2.29 PSP cradle . . . 21

2.30 Tailcone with fins . . . 22
2.31 Overview of the assembled REC section . . . 23
2.32 Sectional view first deployment . . . 24
2.33 Explosion view of first deployment . . . 24
2.34 SD . . . 25
2.35 Explosion view of second deployment . . . 25
2.36 Drogue parachute . . . 26
2.37 Inflated main parachute . . . 26
2.38 Main parachute bag . . . 27
2.39 Overview of eyebolt . . . 27
2.40 Pressure plate connection bolt . . . 28
2.41 Rotatable swivel . . . 28
2.42 Line with thimble . . . 28
2.43 Softshackle . . . 29
2.44 Shockabsorber manufactured for flight . . . 29
2.45 Power management and distribution . . . 30
2.46 Main batter pack . . . 30
2.47 Small battery pack . . . 31
2.48 Avionics stack . . . 32
2.49 Flight computer . . . 33
2.50 Sensor board . . . 33
2.51 Black box . . . 33
2.52 Backplane PCB . . . 34
2.53 Recovery interface PCB . . . 34
2.54 CANary PCB . . . 35
2.55 Sun sensor controller PCB . . . 35
2.56 Sun sensor PCBs . . . 35
2.57 Overview of the arming system . . . 36
2.58 Arming PCB . . . 37
2.59 Telemetry main board . . . 38
2.60 RF Frontend PCB . . . 38
2.61 GNSS PCB . . . 39
2.62 Antenna section . . . 39
2.63 State machine . . . 40

2.64 Automatic state detection 41
2.65 Payload structure 45
2.66 Payload gimbal 45

3.1 HARPIA CONOPS 46
3.2 HARPIA flight phases 47
3.3 All thrust curves 48
3.4 Trajectory of the flight simulation 49

List of Tables

2.1 Propulsion characteristics 4
2.2 Properties of the wound recovery shell 18

3.1 Flight simulation results 49

Acronyms

ADC analog-to-digital converter.

AGL above ground level.

AST Aerostructure.

ASTG Aerospace Team Graz.

AVI Avionics.

CAN controller area network.

CC combustion chamber.

CFD computational fluid dynamics.

CFRP carbon-fiber reinforced polymer.

CHF critical heat flux.

CONOPS concept of operations.

COPV composite overwrapped pressure vessel.

COTS commercial-off-the-shelf.

CR contraction ratio.

DMA direct memory access.

EMI electromagnetic interference.

ESD electro-static discharge.

EuRoC European Rocketry Challenge.

FD first deployment.

FEA finite element analysis.

FEP fluorinated ethylene propylene.

FF feed forward.

FFC flexible flat cable.

FFG Austrian Research Promotion Agency.

FKM fluoroelastomer.

FMECA Failure Mode, Effects and Criticality Analysis.

FPC flexible printed circuit.

FPGA field programmable gate array.

GFRP glass-fiber reinforced polymer.

GNSS global navigation satellite system.

GSE ground support equipment.

I/O input/output.

I2C Inter-Integrated Circuit.

IC integrated circuit.

IFT Institute of Production Engineering.

IIM Institute of Innovation and Industrial Management.

IMU inertial measurement unit.

IPA isopropanol.

LED light-emitting diode.

Li-Ion lithium-ion.

LNA low-noise amplifier.

LPBF laser powder bed fusion.

MC mission control.

MCU microcontroller unit.

MEOP maximum expected operating pressure.

MOSFET metal–oxide–semiconductor field-effect transistor.

NACA National Advisory Committee for Aeronautics.

O/F oxidizer-to-fuel ratio.

PA power amplifier.

PCB printed circuit board.

PCIe Peripheral Component Interconnect Express.

PEEK polyether ether ketone.

PID proportional integral derivative.

PRD pressure relief device.

PRO Propulsion.

PSD photo-sensitive diode.

PSP pitot-static probe.

PTFE polytetrafluoroethylene.

PWM pulse-width modulation.

PWR pressurized water nuclear reactor.

QD quick disconnect.

QFH quadrifilar helix.

RANS Reynolds-averaged Navier-Stokes.

RC rocket candy.

REC Recovery.

RF radio frequency.

RSSI Received Signal Strength Indicator.

SD second deployment.

SF safety factor.

SLA stereolithography.

SLS selective laser sintering.

SoM system-on-module.

SPI Serial Peripheral Interface.

SRAD student researched and developed.

TMR total momentum ratio.

TPU thermoplastic polyurethane.

TU Graz Graz University of Technology.

TVS transient-voltage-suppression.

UART universal asynchronous receiver-transmitter.

UDP User Datagram Protocol.

UPS uninterruptible power supply.

USB Universal Serial Bus.

VVO vent valve override.

WLAN wireless local area network.

Glossary

3D printed Additive manufacturing method where material is deposited, joined or solidified layer by layer under computer control.

ALCEDO 9 km Hybrid rocket designed by the Aerospace Team Graz 2023/24 for the European Rocketry Challenge.

AVES 3 km Solid rocket designed by the Aerospace Team Graz 2020/21 for the European Rocketry Challenge.

AVES II 3 km Solid rocket designed by the Aerospace Team Graz 2021/22 for the European Rocketry Challenge.

backplane PCB that serves as the interconnection between the avionics stack and the rest of the rocket.

black box Hardened data storage device designed to survive ballistic impacts.

CANary Control and data acquisition module connected via CAN bus.

CATS Vega COTS flight computer used for official tracking by EuRoC.

Cold-Flow A test of the rocket propulsion system and other required systems without ignition.

COLIBRI Payload developed for a Bachelor thesis, it records out of the nosecone after drogue deployment and is spin stabilized.

coupling tube Tube for separable connection between nosecone and recovery shell.

CubeSat Miniaturized satellite with form factor of a 100 mm cube.

drogue parachute A small parachute deployed at apogee, to stabilize the vehicle's attitude, and reduce its descent rate sufficiently to permit the main deployment event.

E-Reg Electronically regulated ball valve to pressurize the tanks.

filling station Aluminum frame containing fluid systems used to pressurize and fuel the rocket remotely. Additionally used to mount the gas bottles.

flight computer Onboard system that manages the control, and data processing functions of the vehicle during flight.

FreeRTOS Real-time operating system for embedded systems.

Gallus Demonstrator liquid engine designed by the Aerospace Team Graz in autumn/winter 2025 to test feasibility of making a liquid engine within a year.

HALCYON 3 km Hybrid rocket designed by the Aerospace Team Graz 2022/23 for the European Rocketry Challenge.

HARPIA 9 km Liquid rocket designed by the Aerospace Team Graz 2025/26 for the European Rocketry Challenge.

Hot-Fire A test of the rocket propulsion system and other required systems with ignition.

ISPIDA 9 km Hybrid rocket designed by the Aerospace Team Graz 2024/25 for the European Rocketry Challenge.

KESTREL Kinetic Evaluation of Shockforce, Trajectory, and Recovery Element Linkage; an SRAD simulation tool developed by the recovery module to model shock forces and dynamic behaviour during parachute deployment, including trajectory and shock cord response.

LoRa Radio communication technique.

main parachute A second, large parachute deployed no higher than 450 m AGL, to reduce the vehicle's descent rate sufficiently to prevent excessive damage upon impact with the ground.

main parachute bag Main parachute deployment bag.

NASA CEA A foundational NASA computer program used to calculate chemical equilibrium compositions and thermodynamic properties for complex mixtures.

nosecone Cone-shaped front part of the rocket.

Penguin Horizontal testbed of the Aerospace Team Graz.

prepreg Composite fibers preimpregnated with a known quantity of partially cured resin.

pyrotechnic mass Mixture used in the engine ignitor consisting of rocket candy, calcium silicide (CaSi), magnesium powder and iron oxide.

radax Radial-axial, a type of airframe joint, describing the angled contact surface and force transfer.

shockabsorber A device to absorb and damp shock forces, by ripping open. When tearing, the energy is absorbed by the breaking seams.

SPATZ test rocket SRAD modular low-cost test rocket developed for flights around 100 m AGL.

tailcone Cone-shaped cover at the rear of the rocket.

TELtalk Custom data transfer protocol.

USIT USIT is a brand name commonly used in German-speaking regions to refer to a certain kind of bonded sealing ring used for flat gaskets.

References

[1] Constantine A.. Balanis. *Antenna theory : analysis and design*. John Wiley, 2016, p. 1072. ISBN: 9781118642061.

[2] Ramesh. Garg. *Microstrip antenna design handbook*. Artech House, 2001, p. 845. ISBN: 9780890065136.

[3] David M.. Pozar. *Microwave engineering*. John Wiley & Sons Incorporated, 2013. ISBN: 9780470631553.

[4] Mrityunjoy Ray, Kaushik Mandal, and Nasimuddin N. "Low-Profile Circularly Polarized Patch Antenna With Wide 3 dB Beamwidth." In: *IEEE Antennas and Wireless Propagation Letters* 18 (Aug. 2019), pp. 2473–2477. DOI: 10.1109/LAWP.2019.2940703.

[5] Warren L.. Stutzman and Gary A.. Thiele. *Antenna theory and design*. Wiley, 2013, p. 822. ISBN: 9780470576649.

[6] Wikimedia contributors. *Atmospheric Pressure vs. Altitude*. 2011. URL: https://commons.wikimedia.org/wiki/File:Atmospheric_Pressure_vs._Altitude.png.

Appendix A: System Data

Table A.1: System Data - Outer dimensions and mass distribution.

Total Length	3940 mm
Length of main body (without PSP)	3736 mm
Diameter	182.4 mm
Mass Tailcone	1960 g
Mass Propulsion Stack	21 610 g
Mass Airframe Avionics Section	1660 g
Mass Avionics Stack	1200 g
Mass Airframe Recovery Section	1060 g
Mass Recovery Subsystem	3750 g
Mass Nosecone	1760 g
Mass Payload	1000 g
Total Mass dry	34.0 kg
Mass Fuel (IPA)	6300 g
Mass Pressurizing Gas (N_2)	2500 g
Mass Oxidizer (N_2O)	15 900 g
Total Mass wet	58.7 kg

Table A.2: System Data - Flight Data.

Target Apogee	9000 m
Velocity off Rail	40.2 m/s
Max. Velocity	612 m/s
Max. Acceleration	89 m/s^2
Time to Apogee	42 s
Total Flight Time	346 s

Table A.3: System Data - Aerostructure.

Drag Coefficient	0.27 to 0.44
Dry Center of Gravity (reference: tip)	2174 mm
Moment of Inertia (long axis)	0.25 kgm^2
Moment of Inertia (short axis)	58.12 kgm^2
Fin Geometry	Trapezoidal

Table A.4: System Data - Recovery.

First Deployment Event	Apogee (9000 m AGL)
Main Deployment Event	450 m AGL
Descent Velocity Drogue Parachute	(29.7 ± 1.3) m/s
Descent Velocity Main Parachute	6.2 m/s
Panel Side Length Drogue Parachute	0.5 m
Diameter Main Parachute	3.2 m
Opening Shock Drogue	5160 N at 200 m/s 1037 N at 100 m/s
Opening Shock Main	2405 N at 46 m/s 1600 N at 32 m/s

Table A.5: System Data - Avionics.

SRAD Standby Time with Umbilical Connection	> 24 h
COTS Standby Time	8 h - 10 h
SRAD Standby Time without Umbilical Connection	3 h
Altitude Kalman Filter Frequency	100 Hz
Processor Frequency	480 MHz
Quantity Sensors (complete rocket without COTS)	76
Quantity PCBs (complete rocket, without COTS)	63
Quantity Cameras (excluding Payload)	7
Telemetry System Type	LoRa (Rocket)
Frequency Range	2400 to 2500 MHz
Bandwidth	1.6 MHz
RF Power	Up to 1.0 W
Data Uplink	Configuration Parameters & Commands
Data Downlink	Rocket Data & Position
Internal Data Rate	64 kB/s
Transmitted Data Rate	6.1 kB/s
Range	> 30 km

Table A.6: System Data - Payload.

Form Factor	1x CubeSat 100 x 100 x 113.5 mm
Type	Active
Deployable	No
Mass	1000 g
Quantity Payloads	1

Table A.7: System Data - Propulsion.

Engine	SRAD Liquid
Fuel	Isopropanol (IPA)
Fuel Mass	6300 g
Oxidizer	Nitrous Oxide N_2O
Oxidizer Mass	15 900 g
Pressurizing Gas	Nitrogen N_2
Pressurizing Gas Mass	2500 g
Total Impulse	39.2 kNs
Average Thrust	4900 N
Burn Time	8.0 s
Fuel Tank Pressure Fuel PRD Opening Pressure Fuel Burst Disc Pressure	42 bar 60 bar 67 bar
Oxidizer Tank Pressure Oxidizer PRD Opening Pressure Oxidizer Burst Disc Pressure	35 bar 55 bar 61 bar
Combustion Chamber Pressure	26 bar
Dry Mass	21 610 g
Length	2569 mm
Ignition Type	Pyrotechnic Ignition

Table A.8: Summary of SF of most critical parts in the Aerostructure subsystem. Given are functional groups (e.g. radax: adhesive joint, screws, radax female and male), and the lowest SF of that working group.

Group	SF	Point of First Failure	Reference
Coupling Tube	8.70	Adhesive joint	Adhesive calculation CALC_AST_01
Recovery-Avionics radax	2.10	Part failure	FEA AST_03
Avionics lower radax	3.00	M4 radax screws	Screw calculations CALC_AST_02
Valvebay radax	1.59	M5 radax screws	Screw calculations CALC_AST_03
Tailcone radax	1.76	M5 radax screws	Screw calculations CALC_AST_02
Rail button piston	1.52	Part failure	FEA AST_05
Holddown hardpoint	1.86	Part failure	FEA AST_07
Holddown Deployment	1.56	Insufficient gas pressure	CALC_AST_05
Holddown Chargecup	6.53	Overload of thread	CALC_AST_06
Nosecone groundplate	1.72	Part failure	FEA AST_01

Table A.9: Summary of SF of the most critical parts in the Recovery subsystem. The listed loads correspond to the maximum loads the respective components experience. For components that are required to withstand the drogue deployment loads, the safety factors are given for the nominal deployment velocity of 100 m/s and, in brackets, for the unlikely deployment velocity of 200 m/s.

Component	Loads	SF	Reference
Shroud Line	1037 N [5160 N]	41.0 [8.24]	Tension scale test Appendix C.10
Rotatable Carabiner	1037 N [5160 N]	22.17 [4.45]	Datasheet Appendix M.2
Softshackle	1037 N [5160 N]	27.00 [5.42]	Tension scale test Appendix C.10
Pressure Plate Bolt	5200 N	2.66	FEA REC_06
40 mm Lash on Bag	1037 N [5160 N]	49.18 [9.88]	Datasheet Appendix M.2
4 mm Line	1037 N [5160 N]	35.67 [7.17]	Tension scale test Appendix C.10
8 mm Lines	1037 N [5160 N]	8.67 [1.74]	Datasheet Appendix M.2
Eyebolt	3000 N	2.78	FEA REC_05
Second deployment	2650 N	3.39	FEA REC_02
Groundplate	5200 N, 3000 N	1.52, 1.51	FEA REC_01

Table A.10: Summary of SF of most critical parts in the Propulsion subsystem. The components, SF, and reference document are given. The load cases are assumed to be twice the maximum expected pressures (oxidizer tank 55 bar, fuel tank 60 bar, combustion chamber 25 bar, pressurant tank 300 bar).

Component	Loads	SF	Reference
Fuel tank	120 bar	1.00	FEA PRO_07
PT-Connector	600 bar	1.73	FEA PRO_08
Fuel tank E-Reg Body	600 bar	1.04	FEA PRO_06
E-Reg Rod	120 bar	3.74	FEA PRO_05
N_2 QD	600 bar	5.62	FEA PRO_23
N_2 Fill Valve Body	600 bar	1.27	FEA PRO_09
Venting pipe	120 bar	8.20	FEA PRO_20
Backseal	600 bar	4.68	FEA PRO_24
Pass-through	600 bar	2.85	FEA PRO_21
Valvebay structure	Thrust and bending	1.07	FEA PRO_18
Oxidizer tank	110 bar	1.00	FEA PRO_13
N2 Manifold	600 bar	1.08	FEA PRO_14
Ox tank E-reg Body	600 bar	1.00	FEA PRO_10
Thrust structure	Thrust and bending	1.12	FEA PRO_17
Feedflange	120 bar	5.90	FEA PRO_12
Feed pipe	110 bar	4.02	FEA PRO_11
Chamber v3.2	50 bar	1.85	FEA PRO_25
Bulkhead v3.2	50 bar	1.34	FEA PRO_26
Chamber v4.0	50 bar	1.49	FEA PRO_27
Bulkhead v4.0	50 bar	1.01	FEA PRO_28
Ignitor	50 bar	1.00	FEA PRO_03

Appendix B: Ground Support Equipment

B.1 Filling Station

The filling station provides all fluid interfaces required for the final launch preparations. It houses the fluid panel with its actuators, valves, and sensors, as well as two mounting positions for oxidizer bottles and one for the pressurant gas bottles. For the mounting of the CO_2 bottle, an addition was made to store the gas for the fire suppression system. An electrical cabinet mounted directly to the filling station supplies power and controls the integrated components. The launch rail electrical cabinet and the safety control box are also connected to the filling station, forming the central interface between the ground support equipment and the launch vehicle.

B.1.1 Fluid Architecture

The fluid architecture of the filling station, shown in Figure B.1, is divided into two independent subsystems: one for the oxidizer and one for the pressurant. Both subsystems connect their respective supply bottles to the rocket via the QDs.

The oxidizer subsystem features two independent supply lines, each connected to a dedicated oxidizer bottle and equipped with manual fill and vent valves. Downstream of the servo-actuated fill valves, each line incorporates a pressure sensor, a temperature sensor, and a solenoid-operated vent valve. The vent valve enables controlled depressurization of the fill line before disconnecting the oxidizer QD. Continuous monitoring of pressure and temperature in both oxidizer lines ensures safe and reliable operation throughout the tanking process.

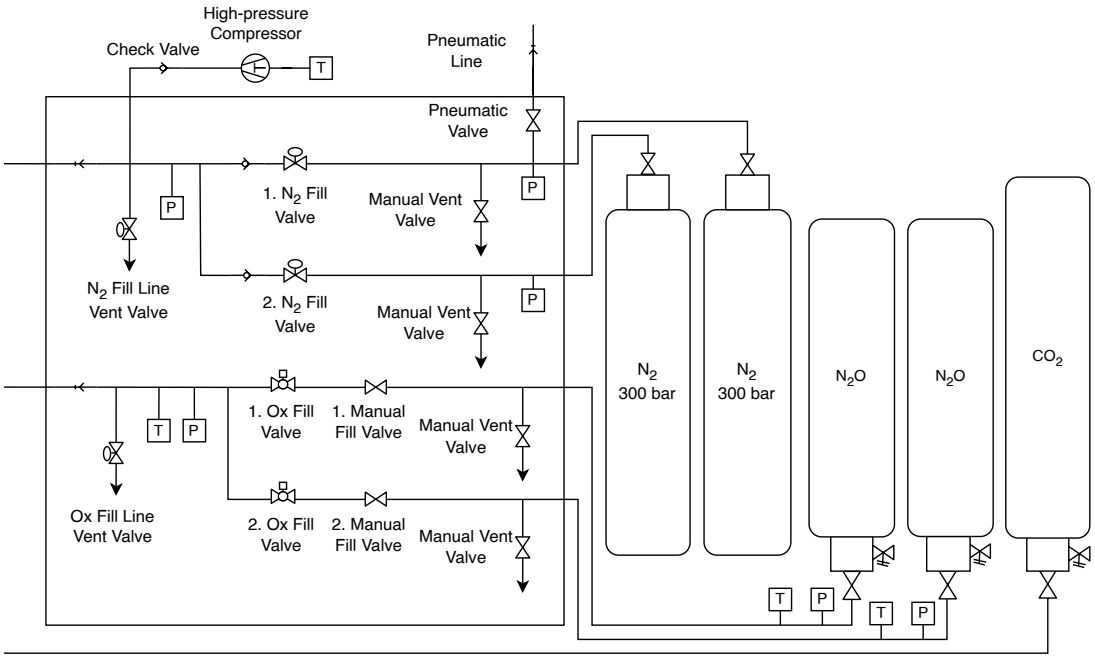


Figure B.1: Schematic representation of the fluid subsystem architecture. Shown are the two main lines for oxidizer (N_2O) and pressurant (N_2), as well as the CO_2 line for fire suppression.

The pressurant subsystem is connected to two N_2 bottles, each equipped with a pressure sensor, a manual vent valve, and a solenoid-actuated fill valve. Since solenoid valves do not inherently prevent reverse flow, check valves are installed directly downstream of each fill valve to isolate the supply bottles from the pressurization line. Downstream of the check valves, the lines merge and pass through an additional pressure sensor, a solenoid vent valve, and a filter before reaching the QD interface.

A compressor is connected to the pressurization line via a check valve and remains isolated from the N_2 bottles. When required, it supplies ambient air instead of nitrogen as a fallback pressurant. This operating mode is acceptable, as previous test campaigns successfully used compressed air during system development. Similar to the oxidizer subsystem, the solenoid vent valve enables controlled depressurization of the line before disconnecting the QD.

B.1.2 N_2 Purging

The pneumatic line, which can be seen at the top of the fluid diagram in Figure B.1, is not only used for pneumatic pressure but also for purging the rocket. A pneumatic line delivers N_2 into the lower fluid of the rocket. The line reaches barely into the hull and is fastened to the launch rail, which holds back the line that is pulled out of the fluid system during launch.

B.1.3 Filling Station Electrical Cabinet

The filling station electrical system operates with a 400 V/16 A main power supply and a 24 V/6 A low voltage supply for the control electronics. Two CANary PCBs manage sensor readouts and actuator controls and connect to a flight computer housed in the electrical cabinet. The filling station features its own telemetry link to the mission control. The cabinet door has indicator lamps that display the system's current state. At the same time, additional switches and buttons provide manual overrides for critical functions, such as vent valves and a reset button for the 24 V systems.

To ensure reliable operation, sensor readout boards are spatially separated from high-power actuators; the CANary PCBs are placed in dedicated electrical cabinets, and sensor cables are kept as short as possible and shielded. Main power consumers, including the compressor, are connected to different phases than the control circuitry, further reducing potential interference and spreading the load over multiple power phases.

The filling station is connected to the launch rail electrical cabinet, which hosts the pneumatic actuators for the QDs, electrical supply for cameras, and an additional CANary.

B.1.4 Safety Control Box

The Safety Control Box provides personnel protection by enabling safe remote operation of the rocket's COTS/SRAD recovery arming systems from a 15 m distance.
A single key operates all key switches, momentary switches for recovery arming as well as the VVO actuation, and a latching switch for pyrotechnical engine ignition arming and holddown ignition arming. The key cannot be removed when engine/holddown ignition is armed, or vent valve override is active, preventing simultaneous activation of ignition arming and vent valve systems. Push-buttons handle disarming the recovery igniters COTS

and SRAD systems, as well as the emergency stop (disconnecting 230 V actuators), while dedicated lamps indicate recovery arming system status.



Figure B.2: Safety Control Box.

B.2 Launch Rail

The launch rail guides the rocket on the first 12 m of its ascent to produce the velocity necessary for stable flight. The rail is constructed from four 3 m truss segments, with three feet that provide stabilization and are weighted down with sandbags or concrete weights. Additionally, steel cables are tensioned between the top segment of the launch tower and the legs. During assembly, a winch system mounted on the back leg and base is used to erect the launch rail from a horizontal position to an inclination of 84° ± 1°; that position is secured by a stopper foot that prevents further elevation and by tightening the steel cables. To improve stability during erection, two corner brakes distribute the load on the winch assembly pulley. In principle, the structure is comparable to the official EuRoC launch rail. The launch rail includes a plethora of sensors and actuators, including sensors for wind speed and direction, the holddown mechanism, the launch rail electrical cabinet, the QD systems for the fluid lines, and power and data connections for the rocket. The following section discusses many of these components in detail.

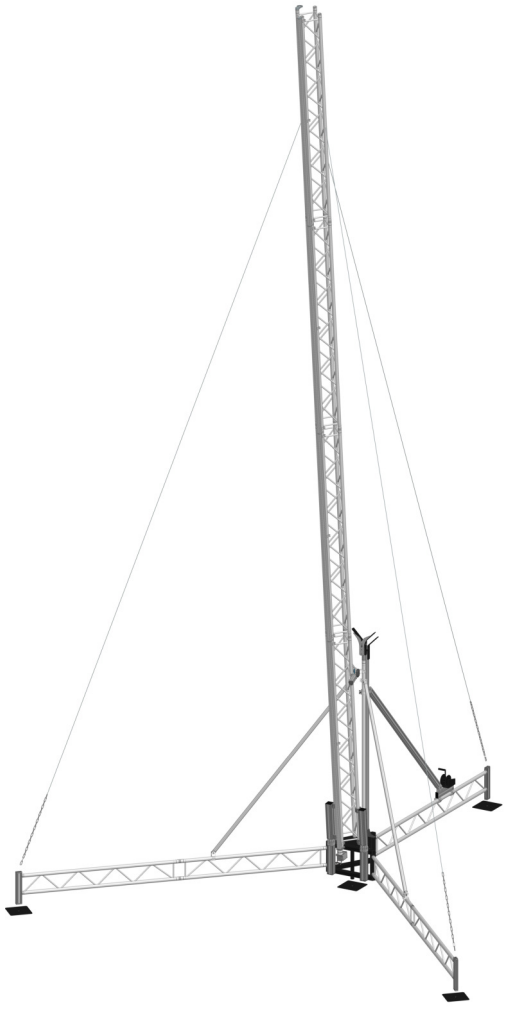


Figure B.3: Assembly of the launch rail.

B.2.1 Fluid Umbilicals

The launch rail features two fluid umbilicals, one for the oxidizer and one for the pressurizing gas, both utilizing quick disconnects (QDs) with dissimilar connection dimensions to prevent incorrect attachment. The oxidizer umbilical is located beneath the oxidizer tank, while the pressurant umbilical is positioned above the fuel tank. To minimize installation space and structural complexity, both umbilical connections are arranged radially, requiring them to disconnect and swing clear of the launch vehicle prior to liftoff.

Remote disconnection is achieved using two pneumatically actuated cylinders that retract the locking sleeves of the QDs. Each umbilical assembly is spring-loaded and mounted to a pivoting aluminum arm. Once released, the stored spring energy rotates the arm away from the rocket, providing sufficient clearance for launch. As a redundant means of operation, both umbilicals can also be manually disconnected from a distance of approximately 15 m using pull ropes attached to the release mechanism.

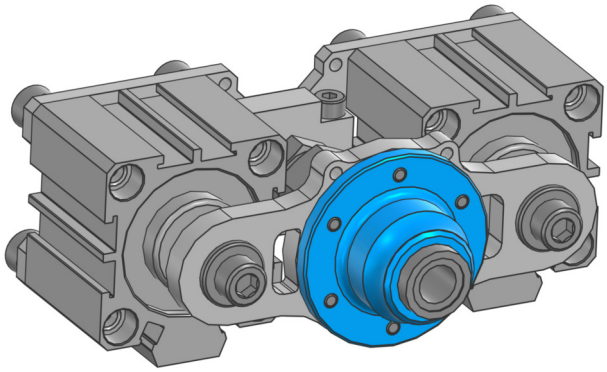


Figure B.4: Assembly of the oxidizer quick disconnect.

B.2.2 Launch Rail Electrical Cabinet

The primary function of the launch rail electrical cabinet is to provide electrical connectivity between the rocket and the filling station, as well as to manage actuators, sensors, cameras, and other devices located in the vicinity of the launch rail.

It connects to the filling station via a Harting connector on the side of the electrical cabinet. Twenty additional connector interfaces are responsible for rocket power supply, rocket arming signals, holddown thrust load cells, VVO signals, co_2 purge control signals, and camera power supplies.

The DC voltage used to charge the rocket's battery pack is also supplied by a separate, dedicated power supply unit located inside the cabinet. The cabinet features a CANary PCB, which is supplemented by two I/O extension PCBs. Because safety also plays an extremely important role, especially around the launch rail, the VVO systems are also housed in the cabinet; dedicated DC-DC converters supply them with the necessary power, and the CANary operates them. In addition, a valve block at the bottom of the cabinet, which is also controlled by the CANary's I/O board, is responsible for pneumatically controlled actuators, such as the QDs and the insulation deployment.

B.2.3 Electrical Umbilical

The electrical umbilical functions as a wired connection between the rocket and the GSE while the rocket is on the launch rail. It uses a Type-C USB cable with a non-standard pin assignment, chosen for its compact connector, high number of contacts, and 240 W power rating. The connector on the rocket body is situated at the top of the avionics tube radax. It angles downward to allow automatic unplugging during lift-off.

One of the umbilical's primary functions is to supply auxiliary electrical power to the rocket, keeping the onboard battery pack charged until lift-off. In addition to power delivery, the cable carries several critical signals: the holddown ignition signal, two-way reset signals, and the recovery arming signals for the rocket's SRAD and COTS flight computers. The reset lines allow for remote resetting of the rocket using the filling station and vice versa. On the GSE side, the electrical umbilical connects to the launch rail electrical umbilical PCB, which is then connected to the launch rail electrical cabinet mounted at the launch rail.

B.2.4 Vent Valve Override System

In case the rocket's onboard electronics become unresponsive, the entire system can be vented safely via the safety control box using four key switches. These four switches actuate the vent valve override (VVO) system via its own umbilical cable, which connects the launch rail electrical cabinet with a magnetic connector in the Valvebay panels of the rocket. This system allows individually overriding the oxidizer tank bottom venting solenoid, the fuel depressurization solenoid, the n_2 filling servo motor, and the upper oxidizer venting servo motor of the rocket.

B.2.5 Holddown

The holddown mechanism is integrated into the launch rail and securely retains the rocket until it reaches sufficient thrust for stable flight. The system is designed and tested to withstand the axial forces during ignition and to reliably release the rocket during a nominal launch procedure.

The system uses a pyrotechnically actuated release pin that mechanically connects the launch rail to a reinforced hardpoint in the rocket's tailcone. The release pin sits inside a housing equipped with pyrotechnic igniters that produce the pressure needed to eject the pin under full load from the rocket's thrust. The housing connects to two load cells, arranged in series for redundancy, that directly measure the thrust acting on the rocket. Figure B.6 shows the complete system, and Figure B.7 shows a cut view.

As soon as the required thrust for stable flight is measured (determined from flight simulations) and the ignition state is confirmed, the CANary in the launch rail electrical cabinet triggers the pyrotechnic igniters. The rocket's flight computer can also trigger the igniters if the CC pressure is stable. The pressure generated by the igniters acts on the rear face of the pin, producing an axial force that fully ejects the pin from the rocket hardpoint and releases it for flight. All igniter channels are also secured via an ignition arming relay, as shown in Figure B.5, which must be actuated with a key switch in the safety control box to enable the ignition relays. A 12 V battery in the filling station powers the igniters.

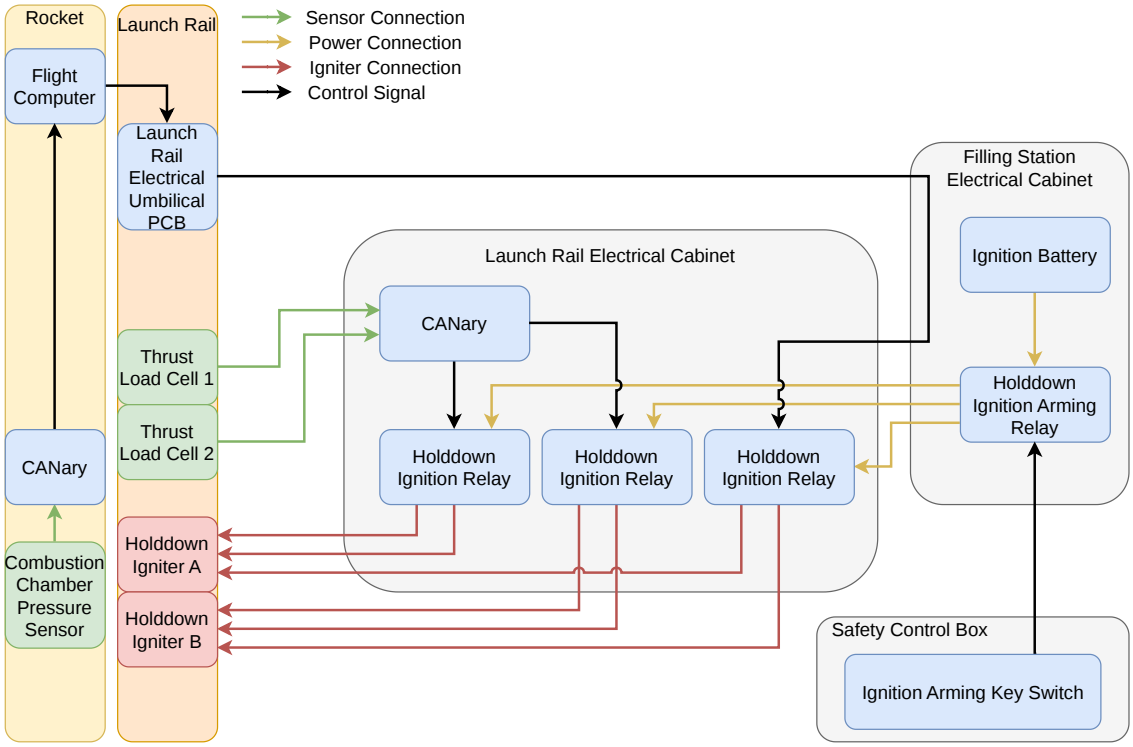


Figure B.5: Electrical wiring of the holddown system.

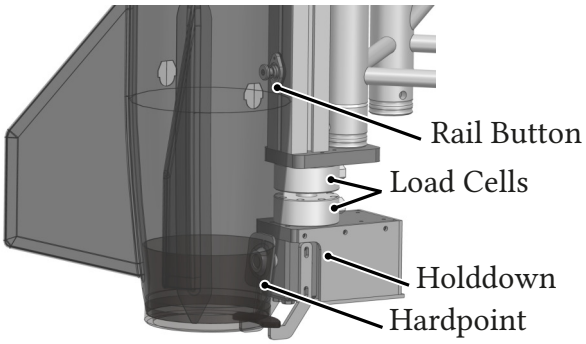


Figure B.6: Holddown with the hardpoint in the tailcone.

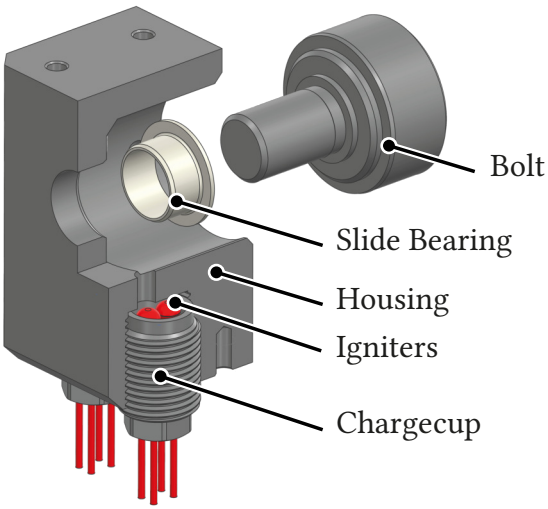


Figure B.7: Holddown in an explosion cut view.

B.3 Mission Control

The telemetry receiver on the ground is built around the same main board used for the rocket telemetry system, with an Ethernet extension board for network connectivity. The mission control is centered around a dedicated server that runs the custom control panel, stores received telemetry data, and provides real-time monitoring and visualization. Safety-critical

physical controls, including the arming key switch, ignition button, and status indicators, are integrated into a separate mission control box.

The telemetry receiver node and the mission control server communicate over UDP using a custom data transfer protocol, TELtalk. The connection between mission control and the ground support equipment at the launch rail is established through a COTS 5 GHz wireless bridge, the UniFi Device Bridge Pro, which is specified for link distances of up to 5 km. Omnidirectional antennas are used for the telemetry link to the rocket, avoiding the need to actively track the rocket during flight.

Additionally, the CATS Vega ground station is used as a redundant mission control system to track the rocket's location.

B.3.1 Mission Control Rack

Most mission control components are built into a flight case rack. This makes transportation simple and allows for a quick setup. The rack houses a server running the mission control software, a network switch, and a wireless local area network (WLAN) router for network access. To ensure continued operation during a power outage, an uninterruptible power supply (UPS) provides temporary power to critical systems.

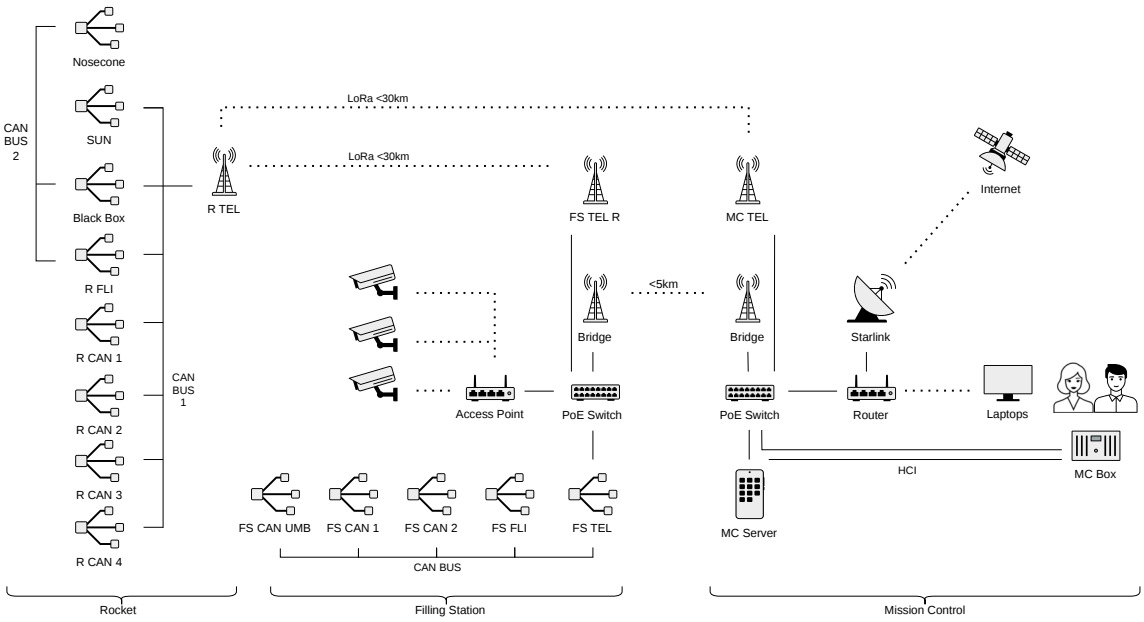


Figure B.8: Network Topology of HARPIA, filling station and mission control.

B.3.2 Mission Control Box

The separate mission control box integrates physical interfaces such as the arming key switch, ignition button, and critical status indicators. For safety, the arming key switch and the ignition button are connected in series, so both must be actuated before the ignition command is sent to the flight computer. The software also checks this condition to ensure both inputs are active. The ignition button sends a signal only when pressed and removes it when released.

The box can also be used to send an abort signal or actuate the rocket vent valves, including the vent valve override, if the server is unavailable. It contains indicator lights showing the connection status of the telemetry nodes, as well as the arming state of the ignition and the recovery system.

B.3.3 Mission Control Software

The mission control software is running on the server in the rack and hosts the custom control panel, manages data storage, and provides real-time visualization.

The nodes communicate with the mission control server over User Datagram Protocol (UDP) using TELtalk. Data exchange between the mission control and the filling station at the launch rail is done via a COTS wireless link (Unifi Device Bridge Pro) rated for a distance of 5 km. To simplify operations, mission control uses omnidirectional antennas, eliminating the need to track the rocket during flight.

The Python backend application reads and writes TELtalk protocol packets and stores the resulting data in a PostgreSQL database. Grafana accesses this database directly for visualization and monitoring. The custom React frontend provides command execution and communicates with the backend via a GraphQL API. The entire system is dockerized to ensure rapid deployment and reproducibility.

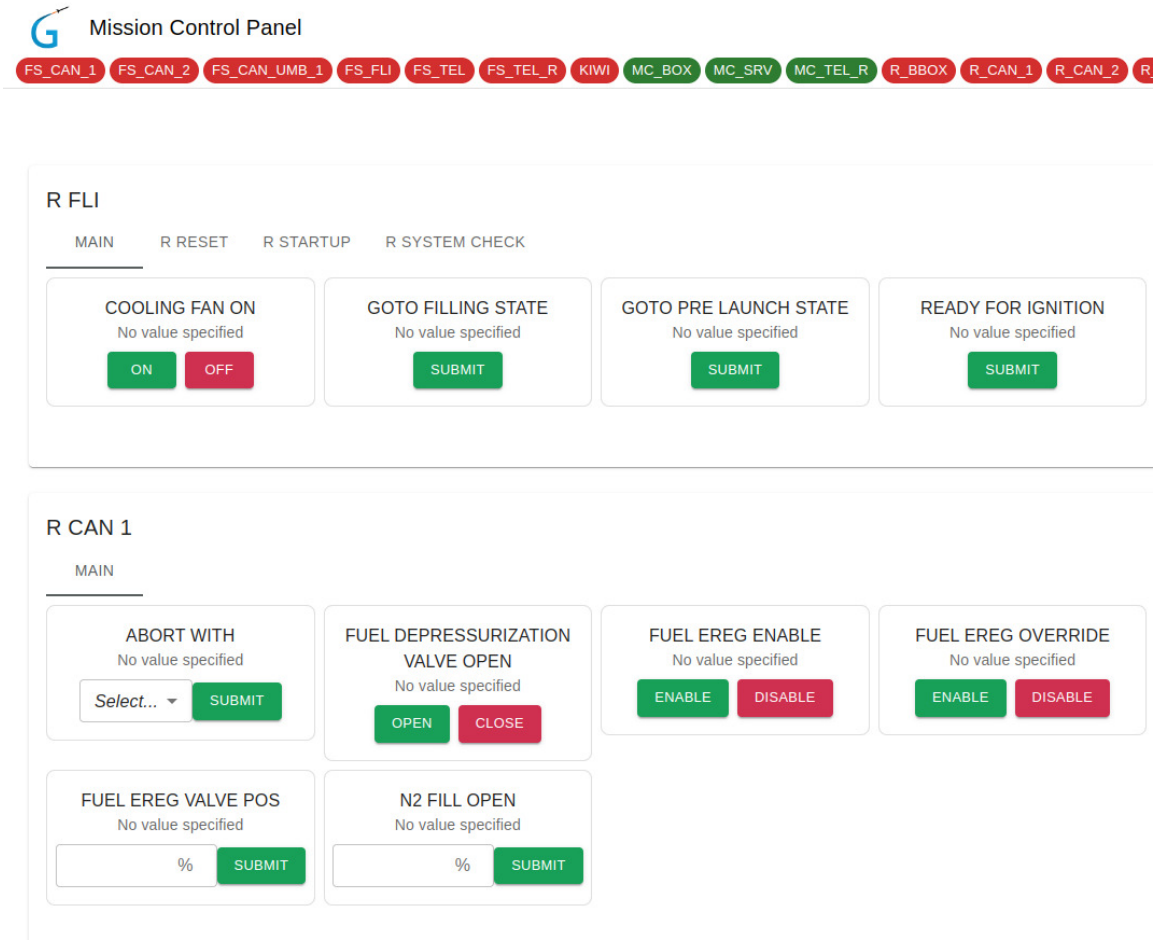


Figure B.9: Mission Control Panel.

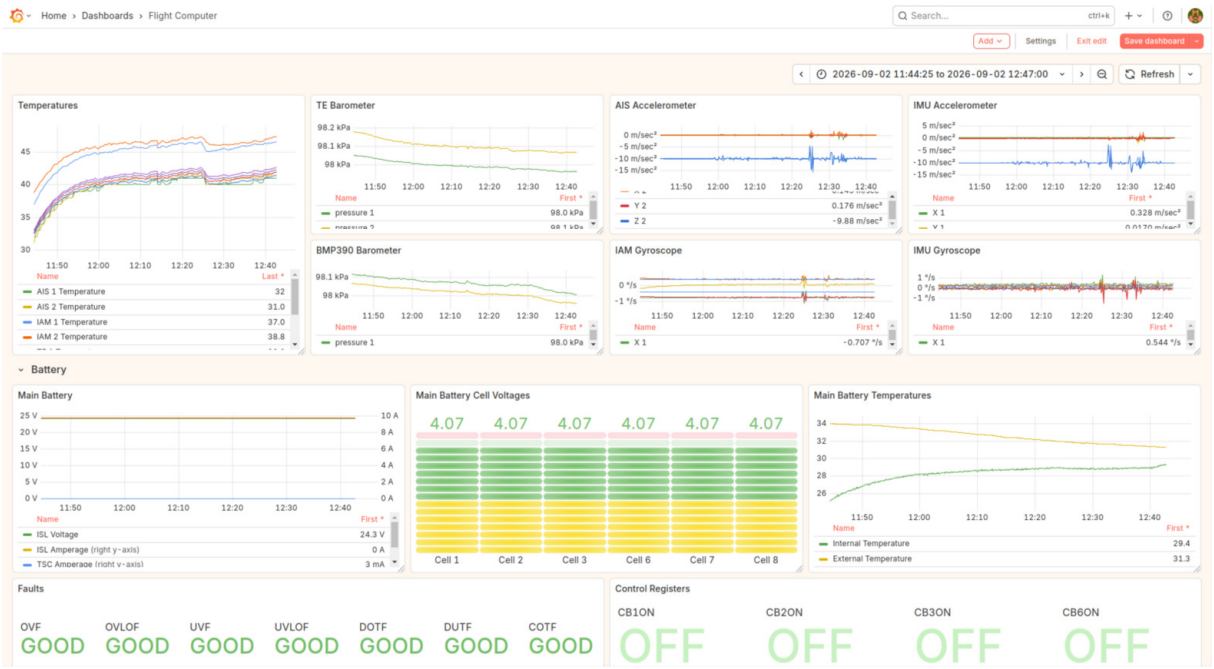


Figure B.10: Mission Control Grafana.

Furthermore, the mission control server connects to IP cameras located at the filling station. These cameras provide real-time visual feedback, enabling reliable monitoring of the tanking process.

B.3.4 Antennas

Omnidirectional quadrifilar helix (QFH) antennas are used at the mission control to receive LoRa transmissions from the rocket. This removes the need for manual rocket tracking and provides more consistent reception as the rocket's orientation and position change during flight.
The antennas are designed for operation around a center frequency of 2.44 GHz within the 2.4 GHz ISM band. They provide a bandwidth of approximately 60 MHz and use right-hand circular polarization. The bandwidth over which the axial ratio remains below 3 dB is approximately 10 MHz and is centered at 2450 MHz.



Figure B.11: Telemetry receiver with QFH antenna.